
GAZİ ÜNİVERSİTESİ
Gazi
1926

PREDICTION OF COVID 19 DISEASE USING CHEST X-RAY IMAGES BASED ON DEEP LEARNING

Ismael Abdullah Mohammed AL-RAWE

IN PARTIAL FULFILLMENT OF THE REQUIREMENTS
FOR THE DEGREE OF MASTER OF SCIENCE
IN COMPUTER ENGINEERING DEPARTMENT

GAZİ UNIVERSITY
GRADUATE SCHOOL OF NATURAL AND APPLIED SCIENCES

JANUARY 2024

ETHICAL STATEMENT

I at this moment declare that in this thesis study, I prepared the thesis writing rules of Gazi University Graduate School of Natural and Applied Sciences;

- All data, information, and documents presented in this thesis have been obtained within the scope of academic rules and ethical conduct,
- All information, documents, assessments, and results have been presented by scientific ethical conduct and moral rules,
- All material used in this thesis that is not original to this work has been exhaustively cited and referenced,
- No change has been made in the data used,
- The work presented in this thesis is original,

or else, I admit all loss of rights to be incurred against me.

Ismael Abdullah Mohammed AL-RAWE

12/01/2024

PREDICTION OF COVID 19 DISEASE USING CHEST X-RAY IMAGES BASED ON DEEP LEARNING

(M.Sc. Thesis)

Ismael Abdullah Mohammed AL-RAWE

GAZİ UNIVERSITY

GRADUATE SCHOOL OF NATURAL AND APPLIED SCIENCES

January 2024

ABSTRACT

Covid 19 disease causes more than one million deaths worldwide each year. Covid 19 diseases are some of the most common medical conditions in the world. Current clinical technologies produce thousands of images, making it impossible for a physician to accurately evaluate them all. A new coronavirus disease (COVID-19) has been causing major lung damage and respiratory problems since December 2019. On the other hand, pneumonia, a type of lung disease, can be caused by the causative COVID-19 virus or another viral or bacterial infection. The prevention, control and treatment of these diseases, as well as the promotion of respiratory health, should be a high priority in global health decision-making. Also, human interpretation of medical images tends to be inaccurate and fails to reveal all data and imaging information. The primary aim of this thesis is to apply deep learning techniques to automatic screening for Covid 19 disease from digital chest X-ray images. The framework for machine learning-based methods mostly consists of the following steps: preprocessing, segmentation, feature extraction and classification. Chest X-ray images are preprocessed and segmented to suppress unwanted distortions and enhance certain image features that are important for downstream processing. Then, using deep learning, relevant features used to classify chest X-ray images are extracted. Finally, the performance of the classifiers has been measured and compared. In this research, we performed a thorough examination of two critical datasets, Covid19-dataset and Chest X-ray (Covid-19 & Pneumonia) dataset, in order to construct machine learning models for COVID-19 identification. Our findings show that dataset quality and complexity have a considerable impact on model performance. Our investigations showed that DenseNet achieved the greatest testing accuracy of 98.04% for Covid19-dataset. This dataset provides a difficult environment for model building, underlining the importance of robust and adaptive algorithms in real-world healthcare applications. Chest X-ray (Covid-19 & Pneumonia) dataset, on the other hand, was built with a simpler scenario and demonstrated flawless training accuracy across all models, with DenseNet obtaining testing accuracy of 95.80%. Results of Chest X-ray (Covid-19 & Pneumonia) dataset have the potential for good accuracy but its simplicity may not adequately represent the complexities of real-world clinical settings. Deep learning algorithms used for Covid 19 disease prediction are supervised learning with high prediction rate. In this thesis, a new Approach is applied for Covid 19 disease prediction using DenseNet and MobileNet based Chest X-Ray Images. The research done in this thesis will enable incredibly rapid diagnosis of clinical scans that radiologists and physicians can use in routine clinical practice. However, estimating spondylolisthesis from X-ray images is more difficult due to the different modalities in the image dataset. This thesis outlines three models that can actually be helpful in detecting Covid 19 disease in the worker. The input image is subjected to several convolution layers. ReLU activation function is used in all convolutional layers. Experiments were made by changing the hyper parameters of the proposed CNN architecture and the proposed models MobileNet and DenseNet performed well with very good accuracy and precision.

Science Code : 92432
Key Words : Covid 19 disease, CAD, machine learning, ANN, CNN, Max-pooling, fully connected layer, classification
Page Number : 109
Supervisor : Assoc. Prof. Dr. Adem Tekerek

DERİN ÖĞRENMEYE DAYALI GÖĞÜS RÖNTGEN GÖRÜNTÜLERİ KULLANARAK COVID 19 HASTALIĞININ TAHMİNİ

(Yüksek Lisans Tezi)

Ismael Abdullah Mohammed AL-RAWE

GAZİ ÜNİVERSİTESİ

FEN BİLİMLERİ ENSTİTÜSÜ

Ocak 2024

ÖZET

Covid 19 hastalığı dünya genelinde her yıl bir milyondan fazla ölüme neden oluyor. Covid 19 hastalıkları dünyadaki en yaygın tıbbi durumlardan bazılarıdır. Mevcut klinik teknolojiler binlerce görüntü üreterek bir hekimin hepsini doğru bir şekilde değerlendirmesini imkansız hale getirmektedir. Yeni bir koronavirüs hastalığı (COVID -19), Aralık 2019 'dan bu yana büyük akciğer hasarına ve solunum sorunlarına neden olmaktadır. Öte yandan, bir tür akciğer hastalığı olan pnömoniye neden olan COVID -19 virüsü veya başka bir viral veya bakteriyel enfeksiyon neden olabilir. Bu hastalıkların önlenmesi, kontrolü ve tedavisinin yanı sıra solunum sağlığının teşvik edilmesi, küresel sağlık karar vermede yüksek öncelikli olmalıdır. Ayrıca, tıbbi görüntülerin insan tarafından yorumlanması yanlış olma eğilimindedir ve tüm verileri ve görüntüleme bilgilerini ortaya çıkarmaz. Bu tezin birincil amacı, dijital göğüs röntgeni görüntülerinden Covid 19 hastalığı için otomatik taramaya derin öğrenme tekniklerini uygulamaktır. Makine öğrenimi tabanlı yöntemler için çerçeve çoğunlukla şu adımlardan oluşur: ön işleme, segmentasyon, öznitelik çıkarma ve sınıflandırma. Göğüs röntgeni görüntüleri, istenmeyen bozulmaları bastırmak ve aşağı akış işleme için önemli olan belirli görüntü özelliklerini geliştirmek için önceden işlenir ve bölümlere ayrılır. Daha sonra, derin öğrenme kullanılarak, göğüs röntgeni görüntülerini sınıflandırmak için kullanılan ilgili özellikler çıkarılır. Son olarak, sınıflandırıcıların performansı ölçülmüş ve karşılaştırılmıştır. Bu araştırmada, COVID -19 tanımlaması için makine öğrenimi modelleri oluşturmak amacıyla Covid19 veri kümesi ve Göğüs X - ışını (Covid -19 ve Pnömoni) veri kümesi olmak üzere iki kritik veri kümesinin kapsamlı bir incelemesini gerçekleştirdik. Bulgularımız, veri kümesi kalitesinin ve karmaşıklığının model performansı üzerinde önemli bir etkiye sahip olduğunu göstermektedir [1].

1. Giriş

Araştırmalarımız, DenseNet'in Covid19 veri kümesi için % 98,04 'lük en yüksek test doğruluğunu elde ettiğini gösterdi. Bu veri kümesi, gerçek dünyadaki sağlık uygulamalarında sağlam ve uyarlanabilir algoritmaların önemini vurgulayarak model oluşturma için zor bir ortam sağlar. Göğüs röntgeni (Covid -19 & Pneumonia) veri seti ise daha basit bir senaryo ile oluşturulmuş ve DenseNet'in % 95,80 test doğruluğu elde etmesiyle tüm modellerde kusursuz eğitim doğruluğu göstermiştir. Göğüs röntgeni (Covid -19 ve Pnömoni) veri setinin sonuçları iyi bir doğruluk potansiyeline sahiptir, ancak basitliği gerçek dünyadaki klinik ortamların karmaşıklığını yeterince temsil etmeyebilir. Covid 19 hastalığı tahmini için kullanılan derin öğrenme algoritmaları, yüksek tahmin oranına sahip denetimli öğrenmedir [2]. Bu tezde DenseNet ve MobileNet tabanlı Göğüs Röntgeni Görüntüleri kullanılarak Covid 19 hastalık tahmini için yeni bir Yaklaşım uygulanmaktadır. Bu tezde yapılan araştırmalar, radyologların ve hekimlerin rutin klinik uygulamalarda kullanabilecekleri klinik taramaların inanılmaz derecede hızlı bir şekilde teşhis edilmesini sağlayacaktır. Bununla birlikte, görüntü veri kümesindeki farklı modaliteler nedeniyle X - ışını görüntülerinden spondilolistezi tahmin etmek daha zordur. Bu tez, çalışanda Kovid 19 hastalığını tespit etmede gerçekten yardımcı olabilecek üç modeli özetlemektedir. Giriş görüntüsü

birkaç evrişim katmanına tabi tutulur. ReLU aktivasyon fonksiyonu tüm evrişimli katmanlarda kullanılır. Önerilen CNN mimarisinin hiper parametreleri değiştirilerek deneyler yapıldı ve önerilen modeller MobileNet ve DenseNet çok iyi doğruluk ve hassasiyetle iyi performans gösterdi.

Bir insanın akciğerleri ve solunum sistemi çevredeki havadan oksijen alır ve karbondioksit verir. Akciğerler, bazıları kalıtsal olabilen çok çeşitli koşullara karşı hassastır, bazıları ise kötü alışkanlıklardan, sağlıksız bir diyetten ve hatta enfeksiyonlardan kaynaklanabilir. Ancak COVID - 19 nispeten yeni bir hastalıktır ve araştırmacılar bir kişinin akciğerleri üzerindeki etkileri hakkında her zaman yeni bilgiler edinmektedir. Araştırmacılar, insan vücudu üzerindeki etkilerin diğer iki koronavirüs enfeksiyonu olan şiddetli akut solunum sendromu (SARS) ve Orta Doğu Solunum Sendromu'nun (MERS) neden olduğu etkilere benzer olduğuna inanıyor. Radyoloji, insan akciğer hastalığının teşhisi sürecinde tutulumun modelini, yerini ve coğrafi dağılımını belirlemekten sorumlu uzmanlık dalıdır. Klinisyenler Covid 19 hastalığını teşhis ederken akciğerlerin oksijen ve karbondioksiti tutma, taşıma ve değiş tokuş etme yeteneklerini değerlendirebilirler. Solunum fonksiyon testleri akciğer hastalığının tipini ve şiddetini belirler. Göğüs görüntüleme, bronkoskopi ve torakoskopi doktorların akciğer hastalıklarını teşhis etmelerine yardımcı olur.

Tüm dünyada çok sayıda insan Covid -19 hastalığının çeşitli türlerinden etkilendi. Özellikle virüsün neden olduğu akciğer hastalıkları, akciğerleri daha fazla fiziksel zorluklara ve hava kirliliğinin olumsuz etkilerine karşı daha savunmasız hale getirmektedir. Covid -19 'un bulaşıcı doğası göz önüne alındığında, bu, en etkili ilacı sunmak için doğru tanının önemini vurgulayarak akciğer fonksiyonunu azaltır. Radyologlar, çeşitli akciğer bozukluklarını keşfetmek ve teşhis etmek için göğüs röntgenlerini birincil tanı aracı olarak kullanarak bu tanı prosedüründe önemli bir rol oynamaktadır. Bu uzman kişiler, Covid -19 'un yanı sıra bronşit, infiltrasyonlar, atelektazi, perikardit, kırıklar ve çok daha fazlası gibi çok çeşitli hastalıkları tespit edebilirler. Şaşırtıcı bir şekilde, her yıl 2 milyondan fazla göğüs radyografisi tedavisi yapılmakta ve bu da onu dünyada en yaygın kullanılan hastalık muayenesi haline getirmektedir. Kovid -19 'un zatürre ve akciğer opaklığı gibi diğer viral enfeksiyonlarla örtüşen semptomları göz önüne alındığında, bireysel hastalıkları güvenilir bir şekilde ayırmak kritik hale geldi. Sonuç olarak COVID, Pnömoni, Akciğer opasitesi, Normal gibi gruplara ayrıldı. Kovid -19 hastalık tablolarının karmaşıklığı, röntgen filmlerinde hastalık özelliklerinin tespit edilmesini ve tanımlanmasını zorlaştırıyor. Daha önce, bu görüntülerin karmaşıklığı ve röntgen görüntülerinde durumları ve bozukluk hastalıklarını analiz etmenin zorluğu nedeniyle etkili gelişme engelleniyordu.

Derin öğrenme algoritmaları, bu zorluklara yanıt olarak akciğer bozukluklarını teşhis etmek için umut verici araçlar olarak gelişmiştir. Çeşitli derin öğrenme algoritmaları kullanarak Kovid -19 hastalık tahminini araştırmak için çeşitli çalışmalar yapılmıştır. Bu gelişmeler, günümüzde kanser tanısı için sinir ağlarına dahil edilen tüberküloz (TB), kronik obstrüktif akciğer hastalığı (KOAH) ve pnömoni gibi diğer akciğer rahatsızlıklarının tanımlanmasına yol açmıştır [3]. Bu bağlamda derin öğrenme uygulaması, akciğer görüntülemede hastalık tanısının doğruluğunu ve etkinliğini artırmaya yönelik büyük bir adım sağlamaktadır. Hastanın göğüs röntgeni genellikle doktor bir hasta hastalığının öyküsünü topladıktan ve fiziksel muayeneyi yaptıktan sonra kontrol edilir. Hastanın tıbbi öyküsünden, fiziksel kontrolünden ve göğüs röntgeninden elde edilen bulgular, semptomların kök nedenini belirlemek için başka hangi tanı prosedürlerinin gerekli olabileceğine dair ipuçları sağlayabilir. Göğüs röntgeninde kalp, akciğerler, kan arterleri ve hava yollarının yanı sıra göğüs ve omurgadaki kemiklerin görüntüleri görülebilir. Göğüs röntgenleri, insan akciğerlerinde veya çevresinde sıvının yanı sıra bir akciğerin etrafındaki havanın varlığını da ortaya çıkarabilir [4-5].

Hastaları tıbbi yardım almaya ve acil servislere gitmeye sevk eden en yaygın semptom göğüs ağrısıdır. Daha yaygın olarak göğüs röntgeni (veya kısaca CXR) olarak adlandırılan göğüs radyografisi, toraksı etkileyen bozuklukların tanımlanmasında kullanılan en popüler radyoloji muayenelerinden biridir [6-7]. Bununla birlikte, radyografi belirsizlik durumlarında karar vermeyi gerektirir ve sonuç olarak, tamamen kusursuz yorumlar veya raporlar sunmak her zaman mümkün değildir. Bu amaçla, radyologların daha kısa sürede tanısal mükemmelliğe ulaşmalarına yardımcı olmak ve hastalar için sağlık hizmetlerinin kalitesini artırmak için Cad olarak da bilinen Bilgisayar

Destekli Tanı oluşturuldu [8]. Cad sistemlerinin amacı, tıp uzmanlarıyla rekabet etmek veya onların yerini almak değildir; daha ziyade, radyologların çalışmalarını destekleyen "ikinci bir görüş" olarak hizmet etmeleri amaçlanmıştır. Radyografiler, BT taramaları, MRG'ler, nükleer tıp, PET taramaları, füzyon görüntüleme, ultrason ve diğer tıbbi görüntüleme tekniklerinin tümü, yaralanmaları ve hastalıkları tespit etmek ve tedavi etmek amacıyla tıbbi görüntüleme çalışması ve uygulaması olan görüntülemenin bir parçasıdır. Radyolog, radyoloji olarak bilinen tıp dalında görüntülemeye odaklanan bir uzmandır. Bu görüntüleme yöntemlerinden bazıları radyasyon kullandığından ve kendinizi radyasyondan nasıl koruyacağınızı anlamak için eğitime ihtiyacınız olduğundan, bu prosedürlerin bir kısmı da radyasyon güvenliği konusunda bilgi sahibi olmanızı gerektirir. Yapay Zeka (AI) ve Bilgisayarlı Görüşü (CV) kullanan teknikler, son on yılda önemli miktarda ilgi ve odak noktası kazanmıştır ve bu eğilimin devam edeceği öngörülmektedir [9]. Tıbbi görüntülerin sınıflandırılması, tipik görevin yanı sıra temel zorluklardan biridir. Kategorizasyon işleminin amacı, bir tıbbi görüntüye görüntünün içeriğine göre tek bir tanısal sonucun mu yoksa birkaç tanısal sonucun mu atanması gerektiğini belirlemektir. Bu bağlamda, kategorizasyonun doğruluğunu artırmak için daha karmaşık sınıflandırma yaklaşımları ve metodolojilerinin geliştirilmesi için önemli miktarda çalışma yapılmıştır. Başlangıçta, resim sınıflandırma sorununu çözmek için iki aşamalı bir süreç kullanılmıştır. İlk aşamanın amacı, özellik tanımlayıcılarını kullanarak bir görüntüden özellikleri manuel olarak çıkarmaktır, ikinci aşamanın amacı ise manuel olarak çıkarılan özellikleri eğitilebilir bir sınıflandırıcıya beslemektir. Bununla birlikte, ilk adımda öznitelik çıkarımı için kullanılan teknoloji, bu tekniğin ne kadar doğru olduğu üzerinde önemli bir etkiye sahiptir. Derin öğrenme, verileri birkaç doğrusal olmayan işleme katmanı aracılığıyla modelleyerek otomatik öznitelik çıkarma ve sınıflandırma sağladığından, resim sınıflandırma amacına ulaşmanın bir yolu olarak incelenmiştir.

Günümüzde klinik görüntüleme, biri yapay zeka olan çok çeşitli testlerden giderek daha fazla unsur içermektedir. Bu bileşenler, derin öğrenme, bulanık kümeler, kaba kümeler, şüpheli analiz, çok hedefli ilerleme, sürü bilgi geliştirme ve makine öğrenmesi dahil olmak üzere birçok çalışmada yaygın olarak kullanılmaktadır. Hastalar, referans noktası olarak gecikmiş test sonuçları kullanılarak klinik gruplarına göre ankete tabi tutulur. Yapay zeka modelleriyle kişiselleştirilmiş enfeksiyon değerlendirme araçları, çok sayıda klinik resim kullanarak klinik fotoğraflarda örüntüleri ve bağlantıları bulma yeteneklerini kullanarak bilgisayar tabanlı zeka odaklı düzenlemelerin başka bir testinde geliştirilmiştir. Bu, klinik tabloların kullanımıyla gerçekleştirilir. Evrimsel sinir ağları tarafından sıklıkla kullanılır. Radyologlar ve doktorlar, birçok disiplinden uzmanların birleşik çalışmaları sayesinde yakında yeni araçlara sahip olacaklar. Radyoloji ve tıbbi görüntü işleme, en etkili ağı belirlemek amacıyla çeşitli yapay zeka algoritmalarının kapsamlı testlerine tabi tutulmuştur. Evrişimsel Sinir Ağları (CNN), segmentasyon, lokalizasyon ve sınıflandırma gibi görevler için tıbbi görüntü işlemede büyük potansiyel göstermiştir. Bu nedenle, göğüs röntgeni görüntülerini ve derin öğrenme yapay zeka teknolojilerini kullanarak COVID -19 hastalık tahmini için çığır açan bir yöntem üzerinde çalışıyoruz.

Akciğerlerdeki anormallikler ölümle sonuçlanabilir; bu nedenle erken teşhis ve zamanında tedavi hayat kurtarabilir ve can kaybını önleyebilir. Akciğer sorunları olan hastalar önemli bir halk sağlığı sorunu olarak kategorize edilebilir. Akciğer bozuklukları için tipik tanı prosedürleri için bir dizi manuel muayene gereklidir. Bu insan müdahalesi çok zaman alır, son derece hataya açıktır ve kullanılan prosedürler her zaman yüksek düzeyde doğruluk garanti etmez. Bu nedenle, oftalmoloji alanındaki gerçek uygulamalar için otomatik yöntemler son derece önemlidir. Bu otomatik teknolojilerin çoğu, hastalıkları teşhis etmek için dijital görüntü analizine dayanmaktadır. Görüntü sınıflandırma yöntemi tanıda önemlidir. Bu süreçte, çeşitli benzerlik ölçümlerine dayalı olarak çeşitli anormal görüntüler bir dizi kategoride düzenlenir.

Buradaki zorluk, bu otomatik kategorizasyon sistemlerinin kısa sürede yüksek doğruluk üretmesi gerektiğidir. Ek olarak, otomatik taramalar, hastalıkları doğrularken bir etkiye sahip olmak için en az iki potansiyel son nokta gerektirir. Standart açıklamalı referansları toplama süreci oldukça zaman alıcıdır. Algoritmalar için başvurulabilir veri havuzları oluşturmak, görüntülerin toplanması, gerekli ek açıklamaların sağlanması ve verilerin geniş kullanım için hazırlanmasıyla ilgili

komplikasyonların bir sonucu olarak zorlaşan bir diğer konudur. Görüntüleme cihazlarının eskimesi, bir veri kümesinin ömrünü kısaltır, bu da eski referansların en son ekipman veya çözünürlüklerle uyumlu olması için revizyon gerektirmesi nedeniyle bir zorluk teşkil eder. Akciğerlerin görüntülerinin önceden işlenmesi gerekir, çünkü içlerinde gürültü olabilir. Birkaç görüntü içeren eğitim veri setleri, önemli miktarda zaman alır ve diğerlerine kıyasla yavaştır. Göğüs röntgeni görüntü işlemede en zorlu işlerden biri, önemsiz olmayan içerik içeren görüntülerde ihtiyaç duyulan bölümlerin bölümlere ayrılmasıdır. Ayrıca, segmentasyonun kesinliğinin nihayetinde bilgisayarlı analiz tekniklerinin akciğer hastalığını belirlemede başarılı olup olmadığını belirlediği gerçeğini de dikkatimize sunarlar. Bu nedenle, etkili segmentasyon sorunlu hale gelebilir.

Dünyanın değişim yaşama hızı o kadar hızlı ki, insanların sağlığına giderek daha fazla baskı yapıyor. İklim, çevre ve insanların yaşam tarzındaki olumsuz değişimlerin tümü, insanlar arasında hastalık insidansının artmasına katkıda bulunur. Olumsuz etkilenen organlardan biri de akciğerdir. COVID - 19 'un neden olduğu ölüm oranını azaltmak için uygulamalı zekadan yararlanan etkili bir temassız tanı ve karar destek sistemi geliştirmek. Bu, korona virüsü ile enfekte olmuş kişilerin şiddet seviyelerinin yanı sıra erken teşhisin doğruluğunu artırarak gerçekleştirilebilir. Hastalığın ilerlemesi hakkında daha iyi bilgi edinmek için, COVID -19 resimlerinin görüntü ön işleme, segmentasyon ve sınıflandırılmasında önemli tıbbi ve teknolojik ilerlemeler hala gereklidir. Küresel ölçekte başlıca ölüm nedenlerinden biri olan zatürre, insan yaşamı için ciddi bir tehdit oluşturmaktadır. Dünya çapında tahminen 1,4 milyon çocuk her yıl zatürreye yenik düşmekte ve bu savunmasız nüfus üzerindeki yıkıcı etkinin altını çizmektedir. Şaşırtıcı bir şekilde, bu endişe verici rakamın % 18 'i beş yaşından küçük çocuklara atfedilmektedir. Araştırmacılar, solunum hastalığının kapsamını daha iyi anlamak için Davranışsal Risk Faktörü Sürveyans Sistemi (BRFSS) 2020 anketinden elde edilen verileri analiz etti. Yirmi dokuz eyalette ve DC'de, anket, yetişkinlerin % 9,2 'sinin ve çocukların % 7,5' inin verilen anket döneminde astım olduğunu göstermiştir. Buna ek olarak, kronik akciğer bozuklukları 34,8 milyon Amerikalıyı veya nüfusun % 13,7 'sini etkilemiştir.

Yetişkinler arasında astım ve kronik COVID -19 hastalığının belirli bir alanda ne kadar yaygın olduğunu öğrenmek için çalışmak gerekir. Bunu, 2020 BRFSS durum yaygınlık oranlarını yaş grubuna göre Kronik Hastalık Önleme ve Sağlığı Geliştirme web sitesinin ilçe düzeyindeki yaşa özgü yerleşik popülasyonları ile karşılaştırarak başarıyoruz. Bu yöntem, yerel bölgedeki yetişkin astım ve kronik Covid -19 hastalığı prevalansının kapsamlı bir değerlendirmesini sunarak sağlık manzarasına ilişkin yararlı bilgiler sağlar. Bu nedenle, bu pandemi durumu ve mevcut senaryo göz önüne alındığında, bilgisayarların gücü ve şu anda halka sunulan önemli miktarda veri göz önüne alındığında, yukarıda bahsedilen sorunun çözümüne katkıda bulunmak için iyi bir zaman. Amaç, tıbbi maliyetleri düşürmek ve derin öğrenme yöntemlerini kullanarak gerekli tıbbi bakım için ödeme yapamayan kişilere yardım sağlamak amacıyla akciğer hastalığını tahmin etmek için güvenilir bir yöntem oluşturarak topluma daha büyük bir katkı sağlamaktır.

Daha önce, COVID -19 'un diğer viral hastalıklarla benzerlikleri nedeniyle tanımlanması zordu. Bununla birlikte, araştırmacılar X - ışını görüntülerine dayanarak akciğer hastalıklarını doğru bir şekilde sınıflandırabilen derin öğrenme modelleri geliştirmede önemli ilerlemeler kaydetmiştir. Tüberküloz (TB), kronik obstrüktif akciğer hastalığı (KOAH) ve pnömoni gibi akciğer bozukluklarını tahmin etmek için evrişimli sinir ağları (CNN'ler) gibi çeşitli derin öğrenme teknikleri kullanılmıştır. Bu modeller, makine öğrenimi yaklaşımlarını kullanarak görüntülerin sınıflandırılmasında yüksek etkinlik ve performans göstermiştir.

2. Alanyazın Taraması

Babukarthik, R. G., ve diğerleri. [10] and other researchers gave limelight to COVID - 19 Disease as the cases of this disease wer exponentially rising day by day, therefore the need of faster and more economical solution for the medication of COVID -19 was raised, and the prediction by viewing CXR images samples of lung was an urgent issue. Çözüm, etkinliğini hesaplayarak ve VGG16, Squeeze Net, resenet50, Densenet -121 ve resenet18 gibi diğer modellerle karşılaştırarak genetik

Derin Öğrenme CNN üzerinde çalışmaktı. Diğer yöntemlerle karşılaştırma yapıldıktan sonra, analiz performansının sonuçları tatmin edici olmuştur.

Minaee, Shervin ve diğerleri [11] COVID 19 ve dünyanın farklı bölgelerindeki etkilerinden bahsetmiştir. COVID -19 'u tespit etmek, COVID 19 için ilaç bulmanın önemli adımlarından biridir. Teşhis ne kadar hızlı olursa, ilaç uygulaması da o kadar hızlı olur ve daha az Kovid 19 vakası tespit edilir. 5000 'den fazla Göğüs RÖNTGENİ Görüntüsünü içeren veri setini topladılar ve Squeeze Net, DenseNet -12, resNet50 ve resNet18 gibi farklı derin öğrenme modelleriyle test ettiler. Sonuç elde etmek için veri kümesi, yaklaşık 2000 ila 3000 göğüs RÖNTGENİ görüntüsünden oluşan test ve tren veri kümesine ayrılmıştır. Özgüllük oranı % 90, duyarlılık oranı ise % 98 civarında çıkmıştır. Sonuçları elde etmek için deneyin ayrıntılı bir analizi yapıldı. Ağırlıklı olarak aktarılan öğrenme yaklaşımını takip etmişlerdir. Çoğunlukla sınırlı örneklerimiz olduğunda kullanılır. Bu genellikle farklı özelliklerin çıkarılması için yapılır. Veri seti sınırlı olduğundan, tüm özelliği çıkarmak ve daha doğru sonuçlar elde etmek için Konvolüsyonel Sinir Ağının son katmanını ayarladılar. Spesifite, Sensitivite, AUC ve ROC olmak üzere 4 farklı parametreye sahip modelleri kontrol etmişlerdir. Tüm modellerin özgüllüğü ve duyarlılığı % 90 civarında olduğu için bu karşılaştırma oldukça başarılı oldu ve gelecekte daha doğru sonuçlar elde etmek için daha büyük veri kümeleri üzerinde çalışacaklar.

Cohen, Joseph Paul ve diğerleri ve diğer araştırmacılar, [12] erken aşamalarda COVID Tespiti üzerinde çalışmaya karar verdiler çünkü o zamanlar her ülkedeki SICAK NOKTALAR üstel oranda artıyordu. O zaman hiçbir aşılama yapılmadı, bu yüzden bunu tespit etmek ve bu hastalığın ilacı üzerinde çalışmak için büyük bir ihtiyaç ortaya çıktı. Bu, esas olarak farklı ülkelerdeki doktorların COVID'i erken aşamalarda tespit etmelerine yardımcı olmak için yapıldı, böylece sıcak noktalar azaltıldı. Araştırma için veri setlerini oluşturmak için 26 'dan fazla ülkeden göğüs RÖNTGENİ GÖRÜNTÜLERİNİ topladılar. Veri kümesi çok büyük olduğu için önlerinde farklı önyargılar ve sorunlar vardı, bu yüzden bir kıtayı veya bir ülkeyi terk etme tekniğini uyguladılar. Test ve eğitim veri seti için doğru sonuçları elde etmek için farklı ülke veya kıta gruplarını çıkardılar. Esas olarak COVID – 19 'un şiddetini tahmin etmişlerdir. Kullanılan teknik Lojistik Regresyon ve Lineer Regresyon idi. Ardından, 20 'den fazla sonuç içeren Göğüs RÖNTGENİ görüntülerinin ilk veri kümesini oluşturdular.

Panwar, Harsh ve diğerleri ve diğer araştırmacılar, [13] tahmin için makine öğreniminde mevcut olan diğer tekniklerle en başarılı olduğu için çeşitli Derin Öğrenme Teknikleri kullanarak COVID -19 'un Erken Saptanması üzerinde çalışmışlardır. Esas olarak Renk Görselleştirme olan ana yaklaşıma odaklandılar. COVID – 19 tanımalarını, COVID – 19 Hastalığının Göğüs Röntgeni Görüntüleri, COV -2 BT taraması ve pnömoninin göğüs röntgeni görüntüleri adlı 3 veri kümesi izlemiştir. Ayrıca her iki hastalığın semptomları oldukça benzer olduğu için Pnömoni ve COVID – 19 'daki paternleri de tahmin etmişlerdir. Ayrıca, renk Görselleştirme için Grad CAM tabanlı renk görselleştirme tekniğine odaklanmışlardır.

Heidari, Morteza ve diğerleri ve diğer araştırmacılar, [14] bulaşıcı bir hastalık türü olduğu için COVID -19 Hastalığına odaklanmışlardır, bu nedenle bunun tespiti erken aşamalarda çok önemlidir. Ayrıca bu hastalığın yayılmasını mümkün olan en verimli ve etkili şekilde kontrol etmeye yardımcı olacaktır. Burada da GÖĞÜS RÖNTGENİ veri seti tahmin için kullanılır. Bu çalışmada Yeni Cad (Bilgisayar Destekli Teşhis) şemasını test ettiler. Düşündükleri ana sınıflar Pnömoni (Non - COVID), Pnömoni (COVID) ve Normaldir (Non - COVID ve NO Pnömoni). Bu şema modele uygulandıktan sonra, doğruluk yaklaşık % 98 özgüllük ve hassasiyet ile % 94,5 olarak ortaya çıkmaktadır.

Alazab, Moutaz ve diğerleri ve diğer araştırmalar, [15] COVID'e odaklanmıştır çünkü bu hastalık bulaşıcı bir hastalıktır. O dönemde hızla yayılıyordu. Daha doğru sonuçlar elde etmek için 1000 gerçek Göğüs X - Rat Görüntüsü elde ederler. Esas olarak otoregresif entegre hareketli ortalama modeli, peygamber algoritması ve uzun kısa süreli bellek sinir ağı olarak Derin Öğrenme Tekniği ve türlerine odaklanmışlardır. Bundan sonraki 7 gün içinde ölümlerin, iyileşmelerin ve teyitlerin sayısını tahmin ettiler. Tüm Göğüs RÖNTGENİ Görüntülerinin tahmini, Avustralya ve Ürdün gibi kıyı dışı alanlarda yapıldı. Ayrıca, bu modelin daha fazla sayıda bulaşıcının olduğu yerlerde

kullanılabileceğini de bildirmişlerdir. Ölüm tahmini, iyileşen ve doğrulanan vakalar Hindistan, Avustralya ve Ürdün için grafik şeklinde yapıldı.

Tahia Tazin ve diğerleri, [16] röntgen görüntülerinden beyin kanserlerini tanımlamak için CNN olarak da bilinen evrişimli bir sinir ağı kullanılarak yapılan araştırmayı sunuyor. Bu alanda yapılan kapsamlı araştırmaların bir sonucu olarak, sunulan model, bir transfer öğrenme tekniğini kullanırken doğruluğu artırmaya vurgu yapmaktadır. Performans, sınıflandırmaların ne kadar doğru yapıldığına göre değerlendirilmiştir. MobileNetV2 ile % 92 doğruluk, InceptionV3 ile % 91 doğruluk ve VGG19 ile % 88 doğruluk elde edilmiştir. Diğer çeşitli ağlarla karşılaştırıldığında, MobileNetV2 en yüksek doğruluk seviyesini sağlamıştır. Bu doğruluklar, tümörlerin erken tespit edilmesine yardımcı olarak, tedavinin felç veya diğer bozukluklar gibi herhangi bir zararlı fiziksel etkinin başlamasından önce başlamasına izin verir.

Abdelbaki Souid ve arkadaşları, [17] MobileNet V2 modelinin değiştirilmiş bir versiyonunu kullanarak frontal torasik röntgen görüntülerine dayanarak akciğerlerde kategorizasyon ve hastalıkların tanımlanması için bir yöntem sunmuştur. Transfer öğrenimini meta veri kullanımıyla birlikte incelediler ve NIH veritabanını kullandılar. AUC ölçümleri birincil karşılaştırma aracı olarak kullanılmış ve analiz sınıflandırıcılar arasındaki farklılıklara odaklanmıştır. Yazarlar, AUC'yi ortalama 0.81 ve doğruluğun % 90 'ı olarak bulmaktadır. Veri kümesinin yeniden örneklenmesinin modelin performansında önemli bir iyileşme sağladığı sonucuna varmışlardır.

Daha önce de belirtildiği gibi, başta gençler olmak üzere çok sayıda insan covid veya zatürre gibi akciğer hastalıklarından etkileniyor. Bu hastalıklar, uygun tıbbi tesislerin bulunmaması ile birleştirilir. Hastalıktan tam bir iyileşme sağlamak için bu akciğer hastalığının hızlı bir şekilde teşhis edilmesi esastır. En yaygın tanı yöntemi X - ışını taramalarının incelenmesidir; ancak, bu yöntemin doğruluğu radyoloğun yorumlayıcı becerilerine bağlıdır ve radyologlar arasında sıklıkla tartışmalıdır.

Bildiğimiz kadarıyla, ilgili çalışmada daha önce bahsedilen yöntemlerin çoğu, akciğer hastalığının sınıflandırılması için bir genetik algoritma, CNN modeli veya derin öğrenme algoritması geliştirmeye odaklanmıştır. Bununla birlikte, sunulan çalışmanın amacı, düşük güçlü cihazlar için eğitilebilir bir model oluşturmak; akciğer hastalığının sağlam tahmini problemini çözmek; ve kaybolan gradyanlar problemini çözmekti ve bu nedenle bu çalışma uygulandı. Özellikle akciğer hastalığı sınıflandırması için tıbbi görüntü işlemede derin öğrenme modellerinin kullanılması umut verici sonuçlar göstermiştir. Evrişimsel Sinir Ağları (CNN), tıbbi görüntülerde görüntü sınıflandırma, lokalizasyon ve segmentasyon gibi görevlerde başarılı olmuştur. Akciğer hastalıkları söz konusu olduğunda, araştırmacılar göğüs röntgeni görüntülerine dayanarak hastalıkları sınıflandırmak ve tahmin etmek için MobileNet ve DenseNet gibi CNN modellerini kullanmışlardır. Bu modeller, binlerce göğüs röntgeni görüntüsünden oluşan büyük veri kümeleri üzerinde eğitilmiştir.

3. Materyal ve Yöntem

CNN'in görüntüleri çeşitli senaryolarda kategorilere ayırma yeteneği yadsınamaz. Belirli bir veri kümesinin özelliklerine göre performansı artırmak için geliştirilmiş çok sayıda CNN versiyonu vardır. Ayrıca, CNN'ler, sınıflandırma için girdileri hazırlamak için gereken resim hazırlama çabasını otomatikleştirmeyi amaçlamaktadır. İlk olarak, çalışmamızda göğüs röntgeni kategorizasyonu için CNN tabanlı sınıflandırma algoritmalarını benimsiyoruz. Makine öğrenimi algoritmaları son yıllarda büyük ölçüde ilerlemiş olsa da, şu anda kamuya açık birkaç tıbbi görüntü veri kümesi bulunmaktadır. CNN'lerin uçtan uca öğrenme mimarisi, kategorizasyon ve öznitelik çıkarımından sorumludur. CNN'ler havuz oluşturan, tamamen bağlantılı ve evrişimli katmanlara sahiptir. Ağ mimarisinin oluşturulması ve sınıflandırma için yüksek derecede ayırt edilebilir özellik setinin oluşturulması, havuzlama ve evrişim katmanlarının ardışık bir sırayla kullanılmasıyla gerçekleştirilir. Tam bağlantılı katmanlar, kendisinden önce gelen katmanlardan elde edilen özellik setinden yararlanan

bir kategorizasyon performansı gerektirir. CNN model eğitiminde, geleneksel geri yayılım algoritması modelin parametrelerinin önemli bir kısmını değiştirmektedir.

Konvolüsyon işlemi ile üretilen özellik haritasına doğrusal olmayan bir aktivasyon fonksiyonu eklemek için ReLU tekniğini kullanıyoruz. Maksimum havuzlama katmanının amacı, altındaki katmandan getirilen anlamsal olarak uygun özellikleri eşlenik hale getirmektir. Maksimum havuzlama katmanı, önce altındaki katmanı dikdörtgen havuzlama bölgelerine bölerek ve ardından bu bölgelerin her birinin maksimumunu temsil eden değeri belirleyerek aşağı örnekleme işlemini gerçekleştirmekten sorumludur [18].

CNN'lerin son seviyesi, tamamen bağlantılı bir katmanın yanı sıra bir softmax sınıflandırıcısı içerir. Önceki katman ile sınıflandırma katmanı arasında yer alan tamamen bağlantılı katman iletimden sorumludur. Özetle, tamamen bağlı katmanlar üç aşamaya ayrılabilir. Prosedürün ilk aşamasında, konvolüsyon ve havuzlama katmanı sonuçları düzleştirilir ve bir sütun vektörüne dönüştürülür. Bu sütun vektörü, ikinci aşamanın giriş katmanı olarak kullanılacaktır. Bir önceki aşamanın sonuçları, ikinci aşamada özellik analizi için girdi olarak kullanılır ve gerçek etiketleri tahmin etmek için ağırlıklar eklenir. Son adım, sonunda her bir sınıf etiketine uygulanacak tahmin puanlarını seçmektir. Araştırmacılar akciğer hastalıklarını öngörmede çeşitli derin öğrenme modellerinin performansını karşılaştırmışlardır. MobileNet, DenseNet, SqueezeNet, VGG16 ve ResNet gibi modeller, özgüllük, hassasiyet, doğruluk ve alıcı çalışma karakteristiği (ROC) eğrisi altındaki alan gibi metriklere göre değerlendirilmiştir. Bu modeller % 88 ile % 98 arasında değişen yüksek doğruluk oranlarına ulaşmıştır [19].

MobileNet ve DenseNet gibi derin öğrenme modellerinin uygulanmasının, röntgen görüntülerinden akciğer hastalıklarını doğru bir şekilde tahmin etmede başarılı olduğu kanıtlanmıştır. Bu modeller, COVID -19, pnömoni ve akciğer opaklığı dahil olmak üzere hastalıkların erken teşhisinde ve teşhisinde radyologlara ve hekimlere yardımcı olma potansiyeline sahiptir. Tıbbi görüntü işlemede derin öğrenme tekniklerinin kullanılması, radyoloji alanında devrim yaratma ve hasta bakımını iyileştirme potansiyeline sahiptir [20].

4. Sonuçlar ve Tartışma

The prediction results was calculated on the based on numerous variables as Area under ROC (AUC), F1 - score, accuracy, precision, and recall. ROC altındaki alan, tahmin modelinin performansını hesaplamak için kullanılır. İş akışımızı göz önünde bulundurursak, CNN, MobileNet için elde edilen performans matrisi sonucunu ve bu kriterler için önerilen yaklaşımı Tablo 1 'de görmekteyiz. Kesinlik, gerçek pozitif değişken grupları olan tüm doğru pozitif sınıflandırmaların, gerçekten pozitif olması beklenen tüm vakalara oranını dikkate alır. Doğru pozitif tuple sayısının, doğru pozitif olan toplam vaka sayısı içindeki oranı. Hassasiyet ve geri çağırma, F1 olarak belirlenen fonksiyona dahildir.

Elde edilen bu sonucun doğruluğunun karşılaştırılması ve eğitim ve test veri kümesi için grafiksel gösterimi. Önerilen yaklaşımın % 96 ile daha yüksek test doğruluk oranı ve 0.93 ile ROC AUC puanı elde ettik. Doğrulukta, tüm vakalardan tüm gerçek pozitifleri ve tüm gerçek negatifleri içeren tüm doğru sınıflandırmaların oranı. Genellikle 0 ile 1 arasında değişmektedir. Tahminler 1 'e yakınsa, daha fazla tahmin doğrudur.

Kullanılan veri seti için Eğitim ve Doğrulama Doğruluk ve kayıp Grafiği şekil 5 'te gösterilmiştir. Şekilden, sinir ağının her döneminde eğitim ve test kaybının azaldığı açıktır. Eğitim süresi boyunca, doğruluk ve model kaybını hesaplamak için toplam 20 dönem çalıştırılmıştır. Çıkarım aşamasında eğitilmiş model ağırlıklarının kullanılacağı dönemi açıklar.

Test performansının analizi, alıcı çalışma karakteristiği (ROC) aracılığıyla oluşturulmuştur. Doğal CNN yöntemi için bu ROC eğrisi, göğüs röntgeni veri seti görüntülerinden Covid için alanın toplam % 100 'ünü, normal için % 86' sını ve viral pnömoni için % 92 'sini sağlar.

. MobileNet'in bu sonucu, göğüs röntgeni veri setinde olduğu gibi Covid için % 100 bölge, normal için % 90 bölge ve viral pnömoni için % 92 bölge sunmaktadır. ROC eğrisi, duyarlılık ve özgüllük arasında yapılması gereken uzlaşmayı göstermektedir. Sol üst köşeye daha yakın olan eğriler üreten sınıflandırıcılar daha yüksek bir performans seviyesi gösterir.

ROC eğrisi, önerilen yöntemin ROC'sini gösterir. Önerilen bu yöntem ROC eğrisi, kullanılan x - ışını veri setinden Covid için % 100 bölgeyi, normal vaka için % 89 bölgeyi ve viral pnömoni için % 93 bölgeyi göstermektedir. Önerilen yöntem, röntgen görüntüsünün 3 kategorisi arasında Covid ve viral pnömoni vakasını göstermek için yüksek ROC sağlar.

Buna ek olarak, sonuç, DenseNet ve MobileNet yöntemine dayanan önerilen yaklaşımımız ile akciğer hastalığını tanımlamak ve kategorilere ayırmak için bilimsel literatürde son zamanlarda araştırılan diğer dört son teknoloji model arasındaki benzerlikleri ve farklılıkları analiz etmektedir. Bu araştırmada kullanılan veri seti ve metodoloji tabloda gösterilmiştir. Farklı test teknikleri nedeniyle, bu araştırmaların doğruluğu doğrudan karşılaştırılamaz, ancak sunulan istatistikler, önerilen modelimizin doğrulandığını ve diğer modellerle oldukça karşılaştırılabilir sınıflandırma sonuçları ürettiğini açıkça ortaya koymaktadır. Bu durum, bu çalışmaların bildirilen doğruluğunun doğrudan karşılaştırılmasının mümkün olmamasına rağmen geçerlidir.

MobileNet ve DenseNet'in akciğer hastalığını tahmin etme madencilik yeteneğinden yararlanan ve daha yüksek test doğruluk oranı ile sonuçlanan derin yapısı. Sunulan yöntem esas olarak Normal, COVID -19 ve Viral Pnömoni olmak üzere üç enfeksiyon kategorisinin göğüs röntgeni sınıflandırmasına dayanan Evrişim sinir ağını kullanır. Önerilen yaklaşım, MobileNet ve DenseNet yaklaşımının hibrit bir yöntemini kullanarak bu konvolüsyon sinir ağında göğüs röntgeni görüntülerine 8 katman kullandı. Göğüs röntgeni görüntülerinin analizinde test doğruluğu, F1 - skoru, kesinlik, hatırlama ve ROC AUC eğrisi kullanılır. Karşılaştırma araştırmamızda, önerilen yöntem, akciğer hastalığının bilgisayar destekli teşhisi için klinik ortamlarda uygulama potansiyelini destekleyen iyi bir sınıflandırma performansı göstermiştir.

Covid19 - dataset, Chest X - ray (Covid -19 & Pneumonia) ve mevcut araştırma çalışmalarının test doğruluk bulgularını detaylı olarak karşılaştırdık. Özellikle, Covid19 veri setini kullanan önerilen DenseNet tekniği, % 98,04 'lük en yüksek test doğruluğunu elde etti. Bu, Covid19 veri kümesi üzerinde eğitilen DenseNet modelinin, göğüs röntgeni resimlerinden COVID -19 örneklerini belirlemede mevcut araştırma yaklaşımlarından daha iyi performans gösterdiğini göstermektedir.

Akciğer grafisi (Covid -19 & Pnömoni) ile önerilen DenseNet tekniği ile karşılaştırıldığında % 95,80 gibi biraz daha düşük bir test doğruluğu elde edilmiştir. Bu hala saygın bir doğruluk puanı olsa da, Covid19 veri setinin doğruluğundan daha düşüktür. Bu doğruluk eşitsizliği, iki veri kümesi arasındaki veri kalitesi, miktarı veya çeşitliliğindeki farklılıklarla ilgili olabilir. Covid19 veri kümesi, modelin daha iyi genelleme yapmasına olanak tanıyan daha çeşitli ve bilgilendirici görüntüler içerebilir.

Önceki araştırma çalışmalarıyla karşılaştırıldığında, Covid19 veri kümesini kullanan önerilen DenseNet metodolojisi, COVID -19 tespit doğruluğunu artırmada yeni veri kümesinin ve stratejinin önemini göstererek diğerlerini geride bırakmaktadır. Mevcut çalışmalar arasında CT - Scan resimlerine uygulanan Panwar ve ark .' nın Grad CAM yaklaşımı % 95.61 ile en yüksek test doğruluğunu elde ederken, bunu % 94.50 doğrulukla Heidari ve ark .' nın VGG16 modeli yakından takip etmiştir. Gerçek dünyadaki COVID -19 hasta veri setlerinde, Alazab ve ark. bir CNN kullanarak % 94,80 'lik bir doğruluk elde etmiştir. Abdelbaki Souid ve arkadaşları, MobileNet V2 kullanarak göğüs röntgeni görüntülerinde % 90 'lık bir test doğruluğu elde etmişlerdir.

Sonuç olarak, Covid19 veri kümesi ve önerilen DenseNet metodolojisi, COVID -19 tespit doğruluğunda önceki yöntemlerden daha iyi performans göstererek umut verici sonuçlar vermektedir. Veri Kümeleri A ve B arasındaki performans eşitsizlikleri, makine öğrenimi

görevlerinde veri kümesi seçiminin ve kalitesinin önemini vurgulamaktadır. Bu bulgular, göğüs röntgeni görüntülemesini kullanarak COVID -19 tanımlamasını iyileştirmek için devam eden çabaları ilerletmeye yardımcı olmaktadır.

Tezin sonuçları, daha fazla araştırma için potansiyel yönelimlerin tartışılmasıyla birlikte bu bölümde kısaca açıklanmıştır. Bu tezin temel amacı, dijital göğüs röntgeni görüntülerinde Covid 19 hastalığını otomatik olarak tespit etmek için makine öğrenimi ve derin öğrenme tekniklerini kullanmaktır.

Geliştirilmiş test doğruluğu, Mobile Net ve Dense Net'in COVID -19 hastalık tahmini için madencilik yeteneklerinden yararlanan derin yapısının doğrudan bir sonucudur. Göğüs röntgenlerini üç farklı enfeksiyon türüne (Normal, COVID -19 ve Viral Pnömoni) sınıflandırmak için mevcut algoritma büyük ölçüde evrişimli sinir ağlarına dayanmaktadır. Yoğun Ağ yöntemi, göğsün röntgen görüntülerine sekiz katmanlı bir evrişimli sinir ağı uyguladı. Göğüs röntgeni resimlerini test doğruluğu, F1 - skoru, hatırlama, hassasiyet ve ROC AUC eğrisini kullanarak analiz ediyoruz. Önerilen yöntem, karşılaştırma çalışmamızda umut verici bir sınıflandırma performansı gösterdi ve bilgisayar destekli bir akciğer hastalığı tanı aracı olarak klinik ortamlarda kullanım için fizibilitesine güven verdi.

Makine öğrenmesi modelleri kullanılarak COVID -19 tespiti amacıyla, Covid19 veri kümesi ve Göğüs Röntgeni (Covid -19 ve Pnömoni) olmak üzere iki ayrı veri kümesine odaklandık. Bu veri kümelerinin karşılaştırılması, etki alanının sorunları ve beklentileri hakkında yararlı bilgiler sağlar.

Covid19 veri kümesi, % 100 eğitim doğruluğu elde eden tüm modellerin belirttiği gibi daha temel bir senaryoyu tasvir etmiştir. Bu veri kümesi, Dense Net'in % 98,04 'lük bir test doğruluğuyla ortaya çıkmasıyla COVID -19 tespitinde yüksek doğruluk olasılığını göstermiştir. Bununla birlikte, Covid19 veri setinin gerçek dünyadaki klinik ortamların inceliklerini yeterince temsil edemeyebileceğini hatırlamak önemlidir.

Göğüs röntgeni resimlerinden oluşan göğüs röntgeni (Covid -19 & Pnömoni) veri seti, klinik ortamlarda görülen zorluklara yakından benzemektedir. Görüntü kalitesindeki ve diğer özelliklerdeki doğal dalgalanmalar nedeniyle, bu veri kümesi derin öğrenme modelleri için daha zor bir sorun sunmuştur. Testlerimize göre DenseNet, Göğüs Röntgeni (Covid -19 ve Pnömoni) veri setinde sürekli olarak sağlam bir performans sergiledi ve bu da bu sorunlar karşısında dayanıklılığını gösteriyor. Öte yandan, göğüs röntgeni (Covid -19 ve Pnömoni) veri kümesi, gerçek COVID -19 tanımlamasının karmaşıklığını göstererek, modeller arasında daha düşük genel test doğruluklarıyla sonuçlandı.

Her iki veri kümesi arasındaki sayısal bulguların karşılaştırılması, makine öğrenimi modellerinin etkinliğini şekillendirmede veri kalitesinin ve çeşitliliğinin kritik önemini vurgulamaktadır. Covid19 veri kümesi gibi gerçek dünya veri kümeleri, pratik sağlık uygulamalarında iyi performans gösterebilecek modeller oluşturmak için kritik öneme sahiptir. Öte yandan, Göğüs Röntgeni (Covid -19 ve Pnömoni) veri kümesi gibi basitlik veri kümeleri, model yeteneklerini değerlendirmek için yararlı ölçütler olarak hizmet edebilir.

Çalışmada COVID -19 için hatırlama değeri 0.96, viral pnömoni için kesinlik değeri 1 ve normal vaka değeri 0.80 olarak bulunmuştur. Normal F1 - Skoru 0.89, COVID -19 F1 - Skoru 0.98 ve viral pnömoni F1 - Skoru 0.89 'dur. Dens net yöntemi ile 0.94 ROC AUC değeri ve % 98.04 doğruluk elde edilmiştir. Doğruluk ölçüsü, hem gerçek pozitifleri hem de gerçek negatifleri kapsayan doğru sınıflandırmaların toplam vaka sayısına bölünmesidir. Elde edilen sonuçlar, Dense Net yaklaşımının tanı doğruluğu ve göğüs röntgeni resim sınıflandırması açısından native CNN ve Mobile Net yöntemlerinden daha iyi performans gösterdiğini ve üstün tanıma oranlarına sahip olduğunu kanıtlamaktadır. Yüksek Precision ve F1 skoru sayesinde daha az yanlış negatif üretir. COVID negatif olarak yanlış teşhis edilen COVID pozitif bir hastanın diğer hastaları önemli ölçüde enfekte edebileceği göz önüne alındığında, bu enfeksiyonun önlenmesi için çok önemlidir. Eğitilebilir bir

modelin geliştirilmesi ve düşük güçlü cihaz özelliklerinin iyileştirilmesi bu çalışmanın diğer hedefleriydi.

Bu tezde, en önemli göğüs hastalıklarından üçünün (normal (sağlıklı), pnömoni ve Covid -19) otomatik hastalık tanımlaması ve teşhisi dikkate alınmıştır. Bununla birlikte, gelecekte, bu çalışma potansiyel olarak kronik obstrüktif akciğer hastalığı (genellikle KOAH olarak bilinir), astım, ödem, kistik fibroz ve akciğer kanseri gibi diğer birkaç göğüs rahatsızlığına genişletilebilir. Ek olarak, çeşitli özellikler ve sınıflandırıcılar kullanılabilir ve bunların ilgili etkinlik seviyeleri değerlendirilebilir. Önerilen sistemi gerçek zamanlı ortamlarda konuşlandırılabilir hale getirmek için, gerçek zamanlı göğüs röntgeni resimlerinin otomatik tahmini için tek aşamalı derin öğrenme yaklaşımlarının, yani YOLO ve SSD'nin etkinliğini araştırmak için daha fazla araştırma yapılabilir. Gürültülü görüntülerdeki hastalıkları daha iyi teşhis etmek için, gelecekteki araştırmalar diğer model yapılarına ve yeni etiket bağımlılığı mimarilerine bakabilir.

Kaynaklar

1. Kido, S., Hirano, Y. and Hashimoto, N. (2018). *Detection and classification of lung abnormalities by use of convolutional neural network (CNN) and regions with CNN features (R-CNN).* 2018 International Workshop on Advanced Image Technology (IWAIT), Chiang Mai, 1-4.
2. Cozzi, D., Cavigli, E., Moroni, C., Smorchkova, O., Zantonelli, G., Pradella, S. and Miele, V. (2021). Ground-glass opacity (GGO): a review of the differential diagnosis in the era of COVID-19. *Japanese Journal of Radiology*, 39(8), 721-732.
3. Soomro, T. A., Zheng, L., Afifi, A. J., Ali, A., Yin, M. and Gao, J. (2022). Artificial intelligence (AI) for medical imaging to combat coronavirus disease (COVID-19): A detailed review with direction for future research. *Artificial Intelligence Review*, 2, 1-31.
4. Babukarthik, R. G., Adiga, V. A. K., Sambasivam, G., Chandramohan, D. and Amudhavel, J. J. I. A. (2020). Prediction of COVID-19 using genetic deep learning convolutional neural network (GDCNN). *Ieee Access*, 8, 177647-177666.
5. Minaee, S., Kafieh, R., Sonka, M., Yazdani, S. and Soufi, G. J. (2020). Deep-COVID: Predicting COVID-19 from chest X-ray images using deep transfer learning. *Medical Image Analysis*, 65, 101794.
6. Cohen, J. P., Morrison, P., Dao, L., Roth, K., Duong, T. Q. and Ghassemi, M. (2020). Covid-19 image data collection: Prospective predictions are the future. *arXiv preprint arXiv:*2006.11988.
7. Panwar, H., Gupta, P. K., Siddiqui, M. K., Morales-Menendez, R., Bhardwaj, P. and Singh, V. (2020). A deep learning and grad-CAM based color visualization approach for fast detection of COVID-19 cases using chest X-ray and CT-Scan images. *Chaos, Solitons & Fractals*, 140, 110190.
8. Heidari, M., Mirniaharikandehei, S., Khuzani, A. Z., Danala, G., Qiu, Y. and Zheng, B. (2020). Improving the performance of CNN to predict the likelihood of COVID-19 using chest X-ray images with preprocessing algorithms. *International Journal of Medical Informatics*, 144, 104284.
9. Alazab, M., Awajan, A., Mesleh, A., Abraham, A., Jatana, V. and Alhyari, S. (2020). COVID-19 prediction and detection using deep learning. *International Journal of Computer Information Systems and Industrial Management Applications*, 12(7), 168-181.
10. Tazin, T., Sarker, S., Gupta, P., Ayaz, F. I., Islam, S., Monirujjaman Khan, M. and Alshazly, H. (2021). A robust and novel approach for brain tumor classification using convolutional neural network. *Computational Intelligence and Neuroscience*, 2(3), 15-18.
11. Souid, A., Sakli, N. and Sakli, H. (2021). Classification and predictions of lung diseases from chest x-rays using mobilenet v2. *Applied Sciences*, 11(6), 2751.
12. Das, N., Topalovic, M. and Janssens, W. (2018). Artificial intelligence in diagnosis of obstructive lung disease: current status and future potential. *Current Opinion in Pulmonary Medicine*, 24(2), 117-123.

13. Touretzky, D. S., Gardner-McCune, C., Kong, S. C. and Abelson, H. (2022). Artificial intelligence thinking in k-12. *Computational Thinking Education in K-12: Artificial Intelligence Literacy and Physical Computing*, 2, 153-180.
14. Mamdani, M. and Slutsky, A. S. (2021). Artificial intelligence in intensive care medicine. *Intensive Care Medicine*, 47(2), 147-149.
15. Prevedello, L. M., Halabi, S. S., Shih, G., Wu, C. C., Kohli, M. D., Chokshi, F. H. and Flanders, A. E. (2019). Challenges related to artificial intelligence research in medical imaging and the importance of image analysis competitions. *Radiology: Artificial Intelligence*, 1(1), e180031.
16. Han, Z., Jian, M. and Wang, G. G. (2022). ConvUNeXt: An efficient convolution neural network for medical image segmentation. *Knowledge-Based Systems*, 253, 109512.
17. Hosny, A., Parmar, C., Quackenbush, J., Schwartz, L. H. and Aerts, H. J. (2018). Artificial intelligence in radiology. *Nature Reviews Cancer*, 18(8), 500-510.
18. Sunija, A. P., Varun P. Gopi, and Palanisamy, P. (2022). Redundancy reduced depthwise separable convolution for glaucoma classification using OCT images. *Biomedical Signal Processing and Control*, 71, 103192.
19. Khan, Z. Y. and Zhendong, N. (2021). CNN with depthwise separable convolutions and combined kernels for rating prediction. *Expert Systems with Applications*, 170, 114528.
20. Sinha, D. and El-Sharkawy, M. (2019). *Thin mobilenet: An enhanced mobilenet architecture*. 2019 IEEE 10th annual ubiquitous computing, electronics & mobile communication conference (UEMCON). IEEE.

Bilim Kodu : 92432
Anahtar Kelimeler : Covid 19 disease, CAD, makine öğrenimi, ANN, CNN, Max-pooling, tamamen bağlı katman, sınıflandırma.
Sayfa Adedi : 109
Danışman : Doç Dr. Adem Tekerek

ACKNOWLEDGEMENTS

I am elated to share my heartfelt thanks with my beloved parents, my supportive wife, and my amazing children, who have been there for me every step of the way as I worked on this thesis. I am incredibly thankful for the unfaltering support you have given me; your unfaltering belief in me and continual encouragement have been the engine that has propelled me to success. Assoc. Prof. Dr. Adem Tekerek, my respected supervisor, deserves special recognition. Thanks to your outstanding direction, priceless insights, and constant commitment, my thesis was a resounding success. Thanks a lot for all the help you've given me academically; your wisdom and guidance have been invaluable. Everyone on the faculty who has helped me along the way in my master's program has my deepest gratitude. Your dedication to our education and enthusiasm for teaching are extremely motivating. I am grateful for all the time you have spent teaching us new things and giving us the tools we need for our future careers. My good friends have been an incredible source of support and friendship during this journey, and I am eternally grateful to them. I am sincerely appreciative for the companionship and support you have given me during my scholastic journey. You have all played a crucial role in helping me achieve my academic goals, and I am grateful to have such a strong support system. Your presence, encouragement, and motivation have made this academic journey even more rewarding. I am grateful for the memorable moments we shared, the late-night study sessions, and the unwavering support we provided to each other. To everyone who has played a role in my thesis journey, I offer my sincerest appreciation for your invaluable contributions. This achievement would not have been possible without each and every one of you. Thank you all for being an integral part of this milestone in my life.

CONTENTS

Page

ABSTRACT iv

ÖZET v

ACKNOWLEDGEMENTS xvi

CONTENTS xvii

LIST OF TABLES xx

LIST OF FIGURES xxi

SYMBOLS AND ABBREVIATIONS xxiv

1. INTRODUCTION 1

2. LITERATURE REVIEW 9

2.1. Chest X-Ray as a Diagnostic Image 13

2.1.1. Interpretation of chest x-rays 15

2.1.2. Role of chest x-ray in covid 19 disease diagnosis 16

2.1.3. Chest x-ray image datasets 18

2.2. Radiographic Signs and Findings in Chest X-Rays 19

2.2.1. Lung opacities and consolidations 19

2.2.2. Pleural effusion and pneumothorax 19

2.3. Machine Learning Methods 19

2.3.1. Supervised learning 22

2.3.2. Unsupervised learning 23

2.3.3. Reinforcement learning 24

2.4. Deep Learning Methods 25

3. MATERIAL AND METHODS 29

3.1. Research Workflow 29

3.1.1. Stage 1: data collection 30

Page

3.1.2. Stage 2: image preprocessing 31
3.1.3. Step 3: dataset splitting 31
3.1.4. Stage 4: data augmentation 32
3.1.5. Stage 5: feature extraction 32
3.1.6. Stage 6: model training 32
3.1.7. Stage 7: model evaluation 33
3.1.8. Stage 8: prediction on new data 33
3.2. Datasets 33
3.2.1. Covid19-dataset 33
3.2.2. Chest X-ray (Covid-19 & Pneumonia) 36
3.3. Preprocessing Techniques 38
3.4. Feature Extraction Methods 39
3.5. Model Selection 39
3.5.1. Convolutional neural network 39
3.5.2. MobileNet 41
3.5.3. DenseNet 44
3.6. Fitting the Model (Model Setup) 47
3.7. Training and Testing 49
3.8. Performance Criteria 50
3.8.1. Classification confusion matrix 50
3.8.2. F1 Score 51
3.8.3. Accuracy 52
3.8.4. Recall 53
3.8.5. Precision 53
3.8.6. Receiver operation characteristic (ROC) 54
4. PROPOSED METHODOLGY 57

Page

4.1. Classification of Covid 19 Disease Using State of-The-Art Deep Learning Architectures 57

4.2. Proposed Approach 59

4.2.1. Preparation for training model 62

5. RESULTS AND DISCUSSION 63

5.1. Results of Covid19-dataset 63

5.1.1. Result of MobileNet model 63

5.1.2. Result of CNN model 67

5.1.3. Result of DenseNet model 71

5.1.4. Accuracy comparison of CNN, MobileNet and DenseNet 76

5.2. Results of Chest X-ray (Covid-19 & Pneumonia) 77

5.2.1. Results of MobileNet model 77

5.2.2. Result of CNN model 82

5.2.3. Result of Dense Net model 85

5.2.4. Accuracy comparison of CNN, Mobile Net and Dense Net using chest X-ray (Covid-19 & Pneumonia) dataset 90

5.3. Comparison of Covid19-dataset and Chest X-ray (Covid-19 & Pneumonia) dataset results 92

5.4. Comparison of Covid19-dataset and Chest X-ray (Covid-19 & Pneumonia) results with existing researches results 94

6. CONCLUSION 97

6.1. Recommendations for Future Work 98

REFERENCES 101

CURRICULUM VITAE 109

LIST OF TABLES

Table **Page**

Table 2.1. Recent related work of Chest X-ray 12

Table 3.1. Important Parameters 35

Table 3.2. ROC AUC accuracy classification range 55

Table 5.1. Results of the MobileNet performance matrix 63

Table 5.2. Obtained results of performance matrix for CNN 67

Table 5.3. Results of the Densenet Approach's performance matrix 72

Table 5.4. Accuracy results for the CNN, MobileNet, and Densenet methods 76

Table 5.5. Collecting data for the Mobile Net performance matrix from the Chest X-ray (COVID-19 & Pneumonia) dataset 78

Table 5.6. Obtained results of performance matrix for CNN using Chest X-ray (Covid-19 & Pneumonia) dataset 82

Table 5.7. Obtained results of performance matrix for Dense net using Chest X-ray (Covid-19 & Pneumonia) dataset 86

Table 5.8. Obtained results of Accuracy for CNN, MobileNet and Densenet method ... 91

Table 5.9. Comparison of Covid19-dataset and Chest X-ray (Covid-19 & Pneumonia) dataset Results 93

Table 5.10. Comparison of Covid19-dataset and Chest X-ray (Covid-19 & Pneumonia) Results with Existing Researches Results 95

LIST OF FIGURES

Figure **Page**

Figure 1.1. Samples from the dataset: Normal (healthy), pneumonia and COVID-19 .. 7

Figure 2.1. Steps of detection the chest X-ray condition 14

Figure 2.2. Steps of an AI tool to classify chest X-rays 17

Figure 2.3. ML approaches 22

Figure 2.4. Process of Supervised learning 23

Figure 2.5. Indicts of Unsupervised Learnin 24

Figure 2.6. Reinforcement Learning process 25

Figure 3.1. Proposed methodology flow for covid detection 30

Figure 3.2. Training and testing data distribution of Covid19-dataset 35

Figure 3.3. Some Sample Images for Train the model 36

Figure 3.4. Training and testing data distribution of Chest X-ray (Covid-19 & Pneumonia) dataset 38

Figure 3.5. Architecture of used CNN model 40

Figure 3.6. Dense-MobileNet model 42

Figure 3.7. Normal Convolution operation 43

Figure 3.8. Depth Wise Convolution 44

Figure 3.9. Training Process Hyper-parameter 48

Figure 3.10. Confusion matrix 51

Figure 3.11. Receiver operating characteristics 54

Figure 4.1. Convolution neural network architecture 59

Figure 4.2. A flow chart representing the proposed method 61

Figure 5.1. Confusion matrix of MobileNet 64

Figure 5.2. Graph of Obtained results of test accuracy for MobileNet 65

Figure 5.3. Training accuracy and testing accuracy of MobileNet model 65

Figure 5.4. Training loss and testing loss of mobile Net model 66

Figure **Page**

Figure 5.4. ROC curve for MobileNet 66

Figure 5.6. Graph of Obtained results of performance matrix for CNN..... 68

Figure 5.7. Confusion matrix of CNN 69

Figure 5.8. ROC curve for CNN..... 70

Figure 5.9. Training Accuracy and Testing accuracy of CNN model 71

Figure 5.10. Training Loss and Testing Loss of CNN model..... 71

Figure 5.11. Graph of Obtained results of performance matrix for Densenet Approach..... 73

Figure 5.12 Confusion matrix of DenseNet..... 74

Figure 5.13. Training accuracy and testing accuracy of dense Net method 74

Figure 5.14. Training loss and testing loss of dense Net method 75

Figure 5.15. ROC curve for DenseNet method..... 75

Figure 5.16. Graphical representation of obtained result of accuracy 77

Figure 5.17. Graph of Obtained results of test accuracy for MobileNet using Chest X-ray (Covid-19 & Pneumonia) dataset 78

Figure 5.18. ROC curve for MobileNet using Chest X-ray (Covid-19 & Pneumonia) dataset..... 79

Figure 5.19. The MobileNet Model's Confusion Matrix with the Chest X-Ray (COVID-19 and Pneumonia) Dataset 80

Figure 5.20. Training and Testing Accuracy of Model using Chest X-ray (Covid-19 & Pneumonia) dataset 81

Figure 5.21. Training and Testing Loss of Model using Chest X-ray (Covid-19 & Pneumonia) dataset 81

Figure 5.22. Graph of Obtained results of test accuracy for CNN using Chest X-ray (Covid- Pneumonia) dataset..... 82

Figure 5-23. ROC curve for CNN using Chest X-ray (Covid-19 & Pneumonia) dataset..... 83

Figure 5.24. Confusion Matrix of CNN Model using Chest X-ray (Covid-19 & Pneumonia) dataset 84

Figure 5.25. Training and testing accuracy of model using Chest X-ray (Covid-19 & Pneumonia) dataset 85

Figure **Page**

Figure 5.26. Training and testing accuracy of model using Chest X-ray (Covid-19 & Pneumonia) dataset 85

Figure 5.27. Graph of Obtained results of test accuracy for Dense net using Chest X-ray (Covid-19 & Pneumonia) dataset..... 87

Figure 5.28. Graph of Obtained results of test accuracy for Dense net using Chest X-ray (Covid-19 & Pneumonia) dataset..... 87

Figure 5.29. Confusion matrix of densenet model using chest X-ray (Covid-19 & Pneumonia) dataset 88

Figure 5.30. Training and testing accuracy of model using chest X-ray (Covid-19 & Pneumonia) dataset 89

Figure 5.31. Training and testing loss of model using chest X-ray (Covid-19 & Pneumonia) dataset 90

Figure 5.32. Graphical representation of obtained result of accuracy using Chest X-ray (Covid-19 & Pneumonia) dataset..... 92

Figure 5.33. Comparison of Covid19-dataset and Chest X-ray (Covid-19 & Pneumonia) dataset Results..... 93

SYMBOLS AND ABBREVIATIONS

The symbols and abbreviations used in this study are presented below, along with their explanations.

Abbreviations	Explanations
AF	Activation Function
AI	Artificial Intelligence
ANN	Artificial Neural Network
AUC	Area Under ROC
BN	Batch Normalization
BOW	Bag of Words
BP	Back Propagation
BRFSS	Behavioral Risk Factor Surveillance System
CAD	Computer Aided Diagnosis
CLH	Continuous Local Histogram
CNN	Convolutional Neural Networks
COPD	Chronic obstructive pulmonary disease
CT	Computed Tomography
CV	Computer Vision
CXR	Chest X-ray
DBN	Deep Belief Networks
DL	Deep Learning
DNN	Deep Neural Network
FP	False Positive
GA	Genetic Algorithm
GM	Gradient Magnitude Histograms
HENC	Hybrid Evolutionary Neural Network Classifier
HNN	Hopfield Neural Network
MERS	Middle East Respiratory Syndrome
MIAS	Mammographic Image Analysis Society
NN	Neural Networks

Abbreviations	Explanations
MRA	Magnetic Resonance Angiography
MSNN	Multistage Neural Network
PCA	Principal Component Analysis
PET	Positron Emission Tomography
PNN	Probabilistic Neural Network
ReLU	Rectified Liner Unit
ROC	Receiver Operating Characteristic
SARS	Severe Acute Respiratory Syndrome
TB	Tuberculosis
TP	True Positive
VGG	Visual Geometric Group
MRI	Magnetic Resonance Imaging

1. INTRODUCTION

The lungs and respiratory system of a human being take in oxygen from the surrounding air and exhale carbon dioxide. The lungs are susceptible to a broad variety of conditions, some of which can be inherited, while others can be caused by poor habits, an unhealthy diet, or even infections. But COVID-19 is a relatively new illness [1], and researchers are always gaining new information regarding the effects it might have on a person's lungs. They believe the effects on the human body are akin to those caused by two other coronavirus infections, severe acute respiratory syndrome (SARS) and Middle East Respiratory Syndrome (MERS) [2]. Radiology is the specialty that is responsible for determining the pattern, location, and geographical distribution of involvement in the process of diagnosing human lung illness [3]. When diagnosing Covid 19 disease, clinicians may assess the lungs' ability to hold, transport, and exchange oxygen and carbon dioxide. Pulmonary function tests determine the type and severity of lung disease. Chest imaging, bronchoscopy, and thoracoscopy help doctors diagnose lung illnesses [4].

Numerous people have been impacted by various kinds of the Covid-19 sickness all around the world. Notably, lung diseases caused by the virus make the lungs more vulnerable to further physical difficulties and the negative effects of air pollution [5]. Given the infectious nature of Covid-19, this reduces lung function, emphasizing the significance of accurate diagnosis in order to offer the most effective medication. Radiologists play an important part in this diagnostic procedure, using chest X-rays as the primary diagnostic tool to discover and diagnose various lung disorders. Aside from Covid-19, these expert individuals may detect a wide range of illnesses, such as bronchitis, infiltrations, atelectasis, pericarditis, fractures, and many more [6]. Surprisingly, over 2 million chest radiography treatments are performed each year, making it the most extensively used disease examination in the globe.

Given the overlapping symptoms of Covid-19 with other viral infections such as pneumonia and lung opacity, it became critical to reliably separate individual diseases. As a result, they were divided into groups such as COVID, Pneumonia, Lung opacity, and Normal [7]. The intricacy of Covid-19 disease pictures makes detecting and identifying disease features in X-rays difficult [8]. Previously, effective development was hampered by the complexity of these images, as well as the difficulty in analyzing situations and disorder illnesses in X-ray images [9].

Deep learning algorithms have evolved as promising tools for diagnosing lung disorders in response to these challenges. Several studies have been conducted to investigate Covid-19 illness prediction using various deep learning algorithms. These advances have led to the identification of other lung ailments such as tuberculosis (TB), chronic obstructive pulmonary disease (COPD), and pneumonia, which are now being included into neural networks for cancer diagnosis [10]. Deep learning application in this context provides a big step toward improving the accuracy and efficiency of illness diagnosis in lung imaging.

A chest x-ray of the patient is often checked after the doctor has finished gathering the history of a patient disease and performing the physical checkup. The findings from the patient's medical history, physical checkup, and chest x-ray can frequently provide clues as to what other diagnostic procedures may be required in order to establish the root cause of the symptoms. Images of heart, lungs, blood arteries, and airways, as well as the bones in chest and spine, can be seen on an X-ray of chest. X-rays of the chest can also reveal the presence of fluid in or around human lungs as well as air around a lung [11].

The most common symptom that prompts patients to seek medical attention and attend emergency rooms is chest pain. Chest radiography, which is more commonly referred to as a chest X-ray (or CXR for short), is one of the most popular forms of radiology examinations used for the identification of disorders affecting the thorax. Nevertheless, radiography entails making decisions under situations of uncertainty, and as a result, it is not always possible to provide interpretations or reports that are completely foolproof [12]. Computer-Aided Diagnosis, also known as CAD, was created for this purpose, to help radiologists achieve diagnostic excellence in less time and to improve the quality of healthcare for patients. The goal of CAD systems is not to compete with or replace medical experts; rather, they are meant to serve as a "second opinion" that supplements radiologists' work [13].

Radiographs, CT scans, MRIs, nuclear medicine, PET scans, fusion imaging, ultrasound, and other medical imaging techniques are all part of imaging, which is the study and practice of medical imaging for the purpose of detecting and treating injuries and illnesses. A radiologist is an expert in the branch of medicine known as radiology, which focuses on imaging [14]. A number of these procedures also need you to be aware about radiation safety since some of these imaging modalities employ radiation and you need training to understand how to protect yourself from radiation [15]. Techniques that utilize Artificial

Intelligence (AI) and Computer Vision (CV) have garnered a significant amount of interest and focus over the last decade, and it is anticipated that this trend will carry on. Classification of medical images is one of the fundamental challenges as well as the typical duty [16]. The purpose of the categorization procedure is to determine whether a medical image should be assigned a single or several diagnostic outcomes based on the content of the image. In this regard, a significant amount of work has been put into the development of more complex classification approaches and methodologies in order to enhance the accuracy of categorization.

Initially, a two-step process was used to resolve the picture classification issue. The first stage's objective is to manually extract features from an image using feature descriptors, whereas the second stage's objective is to feed the manually extracted features into a trainable classifier [17]. However, the technology employed for feature extraction in the first step has a significant impact on how accurate this technique is. Since deep learning provides automatic feature extraction and classification by modeling data through several non-linear processing layers, it was examined as a means of achieving the aim of picture classification.

These days, clinical imaging incorporates more and more elements from a wide range of tests, one of which is artificial intelligence [18]. These components are commonly used in many studies, including deep learning, fuzzy sets, rough sets, dubious analysis, multi-target advancement, swarm knowledge improvement, and machine learning [19]. Patients are surveyed according to their clinical groups using the delayed test results as a point of reference. Tools for personalized infection evaluation with AI models are improved in another test of computer-based intelligence-driven arrangements by utilizing their ability to find patterns and connections in clinical photos using large numbers of clinical pictures. This is accomplished with the use of clinical pictures [20]. Frequently employed by convolutional neural networks.

Radiologists and doctors will soon have new tools thanks to the combined work of specialists from many disciplines. Radiology and medical image processing have seen extensive testing of various AI algorithms in an effort to identify the best effective network. Convolutional Neural Networks (CNN) have demonstrated great potential in medical image processing for tasks such as segmentation, localization, and classification. Because of this, we are working

on a ground-breaking method for COVID-19 illness prediction using chest x-ray images and deep learning AI technologies. [21].

Problem statement

Abnormalities of the lungs can result in death; hence, early detection and treatment in a timely manner can save lives and prevent loss of life. Patients who suffer from lung problems can be categorized as a significant public health issue. A number of manual examinations are required for the typical diagnostic procedures for lung disorders. This human interception takes a lot of time, is extremely error prone, and the procedures used do not always guarantee a high level of accuracy. Therefore, automated methods are of the utmost importance for actual applications in the field of ophthalmology. The majority of these automated technologies rely on digital image analysis to diagnose diseases. The method of image classification is important in diagnosis. In this process, a variety of aberrant images are organized into a number of categories based on various similarity measurements.

A challenge lies in the fact that these automated categorization systems need to produce high accuracy in a short amount of time. In addition, automatic screenings require a minimum of two potential end points in order to have an impact while validating diseases. The process of collecting standard annotated references is rather time consuming. Creating referable repositories for algorithms is another issue that has grown challenging as a result of the complications involved in gathering images, providing the requisite annotations, and preparing the data for broad usage. The obsolescence of imaging devices shortens the lifespan of a dataset, which presents a challenge because the outdated references require revision in order to be compatible with the most recent equipment or resolutions. Images of the lungs need to be preprocessed because there may be noise in them.

Training data sets [22], that contain several images take up a significant amount of time and are slow when compared to others. One of the most challenging jobs in chest x-ray image processing is the segmentation of needed sections in images that contain non-trivial content. They also bring to our attention the fact that the precision of the segmentation ultimately determines whether or not the computerized analysis techniques are successful for determining the lung disease. Because of this, effective segmentation might become problematic.

Motivation and importance of the study

The rate at which the world is experiencing change is so rapid that it is putting an increasing amount of stress on people's health. Unfavorable shifts in climate, the environment, and the way people live their lives all contribute to an increase in the incidence of disease among humans. One of the organs that are adversely impacted is the lung. Develop an efficient contactless diagnosis and decision support system that makes use of applied intelligence in order to cut down on the mortality rate that is caused by COVID-19. This can be accomplished by improving the accuracy of early detection as well as the severity levels of people infected with the corona virus. To acquire a better knowledge of illness progression, significant medical and technological advancement in image preprocessing, segmentation, and classification of COVID-19 pictures is still required.

One of the main causes of death on a global scale, pneumonia poses a serious threat to human life. An estimated 1.4 million children worldwide succumb to pneumonia annually, highlighting the devastating impact on this vulnerable population. Surprisingly, 18% of this concerning figure is attributed to youngsters younger than five years old. To better understand the scope of respiratory sickness, researchers analyzed data from the Behavioral Risk Factor Surveillance System (BRFSS) 2020 survey. In twenty-nine states plus DC, the poll indicated that 9.2% of adults and 7.5% of children had asthma in the given survey period. In addition, chronic lung disorders affected 34.8 million Americans, or 13.7% of the population.

It takes work to learn how common asthma and chronic COVID-19 illness are in a given area among adults. We achieve this by comparing the 2020 BRFSS state prevalence rates by age group with the Chronic Disease Prevention and Health Promotion website's age-specific resident populations at the county level [22]. This method yields a thorough assessment of adult asthma and chronic Covid-19 illness prevalence in the local area, providing useful insights into the health landscape. So, considering this pandemic situation and current scenario, it is a good time to contribute to the solution of above mention problem given the power of computers as well as the substantial amount of data that is currently being made available to the general public. The objective is to provide a greater contribution to the community by creating a reliable method for predicting lung disease, with the goal of

lowering medical costs and providing assistance to people who are unable to pay for necessary medical care using deep learning methods.

Objective of research

The objective of the research work is to develop “A Deep Learning based Prediction model for Covid 19 disease by using Chest X-ray Images on DenseNet and MobileNet”. To identify the presence of as Covid, normal and viral Pneumonia in Chest X-rays pictures employing the image padding technique with deep learning approach.

The research's specific aims include as follows:

- To introduce and give the differences between different deep learning techniques used for Covid 19 disease detection.
- To compare the various deep learning methods for better accuracy
  - To implement a dynamic feature propagation recommended for improving the performance of native CNN models for Covid 19 illness classification using the Mobile Net and Dense Net.
  - To compute a performance matrix based on five assessment metrics: accuracy, precision, recall, f1-score, and AUC.
  - Use the best architecture to detect Covid 19 disease in three categories: Covid, normal, and viral Pneumonia.
  - The results of the suggested model were contrasted with those of a Mobile Net approach and a native CNN methodology. The results showed that the suggested model outperformed the native methods, suggesting that the strategy can be applied in real-world scenarios.

Research methodology

The present research aims at doing and implementing a Novel Approach for Prediction of Covid 19 disease Using Chest X-ray Images based on Dense Net and Mobile Net system to critically evaluate any abnormality in the lung region. The proposed research will contribute to medical science and deep learning area in a significant manner. The system is implemented using a specific set of deep learning technologies.

Python programming, with Anaconda Spyder development tool for debugging, is used to construct the proposed framework. Chest X-ray (Covid-19 & Pneumonia dataset) is the source of the data set that is being considered from the Kaggle public repository. It is made up of pictures that were gathered from several websites' data repositories, including GitHub, Kaggle, Radiohelia, and the Italian Society of Radiology (SIRM) and Fig share is also included. The dataset is arranged in two directories named "train" and "test," and each of these two folders contains three subfolders (COVID19, PNEUMONIA, and NORMAL) [22, 109]. The During the experiment, a total of 6,939 samples were utilized, with each group utilizing 2,313 each class. Some examples of images used are presented in Figure 1.1.

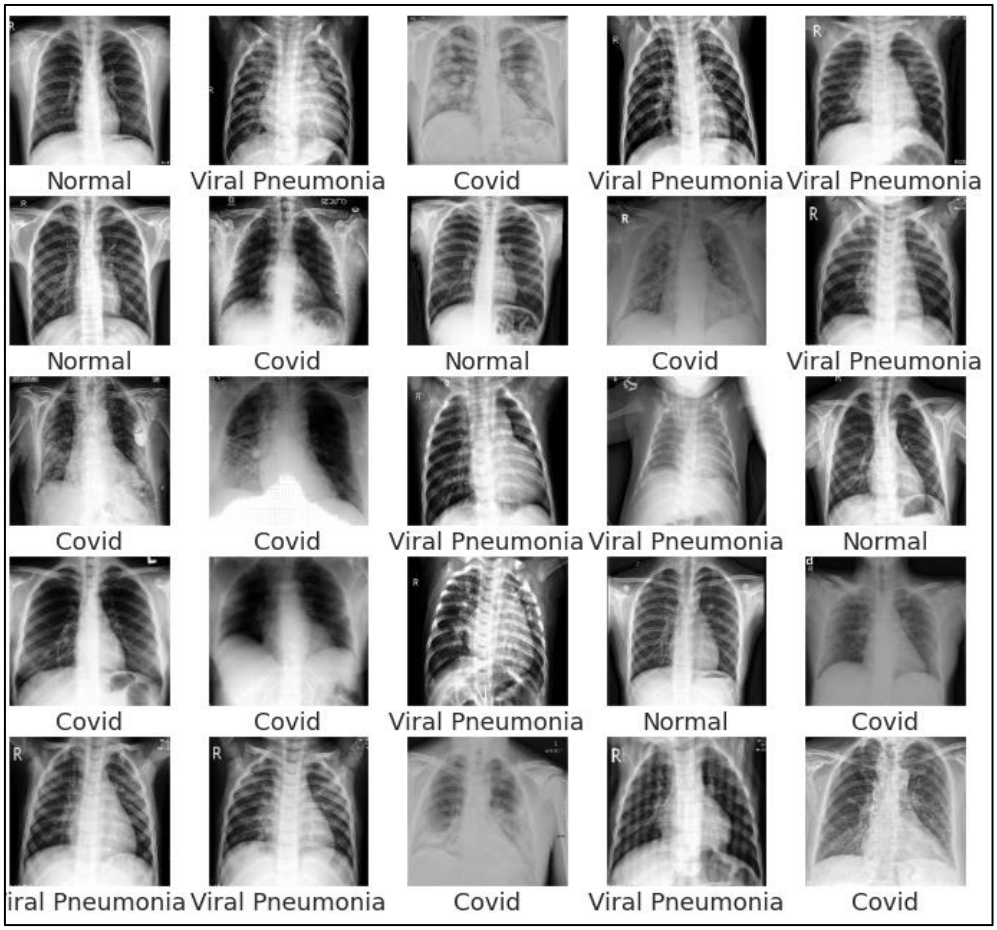


Figure 1.1. Samples from the dataset: Normal (healthy), pneumonia and COVID-19

Scope of the thesis

As part of this investigation, a classification strategy that makes use of neural networks is offered as a potential method for determining the presence of Covid 19 disease i.e., Normal

(healthy), pneumonia and COVID-19 based on chest X-ray images. Using a use case Mobile Net and Dense net model of neural network, this research study was carried out to evaluate the chest X-ray images. The chest X-ray images dataset can be used to categories and forecast lung ailments using the method that has been proposed.

2. LITERATURE REVIEW

Deep learning approaches have proven to be incredibly effective, with many machine learning techniques demonstrating remarkable performance in image categorization. Notably, similar methods are now being used to automate the detection of a variety of disorders [23, 24]. The phrase "machine learning" refers to models that can learn and make intelligent decisions based on large datasets. Speech recognition, translation, and visual perception are just a few examples of the kinds of jobs that deep learning can do with computations and predictions [25, 26]. To better assist doctors and radiologists in their work, researchers are combining their resources. Finding the best network for medical image processing and radiography has involved looking into a number of AI methods [27]. When it comes to medical image processing, CNN have really stood out, particularly for their exceptional performance in picture segmentation, localization, and classification [28].

The primary goal of this chapter is to provide a comprehensive review of the literature, providing a general overview of chest X-ray examinations and the wide range of deep learning and machine learning approaches used in this study for the automatic screening and diagnosis of Covid-19 disease in chest X-rays. Researchers, like Babukarthik et al. [29], have drawn attention to the growing number of COVID-19 cases, underlining the critical need for speedier and more cost-effective treatment options. Their research focuses on predicting whether a person has COVID-19 by studying chest X-ray pictures. They test its fitness and compare it to other models such as VGG16, SqueezeNet, ResNet50, DenseNet-121, and ResNet18 using Genetic Deep Learning CNN. Based on their analytical findings, their model emerged as a top performer after a thorough comparison.

Minaee, Shervin, et al. [30] investigated the global impact of COVID-19 and emphasized the vital role of early identification in its effective treatment. Recognizing the importance of early detection, which leads to faster treatment and fewer cases, the team selected a dataset of over 5000 Chest X-ray pictures. SqueezeNet, DenseNet-12, ResNet50, and ResNet18 deep learning models were subjected to extensive testing.

To optimize results, the dataset was rigorously separated into test and train sets, each including around 2000 and 3000 chest X-ray pictures. Their methods produced an impressive specificity rate of roughly 90% and a sensitivity rate of around 98%. Using a

rigorous study, the researchers primarily used a transferred learning strategy, which is very useful when working with small samples. Given the dataset limits, they fine-tuned the Convolutional Neural Network's final layer for feature extraction, improving result accuracy. Model evaluation included four essential parameters—Specificity, Sensitivity, AUC, and ROC—and all models indicated a remarkable specificity and sensitivity of approximately 90%, laying the groundwork for future efforts on larger datasets.

Cohen, Joseph Paul, et al. [31] and colleagues embarked on early-stage COVID detection, recognizing the world's rising hotspots. In the absence of immunizations, the need to detect and address illness progression became critical. To create a complete research dataset, chest X-ray pictures were obtained from over 26 countries, necessitating the use of methods such as leaving out entire continents or countries to reduce biases. To predict the severity of COVID-19, Logistic Regression and Linear Regression approaches were used, resulting in the production of a robust dataset with over 20 outcomes.

Using a number of well-known deep learning techniques with strong predictive capabilities, Panwar, et al. [32] and their study cohort focused on COVID-19 early detection. Color visualization was their main forte, and they utilized three crucial datasets for it: COVID-19 chest X-ray images, COV-2 CT-scan, and pneumonia chest X-ray images. Researchers painstakingly studied patterns in pneumonia and COVID-19 since the diseases' symptoms are so same. A color visualization tool based on Grad CAM was utilized to enhance the data' interpretability.

Heidari, Morteza, and colleagues [33] focused their attention on COVID-19 disease, noting its infectious nature and the vital need of early identification. The emphasis on early detection not only aids in efficient therapy but also plays a critical role in illness control. They used a chest X-ray dataset to forecast cases of pneumonia, COVID, and normal, and they developed a new computer-aided diagnosis (CAD) system to sort images into these three categories. With sensitivity and specificity close to 98%, the system attained an impressive 94.5% accuracy.

Alazab, Moutaz, and colleagues [34] focused their efforts on the quick propagation of COVID, employing 1000 actual Chest X-RAY Images for more precise results. Predictions were made using Deep Learning Techniques such the prophet algorithm, long short-term

memory neural network, and autoregressive integrated moving average model. Their main focus was on estimating the casualties, cases of recovery, and confirmations for the following seven days, with a special emphasis on non-coastal regions like Jordan and Australia. The model was helpful in regions with high infection rates; it showed visual predictions for India, and Australia.

Tahia Tazin et al. [35] revealed findings from a study that used a convolutional neural network (CNN) to detect brain cancers from X-ray pictures. The study focused on improving accuracy through the use of a transfer learning technique. MobileNetV2 had the highest accuracy (92%), InceptionV3 had 91%, and VGG19 had 88%. These exact classifications aid in early cancer detection, allowing for timely treatment and avoiding negative physical consequences.

Using an adjusted version of the MobileNetV2 model, Abdelbaki Souid et al. [36] developed a method for categorizing and diagnosing illnesses in the lungs based on frontal thoracic X-ray images. The NIH database was used to investigate transfer learning and metadata leveraging. The study produced an average AUC of 0.81 and a 90% accuracy, highlighting the importance of dataset resampling in improving model performance. Given the prevalence of COVID-19 and related respiratory diseases, a precise and timely diagnosis is critical. X-ray scans are a prominent diagnostic technique; nevertheless, their accuracy is dependent on radiologists' interpretation skills, which can be a source of controversy among them.

The suggested work took a different approach than previous methods in the field, which mostly used genetic algorithms, convolutional neural network (CNN) models, or deep learning algorithms to classify COVID-19 illnesses. The goals of the project were to solve the issues of robust lung disease prediction and fading gradients, as well as to construct a trainable model for low-power devices. You can find a summary of the latest relevant work, the approaches used, and the corresponding accuracy in Table 2.1.

Table 2.1. Recent related work of Chest X-ray

Study	Approach	Dataset	Results
[37]	Convolutional Neural Network	NIH Chest X-ray Dataset	Accuracy: 88.2% Precision: 89.6%, Recall: 84.4% F1-score: 0.90 Area Under ROC Curve (AUC): 0.92
[38]	Transfer Learning	CheXpert Dataset	Accuracy: 93.2% Precision: 93.2%, Recall: 90.4% F1-score: 0.95 Area Under ROC Curve (AUC): 0.92
[39]	Generative Adversarial Networks	Kaggle Chest X-ray Dataset	Accuracy: 89% Precision: 85.6%, Recall: 82.4% F1-score: 0.86 Area Under ROC Curve (AUC): 0.89
[40]	Attention Mechanism	ChestX-ray14 Dataset	Accuracy: 92.5% Precision: 90%, Recall: 94% F1-score: 0.95 Area Under ROC Curve (AUC): 0.94
[41]	Ensemble Methods	RSNA Pneumonia Detection Challenge Dataset	Accuracy: 88.6% Precision: 86.6%, Recall: 84.4% F1-score: 0.85 Area Under ROC Curve (AUC): 0.92
[42]	Convolutional Neural Network	MIMIC-CXR Dataset	Accuracy: 90% Precision: 87%, Recall: 92%, F1-Score: 89% Curve (AUC): 0.90
[43]	Transfer Learning	ChestX-ray14 Dataset	Accuracy: 94.5% Precision: 93%, Recall: 94% F1-score: 0.96 Accuracy: 92% Precision: 91%, Recall: 93% F1-score: 0.94 AUC: 0.93
[44]	Convolutional Neural Network	Shenzhen Hospital Dataset	Accuracy: 94.1% Precision: 95%, Recall: 96% F1-score: 0.93 AUC: 0.91
[45]	Transfer Learning	ChestX-ray8 Dataset	Accuracy: 90% Precision: 94%, Recall: 91% F1-score: 0.93 AUC: 0.935

2.1. Chest X-Ray as a Diagnostic Image

Chest X-ray imaging is a cornerstone in medical diagnostics, serving an important role in the detection and monitoring of a variety of lung disorders. This imaging technique uses X-ray radiation to produce comprehensive images of the chest, providing essential insight into the structures and any anomalies within the thoracic cavity [46].

A chest X-ray process involves the patient standing or sitting in front of an X-ray machine. The photons from the X-ray are subsequently directed through the body, interacting with the tissues they come into contact with. The X-ray machine consists of an X-ray tube that emits a precisely controlled number of X-rays and a detector that collects the radiation transmitted through the body. The X-ray beam is focused into the patient's chest, and the image is created as X-ray photons undergo differential attenuation, which is impacted by the variable density and composition of encountered tissues.

This method of diagnosis is especially useful in analyzing illnesses such as pneumonia, lung cancer, tuberculosis, and other pulmonary ailments. Chest X-ray imaging assists healthcare personnel in identifying anomalies, determining the extent of injury or infection, and guiding treatment options by allowing them to examine internal structures. Its broad use extends to emergency situations where rapid assessments of respiratory problems are crucial, and it is commonly incorporated into standard medical examinations.

While chest X-ray imaging provides quick, non-invasive results, it is critical to recognize ionizing radiation exposure. Despite the low doses, healthcare providers follow established safety standards to reduce radiation exposure while prioritizing patient well-being. The advantages of this imaging technology, such as its efficiency and non-invasiveness, frequently exceed the hazards, particularly in urgent diagnostic situations.

Through the incorporation of digital radiography, technological improvements have further refined chest X-ray imaging. This advancement allows for faster image acquisition, higher image quality, and more convenient digital image storage and retrieval. The move to digital platforms improves diagnostic interpretation and seamless exchange among healthcare providers. The detector records the transmitted X-ray photons, producing a grayscale image that represents the variations in X-ray intensity [47]. The resulting chest X-ray image

provides visual information about the bones, lungs, heart, and other thoracic structures. These images are typically viewed and interpreted by radiologists or other medical professionals to identify signs of abnormalities or diseases. The interpretation of chest X-ray images requires expertise and knowledge of anatomical structures and pathological patterns. Radiologists examine the pictures for Covid 19 disease signs such as lung opacities, consolidations, nodules, pleural effusion, and other abnormalities. They assess the size, location, shape, and characteristics of the observed structures to arrive at a diagnosis or recommend further investigations [48].

Despite the widespread use of chest X-ray imaging, it is important to recognize its limitations. Chest X-rays provide a two-dimensional projection of the thoracic cavity, which can sometimes result in overlapping structures and reduced spatial resolution. Additionally, certain conditions or abnormalities may be subtle or difficult to detect on a chest X-ray, necessitating further imaging modalities like computed tomography (CT) or magnetic resonance imaging (MRI) for a more detailed evaluation.

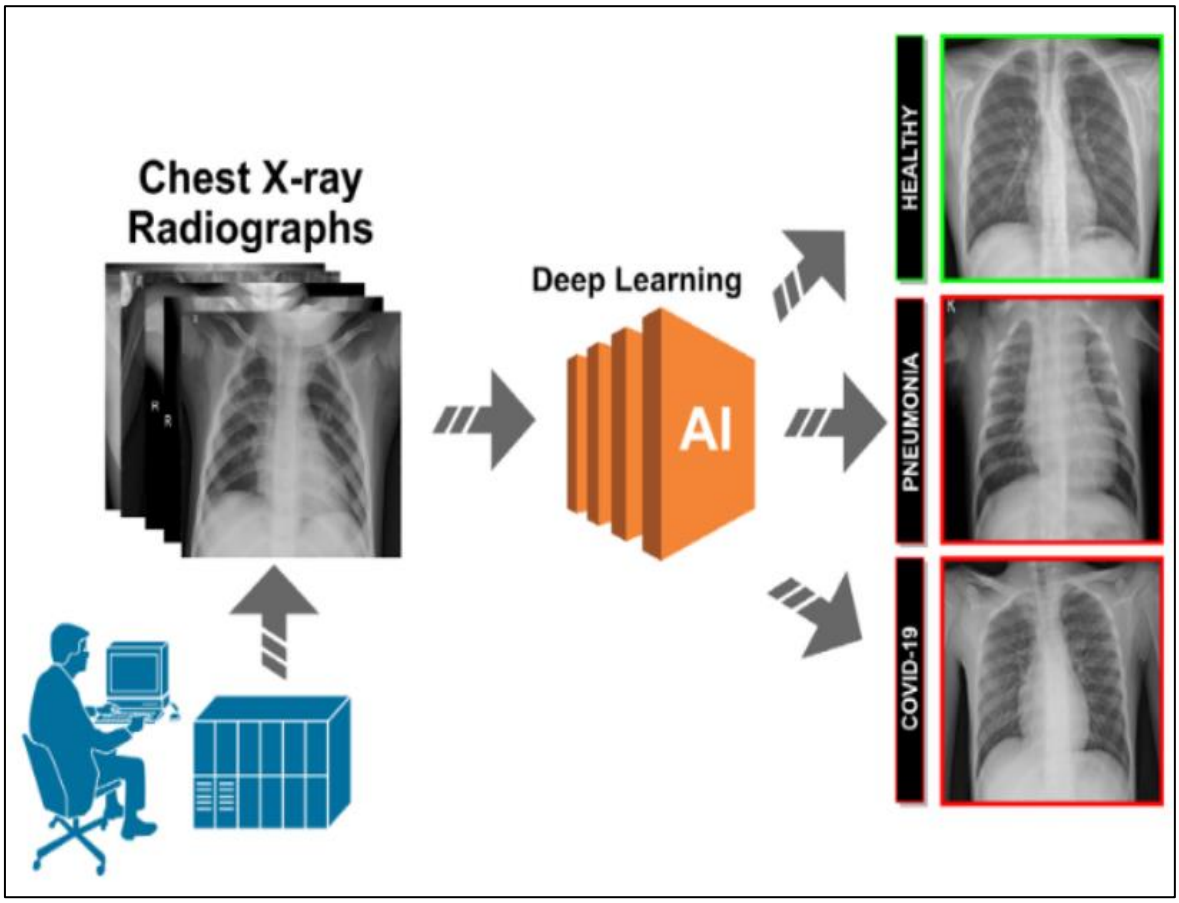


Figure 2.1. Steps of detection the chest X-ray condition [49]

2.1.1. Interpretation of chest x-rays

Interpretation of chest X-rays plays a crucial role in diagnosing Covid 19 disease and assessing thoracic abnormalities. Radiologists and medical professionals carefully analyze chest X-ray images to identify and interpret various anatomical structures and signs of potential diseases. Understanding the key features and abnormalities observed in chest X-rays is essential for accurate diagnosis and appropriate patient management [50]. Chest X-ray images provide valuable information about the lungs, heart, bones, and other thoracic structures. Radiologists examine these images to evaluate the overall quality, positioning, and technical factors affecting image clarity. They look for specific anatomical landmarks and structures, such as the ribs, clavicles, scapulae, and spine, which provide reference points for orientation and localization of abnormalities. Radiologists focus on identifying abnormalities or signs of diseases in chest X-ray images [51]. These abnormalities can include lung opacities, pleural effusion, nodules, consolidations, pneumothorax, and cardiomegaly, among others. Understanding the appearance and characteristics of these findings helps in formulating a diagnosis. For instance, lung opacities refer to areas of increased density or haziness in the lung fields. They can indicate various conditions such as pneumonia, lung infiltrates, or tumors. Radiologists assess the size, distribution, shape, and density of these opacities to differentiate between different pathologies. Pleural effusion, on the other hand, refers to an abnormal collection of fluid in the pleural space surrounding the lungs. It appears as a blunting or haziness of the costophrenic angles or as a meniscus-shaped density on the X-ray image [52]. Radiologists evaluate the amount, location, and characteristics of the effusion to determine its etiology, such as infection, malignancy, or heart failure. Nodules, which are small rounded opacities in the lung fields, can be benign or malignant. Radiologists assess the size, shape, margins, and calcification patterns of nodules to determine their likelihood of being cancerous. The location and presence of associated features, such as lymphadenopathy or metastases, are also important considerations in the interpretation. To interpret chest X-rays accurately, radiologists rely on their expertise, experience, and knowledge of specific disease patterns. They compare the observed findings with normal anatomy and pathological manifestations to arrive at a diagnosis or recommend further investigations, such as additional imaging tests or interventions [53].

It is important to note that the interpretation of chest X-rays can be challenging and subjective, and it requires ongoing education and training to maintain proficiency. Radiologists often collaborate with other specialists, such as pulmonologists or thoracic surgeons, to ensure comprehensive and accurate diagnoses.

2.1.2. Role of chest x-ray in covid 19 disease diagnosis

When it comes to diagnosing and evaluating different types of COVID-19 disease, chest X-ray imaging is crucial. In addition to revealing important details about the lungs, it aids in the detection of anomalies that might point to pulmonary diseases [54]. For efficient patient management and treatment, it is crucial to understand the role of chest X-ray in COVID-19 illness diagnosis. Because of their widespread availability, low cost, and capacity to offer a bird's-eye perspective of the chest, chest X-rays are frequently utilized as the principal imaging modality for assessing COVID-19 disease. Infections, tumors, inflammations, and structural abnormalities are just few of the many lung diseases that they can help detect and evaluate. It is common practice to begin imaging with chest X-rays for diagnosing lung illnesses like pneumonia. They have the ability to show where the lung parenchyma has consolidated, which shows up as localized opacities. In order to establish the degree and severity of the infection, radiologists evaluate the size, position, and distribution of these opacities [55].

Additionally, chest X-rays can help differentiate between bacterial, viral, and fungal pneumonias based on certain radiographic patterns. Chest X-rays also play a critical role in the detection and evaluation of lung tumors. They can reveal suspicious nodules or masses, indicating the presence of lung cancer or metastatic lesions. Radiologists analyze the size, shape, margins, and location of these abnormalities to determine the likelihood of malignancy. Furthermore, chest X-rays may show signs of advanced lung cancer, such as lung collapse, pleural effusion, or lymphadenopathy, aiding in staging and treatment planning. In addition to infections and tumors, chest X-rays assist in diagnosing other Covid 19 disease. For instance, they can reveal signs of chronic obstructive pulmonary disease (COPD), such as hyperinflation, flattened diaphragms, and bullae. They can also show characteristic findings of interstitial Covid 19 disease, including reticular or nodular opacities, honeycombing, or ground-glass opacities. It is important to note that while chest X-rays provide valuable information, they have limitations. The two-dimensional nature of

chest X-rays can result in overlapping structures and reduced sensitivity in detecting subtle abnormalities. In cases where further evaluation is required or when detailed anatomical information is needed, additional imaging modalities like computed tomography (CT) or magnetic resonance imaging (MRI) may be necessary [56].

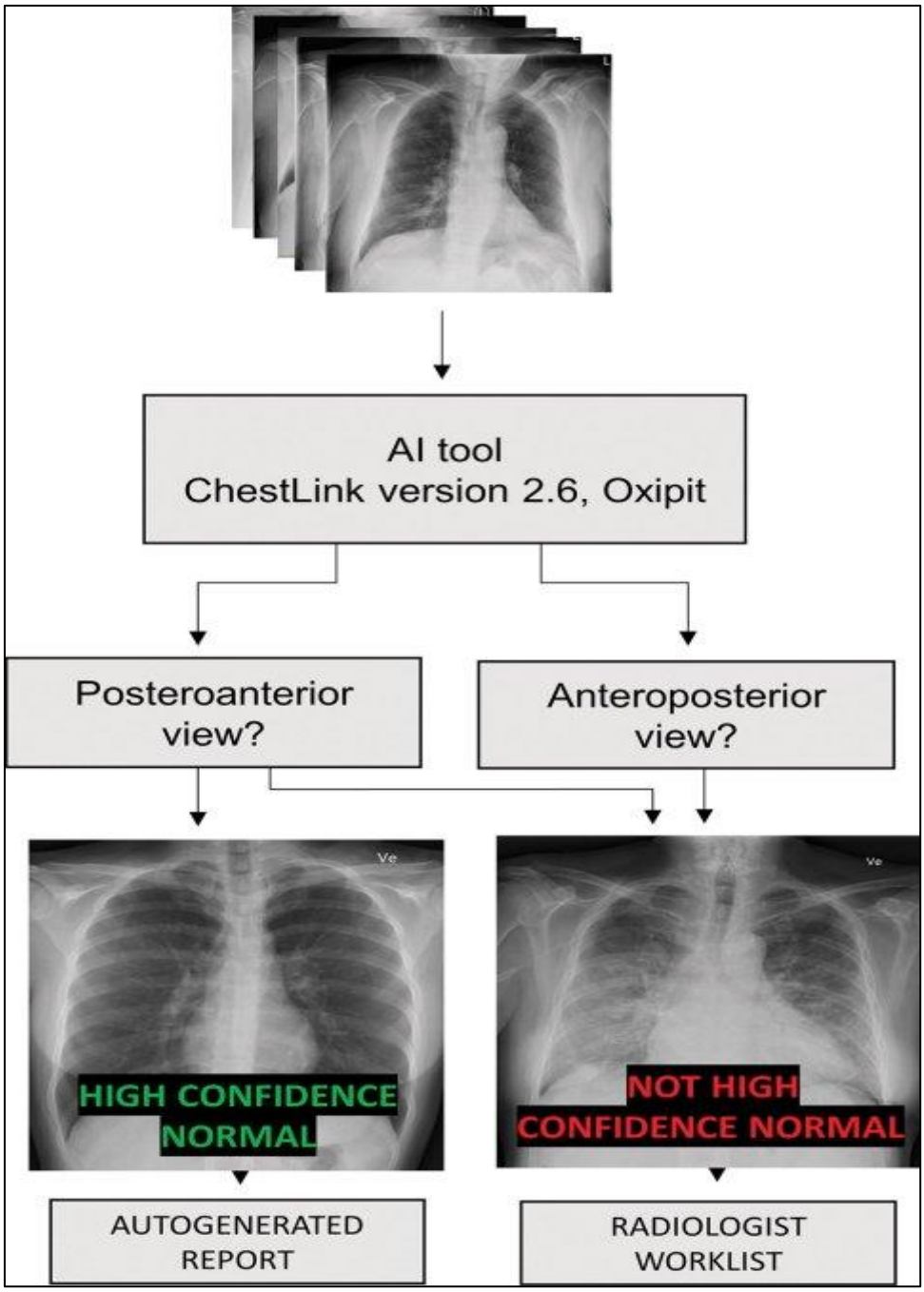


Figure 2.2. Steps of an AI tool to classify chest X-rays [56].

2.1.3. Chest x-ray image datasets

Chest X-ray image datasets play a crucial role in the development and evaluation of deep learning models for Covid 19 disease diagnosis. These datasets are used to train and test the models to achieve accurate predictions. Some of the most commonly used chest X-ray image datasets for deep learning-based Covid 19 disease diagnosis are discussed below:

1. ChestX-ray14: This is one of the most extensively used datasets for deep learning-based chest X-ray image interpretation. It includes 112,120 frontal-view chest X-ray scans of 30,805 different individuals, as well as 14 illness designations for each image. Wang et al. [57] initially presented the dataset in 2017.
2. Pad Chest: This dataset was introduced in 2018 by Bustos et al. [58]. It contains a total of 160,868 chest X-ray images with 174 different radiological findings, including various Covid 19 disease. The dataset also includes metadata such as patient demographics, acquisition parameters, and radiological reports.
3. Montgomery County X-ray Set: This dataset contains a total of 138 posterior-anterior chest X-ray images of patients with active tuberculosis and 80 normal chest X-ray images. The dataset was introduced in 1999 by Jaeger et al. [59] and is commonly used for tuberculosis diagnosis.
4. Shenzhen Hospital X-ray Set: This dataset contains a total of 662 frontal-view chest X-ray images, including 326 normal images and 336 images with tuberculosis. The dataset was introduced in 2018 by Jaeger et al. [60].
5. CheXpert: This dataset contains a total of 224,316 chest X-ray images of 65,240 patients, along with radiologist-labeled disease labels. The dataset was introduced in 2019 by Irvin et al. [61].

The dataset used in this research is described in the section 3.2. These chest X-ray image datasets have played a significant role in the development of deep learning-based models for Covid 19 disease diagnosis and have enabled researchers to achieve high accuracy in disease detection.

2.2. Radiographic Signs and Findings in Chest X-Rays

Chest X-rays provide valuable information about the thoracic cavity and can reveal various radiographic signs and findings indicative of different Covid 19 disease. Understanding these signs and findings is essential for accurate interpretation and diagnosis. The following are some common radiographic signs and findings observed in chest X-rays [62].

2.2.1. Lung opacities and consolidations

- Lung opacities refer to areas of increased density in the lung parenchyma, indicating abnormalities. They can be caused by infections, inflammation, edema, or tumors. Opacities may appear as hazy areas, nodules, or consolidations.
- Consolidations occur when the lung tissue becomes solid due to the filling of alveoli with fluid or inflammatory exudates. They often indicate pneumonia or other infectious processes [63].

2.2.2. Pleural effusion and pneumothorax

The buildup of fluid in the region surrounding the lungs, known as the pleural effusion, is a medical condition. It appears as a blunted costophrenic angle and meniscus sign on chest X-rays.

- Pneumothorax occurs when air accumulates in the pleural space, causing lung collapse. It appears as a hyperlucent area with absent lung markings [64].

2.3. Machine Learning Methods

Machine Learning (ML) is a pattern recognition technology that may be applied to the interpretation of medical imaging reports. ML is a dominant technique for assisting in medical representation analyses, but in most situations, it begins with the computation of picture attributes that are deemed to be significant in the process of creating the prediction or diagnostic of interest [65]. This is true even if machine learning can aid in the rendering of medical diagnostics. Following that, the machine learning algorithm system will identify which image attributes work together to generate the most accurate image categorization or

the most accurate computation of some metric for the specific image region. Deep learning is a very new technology that has just recently gained popularity. One advantage of utilizing this method is that it eliminates the need for the first step of calculating and identifying picture attributes; rather, feature identification occurs as part of the learning process. ML has already been deployed in the field of medical imaging, and its significance will only rise in the next years. Those who work in medical imaging need to have a solid understanding of how machine learning functions. Machine learning is currently being employed in a wide variety of fields that are not related to health. It plays an important part in a variety of activities, including speech recognition and translation between languages, autonomous navigation of cars, and product suggestions [66].

The term "machine learning" refers to a set of computing algorithms and approaches that allow computers to acquire new skills and become better at what they do over time. Data analysis, pattern recognition, computer vision, NLP, and countless more domains make extensive use of these techniques [67].

Machine learning relies on a number of different approaches, each with its unique features and potential uses. A few of the most popular ones are these:

1. Supervised Learning: When the goal variable or output is known, this technique uses labelled data to train a ML model. By analyzing the input-output pairs, the model is able to learn and extrapolate new information. Neural networks, SVMs, DT, RF, and LR are some of the most popular supervised learning methods.
2. Unsupervised Learning: When the objective variable is unknown, unsupervised learning is used to train a model instead of supervised learning, which uses labeled data. The objective is to unearth the data's latent structures, correlations, or patterns. Clustering algorithms like hierarchical clustering, and GMM are common unsupervised learning algorithms. PCA and t-distributed stochastic neighbor embedding (t-SNE) are examples of dimensionality reduction approaches.
3. Reinforcement Learning: The main goal of this approach is to teach an agent how to navigate its surroundings and perform activities that will maximize a reward signal. By receiving rewards or penalties according to its activities, the agent is able to learn by doing. Several activities have found success with reinforcement learning, including game playing (e.g., AlphaGo), autonomous driving, and robots.

4. Deep Learning: A branch of ML, DL focuses on ANNs, and more specifically, ANNs having several layers. Computer vision, NLP, and speech recognition are just a few of the many areas where these networks have proven to be highly effective. They can automatically develop hierarchical representations of data. Among the many deep learning architectures available, two of the most well-known are RNNs and CNNs.
5. Transfer Learning: Employs models that have been trained on massive datasets for a different task. Making use of the knowledge acquired from a single task, the model may potentially generalize and adjust to new problems with less labeled data. When labelled data is limited or model deployment time is of the essence, transfer learning has shown to be a viable option.
6. Ensemble Learning: To achieve better results, ensemble learning integrates numerous ML models. Ensemble approaches produce better outcomes by lowering the likelihood of overfitting and increasing the likelihood of generalization by combining predictions from multiple models. Stacking, bagging, and boosting are common ensemble approaches. Examples of boosting algorithms are AdaBoost and Gradient Boosting.
7. Bayesian Methods: To account for ambiguity and arrive at forecasts, Bayesian approaches employ probability theory. These techniques use Bayes' theorem to update previously acquired knowledge based on new observations. Numerous applications rely on Bayesian inference and Bayesian networks. These include medical diagnosis, recommendation systems, and spam filtering, among others.

It should be noted that new approaches and techniques are produced on a regular basis in the field of machine learning. To overcome obstacles and enhance the capabilities and performance of machine learning algorithms, researchers and practitioners are constantly looking for new and creative ways to do things. The graphic shows how the ML methods.

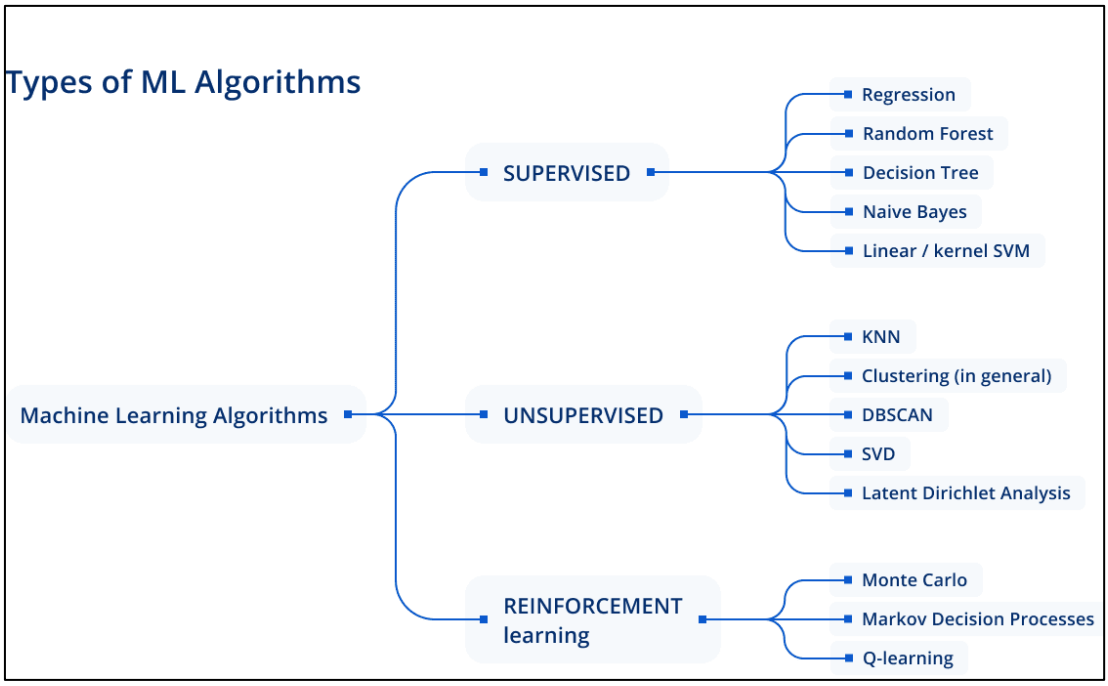


Figure 2.3. ML approaches [67]

2.3.1. Supervised learning

Supervised learning is a machine learning approach in which a model trains from labeled training data to generate predictions or categorize fresh, unseen data. The training dataset in supervised learning comprises of input features (independent variables) and matching output labels (dependent variables) or goal values. By reducing the difference between its projected outcomes, the model hopes to discover the underlying link between the input attributes and the output labels. Once trained, the model may use this previously learnt connection to generate predictions on fresh, previously unknown data [68].

Image classification, voice recognition, medical diagnosis, and natural language processing are just a few of the many disciplines that have widely utilized supervised learning.

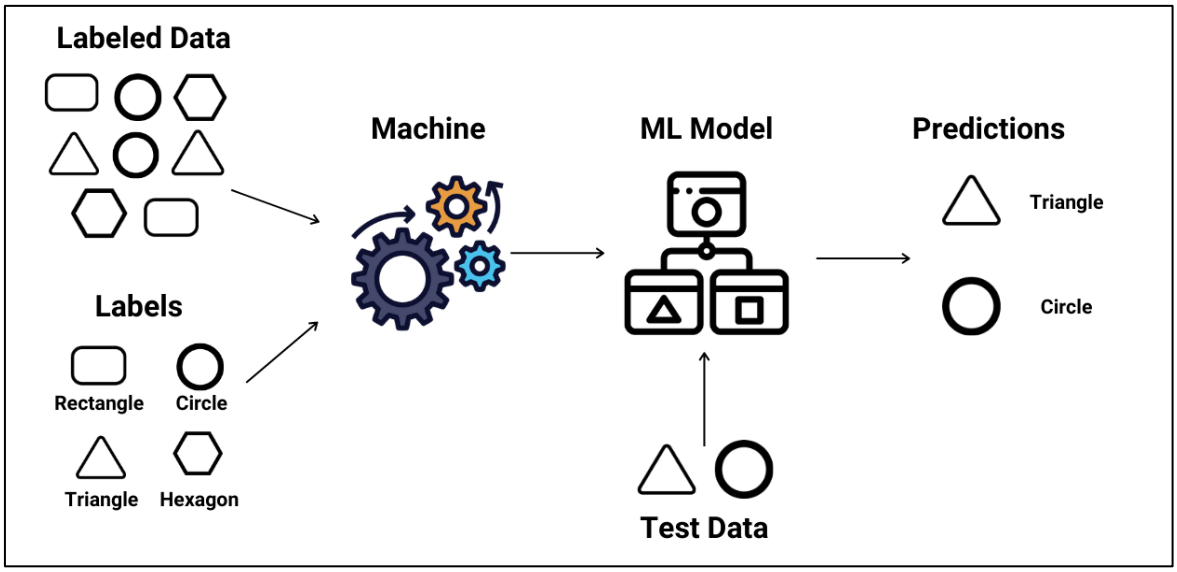


Figure 2.4. Process of Supervised learning [69]

2.3.2. Unsupervised learning

In unsupervised learning, models learn structures and patterns in unlabeled data without human intervention or labelled samples. Unsupervised learning algorithms set out to discover patterns, correlations, or structures in the data independently, as opposed to supervised learning [70].

Without prior knowledge of the right output labels, the model in unsupervised learning investigates the data in search of significant patterns. Clustering and dimensionality reduction are two examples of such tasks; in the former, the model groups data points that are related and in the latter, it finds a lower-dimensional representation of the data while retaining its key properties.

Unsupervised learning has numerous applications, including anomaly detection, customer segmentation, recommender systems, and exploratory data analysis.

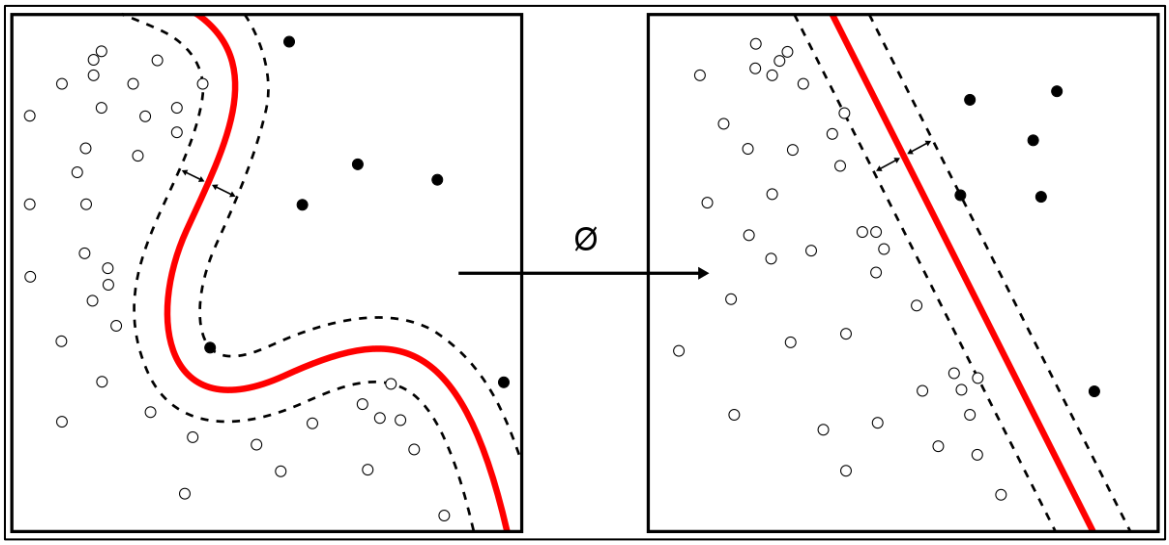


Figure 2.5. Indicts of Unsupervised Learning [71]

2.3.3. Reinforcement learning

One kind of machine learning known as "reinforcement learning" teaches agents how to maximize their reward signals through specific interactions with their surroundings. In this model, the agent learns by doing, with incentives and punishments serving as feedback on its performance.

Agents engage in environmental behaviors in reinforcement learning, with feedback in the form of rewards or penalties depending on the outcomes of those actions. The objective of the agent is to maximize the cumulative reward over time by learning a policy or set of rules that connect states to actions. As it takes actions to investigate its environment, the agent learns, via trial and error, which behaviors yield bigger rewards. The agent, their surroundings, and the reward signal are the three primary actors in reinforcement learning. The environment changes to a new state and gives the agent a reward when the agent chooses activities depending on its current condition. To maximize the predicted cumulative reward, the agent must learn the best policy [72].

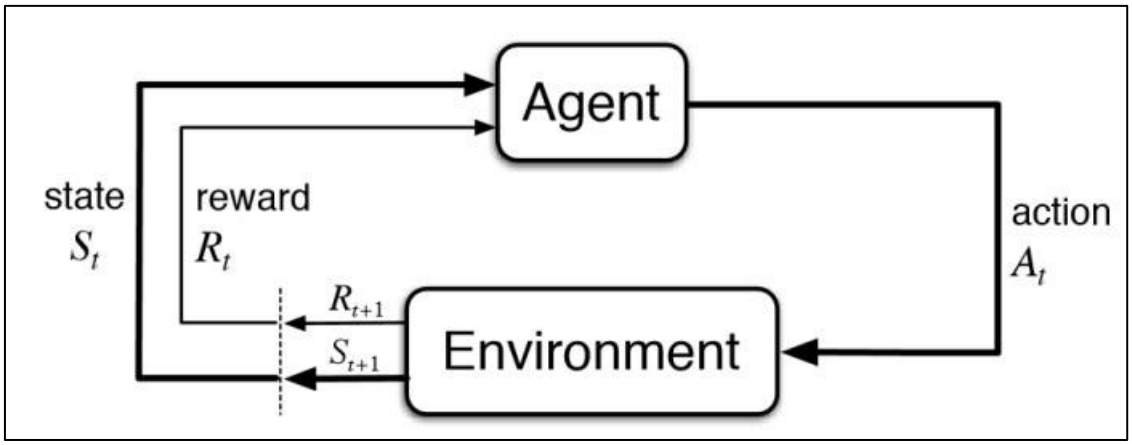


Figure 2.6. Reinforcement Learning process [73]

2.4. Deep Learning Methods

Deep Learning (DL), a fresh area of study the realm of machine learning. It first appeared on the market in 2006. Often referred to by its technical name, "deep neural network learning," "deep learning" is a cutting-edge study topic that has quickly gained in popularity and is yielding impressive results. At the beginning, it was referred to as hierarchical learning [74], and it is currently known as deep learning. In most cases, it incorporates a wide range of research topics associated to shape recognition. The fundamental focus of deep learning is on taking into consideration the following two primary aspects: the use of non-linear processing across a number of stages or layers and the use of either supervised or unsupervised learning [75]. Recently, medical image analysis has made use of deep learning techniques, which have shown promise in several applications like segmentation and registration. Many people are looking to DNNs, and more specifically CNNs, to solve the problems associated with medical imaging [76].

It used to be that human experts like radiologists and doctors were the only ones allowed to evaluate medical images in a clinical setting. Regardless, computer-assisted therapies have just recently started to help researchers and doctors. This is because human specialists may be exhausted and there are vast differences in pathology. While computational medical image analysis is still behind the times when compared to medical imaging technology advancements, it has been making progress with the use of machine learning techniques.

Meaningful feature extraction and representation are the foundations of machine learning's capacity to do its intended tasks. When analyzing data using machine learning, this is indeed the case. Based on their knowledge of the target areas, human professionals have usually designed features that are relevant or task-related. Since human experts are required to develop relevant or task-related qualities, it is difficult for non-experts to employ machine learning approaches in their own research. However, by incorporating feature engineering into the learning step, deep learning has successfully solved these obstacles. In order for deep learning to learn the informative representations on its own, all it needs is a dataset, maybe pre-processed. What this implies is that it does not use a labor-intensive approach to character extraction. Now that computers are doing feature engineering instead of humans, even those without a background in machine learning can leverage deep learning for their own projects, especially in the field of medical picture analysis. Because ML methodology can now be adopted by individuals and feature engineering can be left to machines, this is the case [77].

Finding patterns in photographs is where CNN shines, the most popular deep learning algorithm now in use. Convolutional neural networks (CNNs) mimic the structure and function of the human brain by mimicking its architecture and consisting of trainable neurons with predefined biases and weights. On average, each neuron receives many inputs. The next step is to add up all of the inputs while considering their weights. Then, an activation function is used to provide an output based on the weighted total. The use of convolution layers is what sets convolutional neural networks apart from its non-convolutional counterparts [78]. Three distinct kinds of layer convolutional, pooling, and fully connecte make up a convolutional neural network (CNN). Multiple layers make up a CNN. Simply said, the convolutional layer performs a convolutional operation. A linear view of convolution is possible due to the fact that it is a multiplication of an input by a set of weights. A kernel or filter is the name given to the set of weights. The filter is unable to process the incoming data set due to its size. When you multiply the input by itself, you get the dot product, which is proportional to the size of the filter. After that, we add the dot product value, which gives us one integer. It is the responsibility of this layer to generate the activation. Additional information regarding CNN can be found in the reference number [40]. Two main components are typically used by CNN during learning: feature extraction and categorization. It is common practice to employ a filter or kernel to conduct convolution on the input data during the feature extraction step. The making of a feature map follows.

The CNN will calculate the likelihood that the image matches to a specific label or class during the classification step of the procedure. It is notably beneficial for picture categorization and identification since it automatically learns characteristics rather than requiring the user to manually extract those qualities [79, 80]. Transfer learning is another method that may be used to retrain CNN and apply it to an entirely new field. Transfer learning has been demonstrated to generate improved categorization results [81].

Deep Belief Networks (DBN) are an extra deep learning algorithm. As mentioned in [82, 83], each layer in the DBN serves two distinct functions. The nodes preceding this layer use it as a hidden layer, whereas the ones following it use it as an input layer. This layer fulfils both of these functions. The first RBM is designed to mimic the input used to train a DBN as precisely as possible. Following that. This process is repeated over and over again until all of the layers of the network have been trained. It is possible to utilize DBN to recognize objects contained inside still photos, video sequences, and motion capture data. There is additional information regarding DBN that can be found in [84, 85].

Within the scope of BOVW, image qualities replace "words." Picture features are distinct patterns within an image that can be identified. The primary idea behind BOVW is to characterise a picture as a collection of features, each with its own set of important points and descriptors. An image's key points remain the same no matter how the image is altered, whether it is rotated, resized, or enlarged. This is because key points are the most prominent features of an image. The explanation of the central idea is known as the descriptor. It is possible to build languages with the help of key points and descriptors, and each image can be represented as a frequency histogram of its features. One can determine the class of the image by looking at the frequency histogram and then finding other photos that are similar to the one being analyzed. The classification of tuberculosis was suggested by Lopes and Valiati using the Bag of CNN characteristics [86].

3. MATERIAL AND METHODS

Image processing techniques, as described in reference [59], play a vital role in the initial processing of pictures, comprising critical tasks such as noise reduction, sharpening, deblurring, binarization, contrast enhancement, and object segmentation. The inclusion of unclear, low-contrast, or otherwise defective photos has been extensively reported in research as a serious obstacle to the accuracy of classification algorithms. The use of such photos in machine learning models raises questions about their ability to recognize objects correctly. When confronted with such difficult-to-decipher images, the insertion of metadata becomes critical for the accurate interpretation and categorization of these images within a model. To avoid the need to rely on information for the classification of these complex images, we present a variety of methods for cleaning images before training neural networks.

This chapter looks deeply into how deep learning techniques and Convolutional Neural Networks (CNNs) can be used to accurately classify chest X-ray pictures. Furthermore, we performed extensive evaluations of several pre-processing techniques like as thresholding, blurring, and histogram equalization.

3.1. Research Workflow

In the intricate realm of this COVID detection research workflow as shown in Figure 3.1, several pivotal stages emerge as the linchpins to crafting a precise and efficacious detection framework.

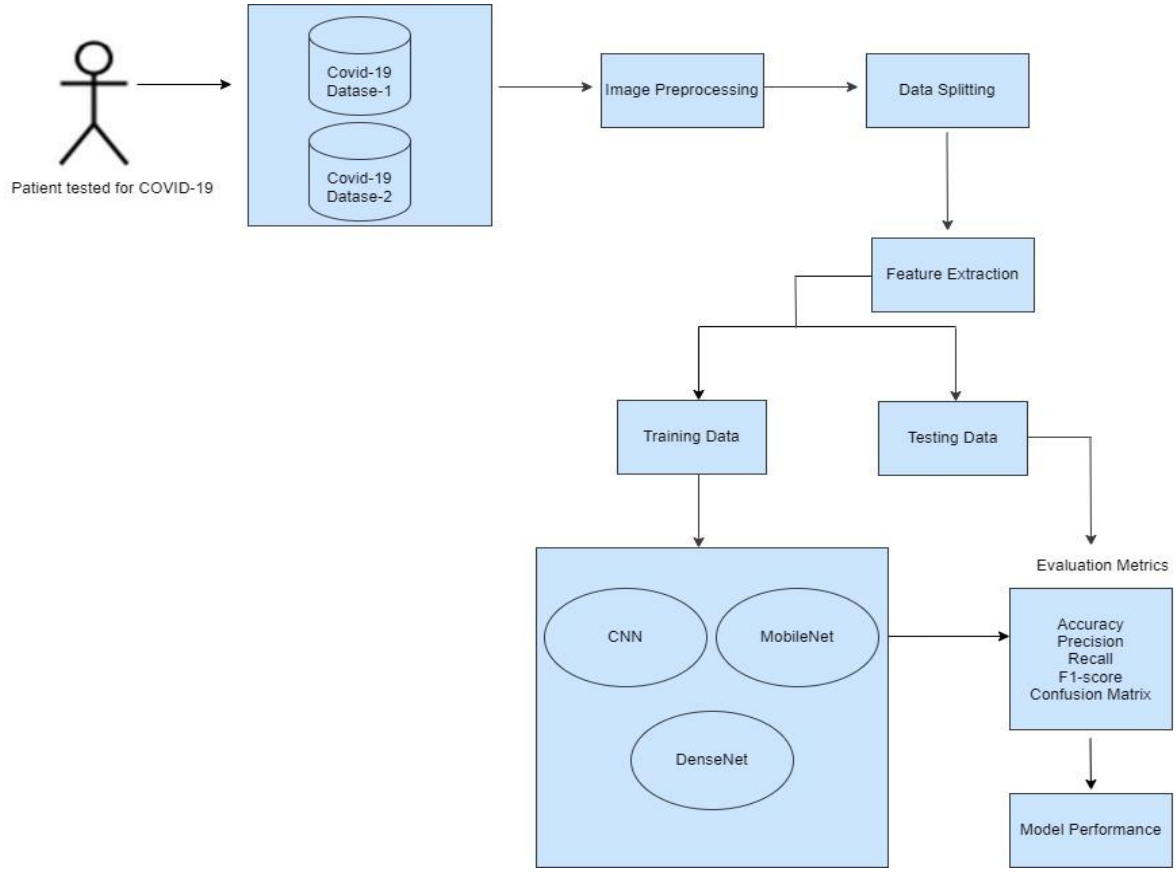


Figure 3.1. Proposed methodology flow for covid detection

3.1.1. Stage 1: data collection

Initiating this odyssey is the cardinal task of amassing an exhaustive repository of thoracic X-ray depictions. This repository demands an eclectic compendium of visuals spanning the gamut from COVID-19 afflicted subjects, individuals in the prime of health, to those grappling with viral pneumonia. To substantiate credibility, these visual portrayals necessitate an echelon of excellence, with conspicuous demarcations signifying the subjects' COVID-19 status.

The first critical step is to collect a large collection of chest X-ray pictures. This dataset should include photos from COVID-19 patients, normal patients, and patients with viral pneumonia. These photos should be of high quality and clearly labelled with the patient's COVID-19 status to ensure reliability.

3.1.2. Stage 2: image preprocessing

Following the assemblage of the repository, the mandate extends to the art of visual preening. This delicate maneuver ensures that all visual manifestations adhere to a standardized paradigm concerning dimensions and aspect ratio. Canonical procedures encompass resizing the visual renderings, grayscale conversions where requisite, and the normalization of pixel values, thus rendering them amenable for meticulous scrutiny and analysis.

It is critical to preprocess the photos after collecting the dataset. This step guarantees that all photos have the same size and format. Typical preprocessing operations include scaling images, turning them to grayscale if necessary, and normalizing pixel values to prepare them for analysis.

3.1.3. Step 3: dataset splitting

The efficacy of the deep learning model's training and evaluation hinges upon the judicious partitioning of your repository into three distinct strata: the training cohort, the testing, and the testing cohort. The training corpus is consecrated to honing the model's acumen, whilst the testing set serves as the crucible for assessing its mettle during the formative phases. Lastly, the testing domain serves as the crucible for ascertaining the model's universalizability. We chose an 80% training and 20% testing dataset split, as it yielded the highest accuracy compared to other percentages. Common allotment proportions typically approximate 80% for training, 10% for testing, and 10% for testing.

Separate your dataset into training and testing sets for optimal deep learning model training and analysis. There are three sets of data used in machine learning: the training set, the testing set, and the evaluation set. The training set is used to train the model, and the evaluation set measures how well the model generalizes. The usual distribution is as follows: 80% training, 10% testing, and 10% testing.

3.1.4. Stage 4: data augmentation

To engender an exponential augmentation of your training repository and bestow upon your model an aura of invincibility, contemplate the strategic deployment of data amplification stratagems. These stratagems pivot on the whims of stochastic transformation, as extant visuals are subjected to capricious modulations comprising cropping, mirroring, and rotation—yielding a panoply of avant-garde variations. Data amplification functions as a linchpin, enhancing the model's aptitude in parsing the intricate tapestry of COVID-19 patterns.

Consider using data augmentation techniques to enlarge your training dataset and improve model robustness. To create new variations, these approaches entail applying random adjustments to existing images, such as cropping, flipping, and rotating. Data augmentation improve the quality and visibility of image, which becomes easier to understand by the model. Data augmentation can help improve the model's recognition of COVID-19 patterns.

3.1.5. Stage 5: feature extraction

The ardent champions in your arsenal, Convolutional Neural Networks (CNNs), ascend to the fore, armed with the singular mission of distilling salient features from the canvas of thoracic X-ray portraits. These neural denizens are meticulously trained to discern the telltale patterns and intricate nuances underpinning COVID-19 manifestations. The extracted features, akin to precious gems, form the currency of exchange for the impending machine learning contrivance.

To extract relevant information from chest X-ray pictures, Convolutional Neural Networks (CNNs) are used. CNNs are trained to recognize patterns and features related to COVID-19. The retrieved features are used as input for the machine learning model that follows.

3.1.6. Stage 6: model training

The chosen archetype is then inducted into a rigorous regimen of conditioning, anointed with the elixir of features extracted in the antecedent phase. Depending on the properties of the dataset and your desired performance goals, choose a suitable deep learning model, such as

a CNN, or a neural network. Using the extracted features from the previous step, train the chosen model.

3.1.7. Stage 7: model evaluation

Using the testing set, assess the trained model's performance. Assess the model's accuracy, precision, recall, F1 score, and other relevant variables using appropriate evaluation metrics. This stage determines whether the model is ready to be deployed on new data.

3.1.8. Stage 8: prediction on new data

Once the model emerges from the gauntlet of scrutiny, battle-hardened and validated, it stands ready to unfurl its prophetic mantle upon new entrants to its domain—the thoracic X-ray portraits. Here, the model bequeaths unto each visage probability scores, a numeric testament to the likelihood of COVID-19's insidious embrace.

In this step we utilized the trained model to predict the COVID-19 status of new chest X-ray pictures once it has been properly evaluated and proved to perform well. For each image, the model will generate a probability score reflecting the possibility that the patient is infected with COVID-19.

Importantly, the features of the dataset and the deep learning model employed might affect the specifics of each step. The construction of an accurate and dependable COVID-19 detection system is the goal of this comprehensive procedure.

3.2. Datasets

This research two datasets to make broader comparison for this research. Both the datasets are publically available on the kaggle. Let’s discuss each datasets insight separately;

3.2.1. Covid19-dataset

This dataset (Covid19-dataset) has been painstakingly divided into two groups: those with tuberculosis and those with normal health conditions. These datasets are freely available to

the public via Kaggle and have been generously given by the National Institutes of Health (NIH) [22]. A thorough preparation process is carried out prior to using the input data for network training to guarantee that the data is optimized and ready for use.

According to Figure 3.2, dataset distribution consists of a train set and a test set, each of which has three separate classes: COVID-19, Normal, and Viral pneumonia. There are 70 images for COVID-19, 70 images for normal patients, and 111 images for viral pneumonia in the train set. The test set includes 20 COVID-19 photos, 20 normal cases, and 26 viral pneumonia images.

This dataset distribution is balanced in that each class has an approximately similar amount of photos in both the training and test sets. This balance is critical in order for the machine learning model to learn and categories the various image classes with equal accuracy. However, when analyzing this dataset distribution, there are a few things to keep in mind:

The number of photographs in each class may not adequately reflect the true prevalence of certain medical disorders in the general community. For example, because COVID-19 is more common than viral pneumonia, there may be a greater representation of COVID-19 photos in the collection.

The dataset may not cover the full range of disease severity within each class. Some COVID-19 patients may have more severe symptoms, and their X-ray images may be included more frequently, thereby influencing the dataset's representativeness.

When evaluating the performance of your machine learning model on this dataset, it is critical to take these factors into account. While the distribution appears to be fairly balanced, it is important to realize that the dataset may not completely reflect real-world prevalence and severity, which can affect the model's performance. Overall, this dataset distribution provides a solid foundation for training and assessing a COVID detection machine learning model.

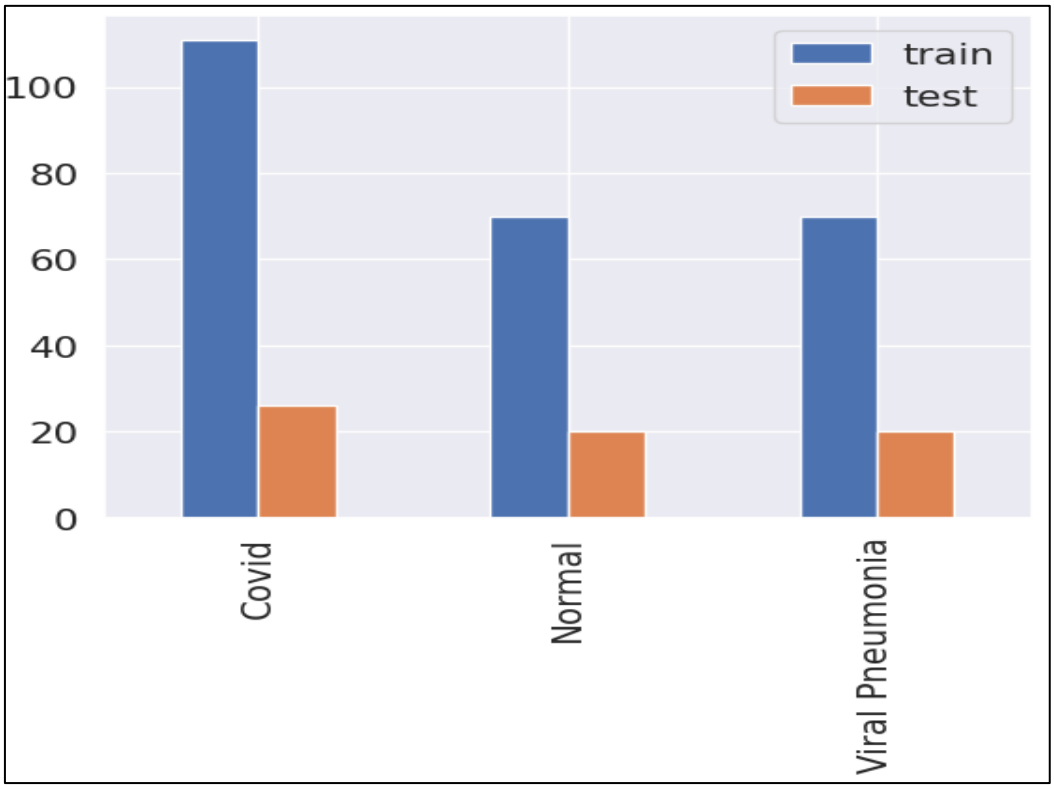


Figure 3.2. Training and testing data distribution of Covid19-dataset

The following Table 3.1 shows some important parameters that are defined in model.

Table 3.1. Important Parameters

Input target size	256 x 256
Colour mode	input samples of chest X-rays are set to grayscale
Batch size	10
Class mode	Three (Normal, Covid & Viral Pneumonia)

Table 3.1 lists the model's essential parameters. These features include a 256 x 256 pixel input target size, a grayscale color mode for chest X-ray samples, a batch size of 10 for processing, and a classification mode with three classes: Normal, Covid, and Viral Pneumonia.

After the data have been preprocessed, the sample images that will be used in the training phase are shown in Figure 3.3.

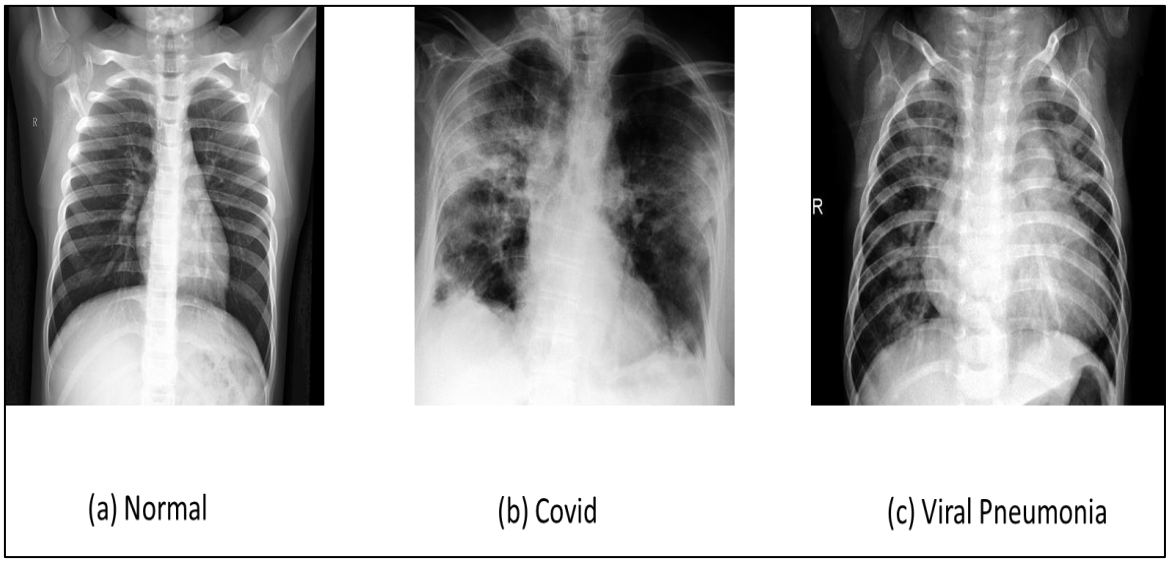


Figure 3.3. Some Sample Images for Train the model

3.2.2. Chest X-ray (Covid-19 & Pneumonia)

The dataset has been painstakingly organized for use in deep learning tasks. It is organized into two primary folders: "train" and "test," which serve different functions in model creation and evaluation. Each of these files contains three subfolders: "COVID19," "PNEUMONIA," and "NORMAL." These subfolders organize the photographs according to their categories.

The dataset contains 5,014 X-ray images in total, representing a wide range of medical disorders and healthy instances. These photos are required for training and testing machine learning models that can recognize various health issues.

A frequent practice is to dedicate a subset of the dataset for testing to ensure a robust evaluation of model performance. In this scenario, 20% of the total photos have been reserved for testing. This separation enables that the model's performance can be evaluated on data that it did not see during training, providing a reliable measure of its generalization capacity.
Overall, this well-structured dataset makes it easier to design and test machine learning models for detecting COVID-19, pneumonia, and normal patients using X-ray pictures.

This research strategy appears to be comprehensive and well-structured. Each of these phases is critical to the success of your research:

Data Preparation: This research used publically available dataset [101]. Here's the training set of the dataset and the distribution presented in Figure 3.4:

Here's the training set of the dataset:

- COVID-19: 467: This means that the training set has 467 chest X-ray images labelled as COVID-19 instances. These are X-ray images of people who have been diagnosed with COVID-19.
- NORMAL: 1,241: There are 1,241 chest X-ray images in the training set labelled "NORMAL." These photos are considered typical reference X-rays because they show people with no apparent lung anomalies.
- PNEUMONIA: 1,709: Included in the training set are 1,709 chest X-ray images labelled "PNEUMONIA." These photos depict examples of viral or bacterial pneumonia, a disorder with symptoms similar to COVID-19.
- Here's the testing set of the dataset:
- COVID-19: 109: This means that the testing dataset contains 109 COVID-19-labeled chest X-ray pictures. Individuals with COVID-19 have been identified in these photos.
- NORMAL: 342: There are 342 chest X-ray images in the testing dataset labelled as "NORMAL." These photos show X-rays of people who have no significant lung anomalies.
- PNEUMONIA: 1,146: The testing dataset also includes 1,146 images of chest X-rays labelled "PNEUMONIA." These photos represent examples of viral or bacterial pneumonia, a disorder with symptoms similar to COVID-19.

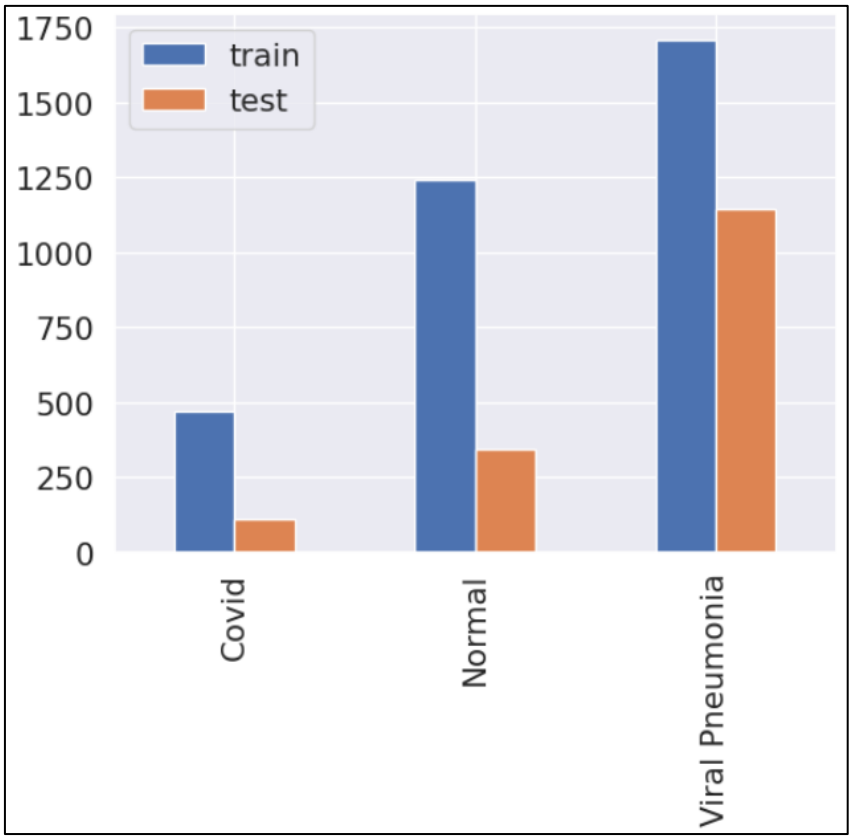


Figure 3.4. Training and testing data distribution of Chest X-ray (Covid-19 & Pneumonia) dataset

3.3. Preprocessing Techniques

Image quality is improved by the use of preprocessing in order to facilitate more accurate analysis of the data it contains. Preprocessing can increase some of the features that are required for a given activity while also reducing any undesirable distortion. The most significant challenge presented by deep learning is overfitting. To lessen the effects of overfitting, the pre-processing stage employs the data augmentation approach. Resizing, scaling, cropping, flipping, and rotating are a few of the more popular data augmentation techniques [97].

The following are some techniques to data augmentation:

1. Resizing: The images are all different sizes, so it is necessary to resize them before moving on to the next step. This is because the differences make it more difficult to prepare the model. All of the images are scaled down to a specific dimension, such as

224 pixels by 224 pixels or 299 pixels by 299 pixels, so that the dataset can be applied to a wider range of situations [61].

2. Flipping or Rotating: The sample size of datasets can benefit from using this method. It is common practice to flip the axis in both the horizontal and the vertical directions.
3. Resizing: It is common method utilized for the purpose of augmentation. There is no requirement for the utilization of complete parts of the images. As a direct consequence of this, the cropping method was implemented by the researchers in order to cut down on duplication.
4. Brightness or Intensity adjusting: Brightness adjustments—both increases and decreases—must be made to images before performing any kind of analysis, as these adjustments are essential to the process.

3.4. Feature Extraction Methods

Since the extracted features define the key elements of the pictures being categorized, feature extraction is a crucial step in the classification process. The extraction of visual characteristics benefits greatly from the use of Convolutional Neural Network (CNN). They are often used in computer vision techniques as well as convolutional neural networks as a direct result of this.

When given input photos, deep learning algorithms, like the convolutional neural network, assign weights and biases (also known as learnable) to distinctive properties or objects, which are then distinguished from one another. CNN requires far less pre-processing than other classification techniques. The manual development of filters is a crucial part of the fundamental approaches; however, given enough training, CNNs are capable of learning these features and filters.

3.5. Model Selection

3.5.1. Convolutional neural network

In this study, models based on Convolutional Neural Network (CNN) were used to recognize Covid-19, Healthy, and pneumonia from digital chest X-rays. The major distinction between neural networks and convolutional neural networks is the use of convolutions in the network

layers to extract and map features for use in training various classifiers or repressors. Convolutional neural networks perform their functions very similarly to neural networks. Convolutions are mathematical operations that go over an image matrix, extracting smaller matrices from it, and then mapping each of those smaller matrices to a single value by making use of the same weight. The output that was produced as a consequence of the earlier input is typically referred to as a feature map or activation map. During the training phase of the process, the kernel weights are altered by employing forward and backward propagation, as well as a variety of various optimizers, learning rates, and other hyper parameters [87]. This is done in order to minimize a loss function.

CNN architecture

CNN layers extract significant features before transmitting them to the fully connected layer, which categorizes them [88]. The CNN structure consists of feature extraction and categorization. Convolution layers, Batch Normalization (BN), ReLU (Rectified Liner Unit), Activation Function (AF), dropout, and max-pooling are all part of the feature extraction stage [89].

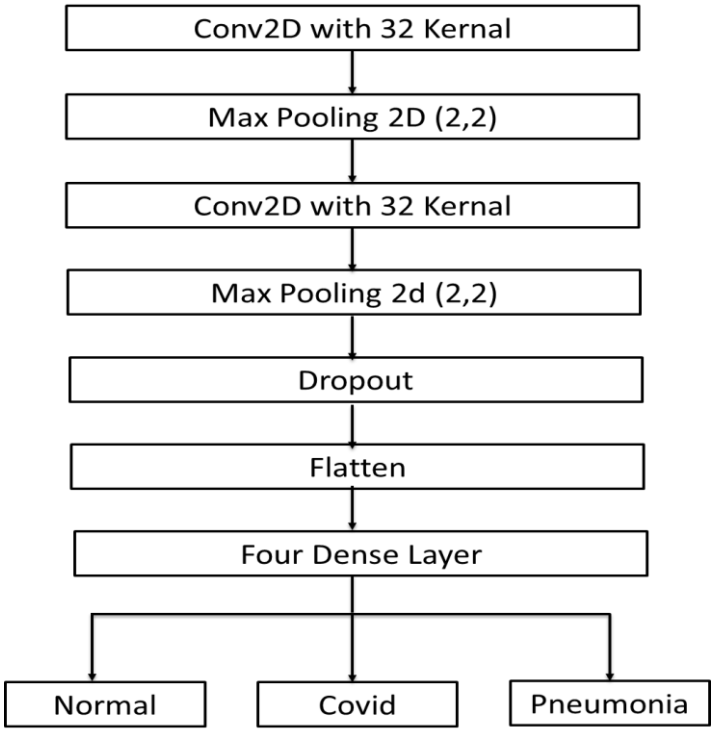


Figure 3.5. Architecture of used CNN model

The block diagram of the used CNN based classification system for lung dieses detection is given in Figure 3.5. To build a CNN model we used following layer as shown in this figure.

1. The Convolutional layer starts with a lower filter value such as 32 and begins to increase it layer wise.
2. Construct the model by beginning with a layer of Conv2D and then moving on to a layer of MaxPooling 2 x 2.
3. It is recommended that the kernel size be 3x3, which is an odd integer.
4. ReLU used for activation function
5. Image width and height are taken into account by the input shape, with the final dimension serving as the colour channel.
6. After the CNN layers, the input is flattened, and the ANN layers are added.
7. Applying sigmoid activation function for binary classification and if the difficulty is multicategory, activation function used is softmax.

3.5.2. MobileNet

One CNN that has found widespread use in embedded and mobile computer vision systems is MobileNet. Lightweight deep neural networks that use depth-wise separable convolutions are the basis of these systems, which have the ability to reduce latency for embedded and mobile devices [90]. The architecture of MobileNet is defined by two distinct steps: depthwise and pointwise convolution. Following the completion of down sampling for each feature map, following two procedures are executed. Now running as depthwise convolution, the first stage primarily focuses on the filtering process. To combine the results, a second pointwise convolution must be executed [91].

In contrast to conventional convolutions, depthwise convolution is conducted only once when dealing with input channels. Incorporating a 1X1 filter convolution into its processes, this layer passes through pointwise convolution to produce a linear output combination. The MobileNet architecture deviates from traditional CNNs in that it uses ReLU and Batch Normalization instead of a single 3X3 convolution. In contrast to more conventional convolutional neural networks, MobileNet takes a novel method [92]. MobileNet uses a depthwise 3X3 convolution kernel first, and subsequently, for each input channel separately,

it uses a pointwise 1X1 convolution. This fresh method improves the network's efficiency without sacrificing precision.

The use of depthwise convolutions by MobileNet is crucial since it reduces the number of parameters compared to networks that use regular convolutions. The end result is a collection of very efficient deep neural networks that are quite low in weight. For the purpose of training tiny, quick classifiers, Google has made available the MobileNet CNN class through its open-source initiative. This method is a huge step forward since it makes it easier to create neural network designs that are both efficient and streamlined.

Depthwise separable convolution

In order to be complete, Dense-MobileNet employs depth-wise separable convolution. This block has two convolutional layers as well as a depth-wise layer. The first layer's input data are the results of the previous depth-wise separable convolution layers' output. As illustrated in Figure 3.6, the dense block structure depicted here has only one dense link [93].

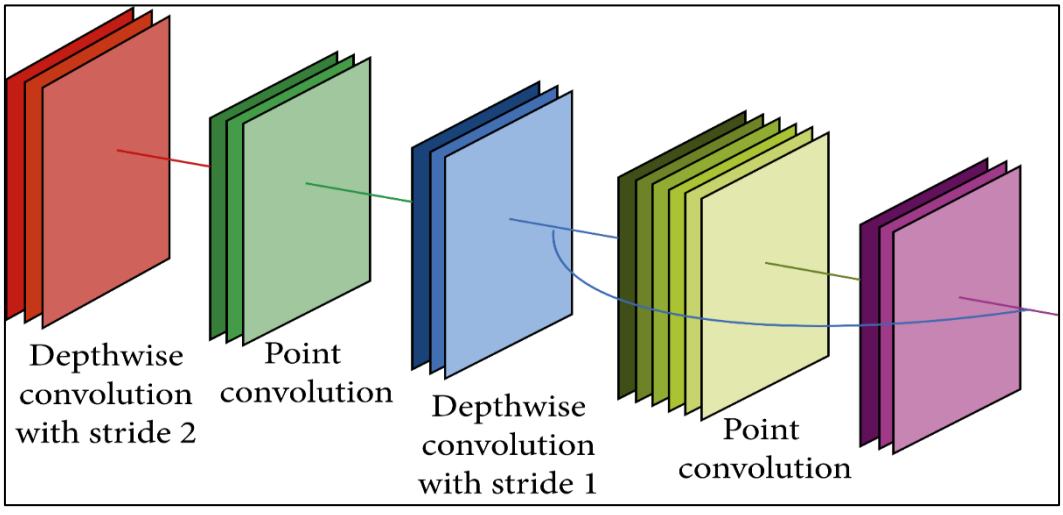


Figure 3.6. Dense-MobileNet model [93]

The normal convolution process is shown in Figure 3.7. Suppose if the input data of size is considered to be D_f x D_f x M in a Normal Convolution process, where D_f x D_f can be the size of the image and M is the number of channels, the result is a Normal Convolution. Let's say there are N filters or kernels, each of which has the dimensions D_k x D_k x M. If an ordinary convolution process is carried out, then the size of the output will be D_p x D_p x N.

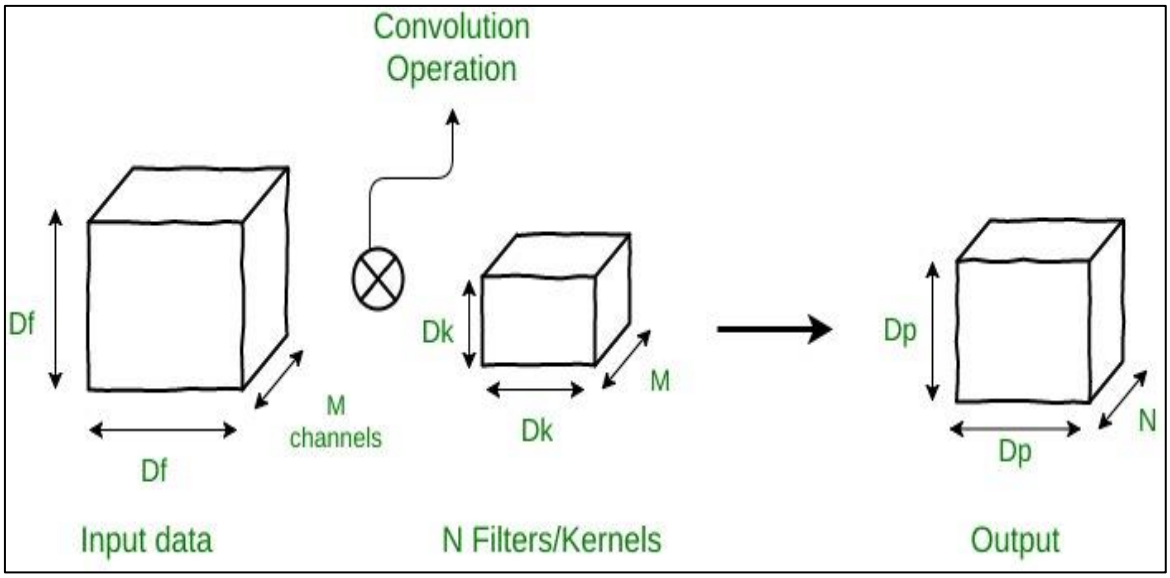


Figure 3.7. Normal Convolution operation

A depth-wise separable convolution is one that is followed by a pointwise convolution. Two distinct approaches are combined to produce a depth-wise separable convolution [94].

- Depth wise Convolution
- Point wise convolution

In the first step, known as depth-wise convolution, we apply a convolution on the input image without making any adjustments to the depth. To this end, we make use of three kernels with the dimensions 5 by 5 by 1. The output of each 5x5x1 kernel is an 8x8x1 image. This is accomplished by iterating one channel of the image and obtaining the scalar products of every 25 pixel group. When stack these images together, we obtain an image that is 8 by 8 by 3. So, in this case, the filters/kernels will be Dk x Dk x 1. Given that the input data contains M channels, M such filters are necessary. Figure 3.8 depicts the output size of Dp x Dp x M.

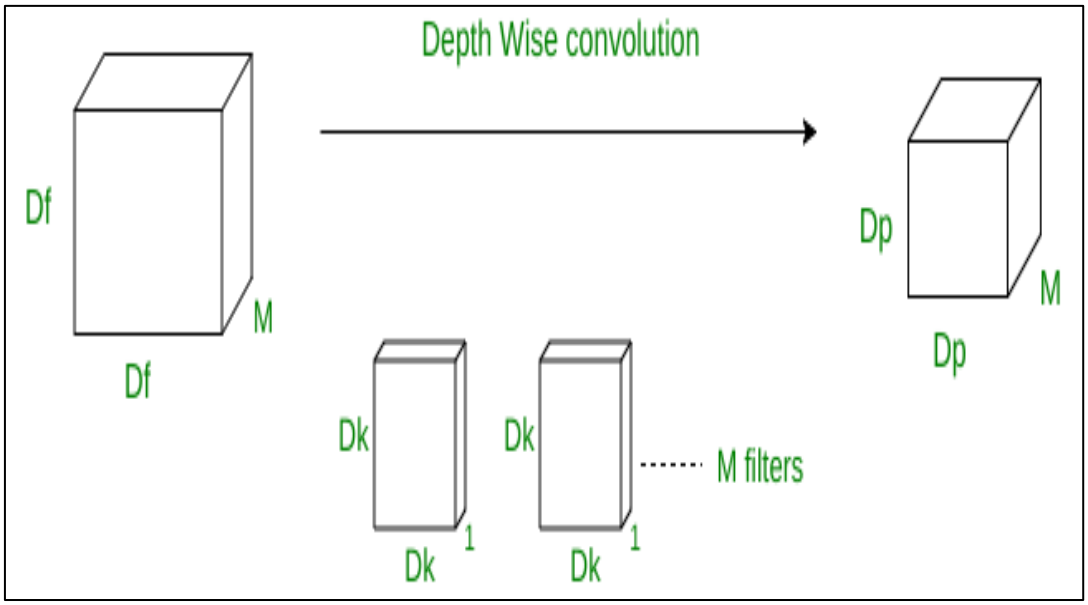


Figure 3.8. Depth Wise Convolution

The second pointwise convolution is so named because it uses a 1x1 kernel, commonly known as a kernel that iterates across all points. The number of channels in the input image is utilized to calculate the depth of this kernel, which is equal to that number. As a result, in order to obtain an 8x8x1 image, we must first run a 1x1x3 kernel over the existing 8x8x3 image. As a result, the dimensions of the filter that will be used to carry out this procedure will be 1 x 1 x M. If we utilize N of these filters, the output size will be Dp times that number multiplied by N.

Therefore, for overall operation:

Total multiplications= Depth wise multiplications + Point wise multiplication (3.1)

Total multiplication = $M * D_k^2 * D_p^2 + M * D_p^2 * N$ (3.2)

So for depth wise separable convolution operation

Total multiplication = $M * D_p^2 * (D_k^2 + N)$ (3.3)

3.5.3. DenseNet

The DenseNet (Dense Convolutional Network) design aims to assist deep learning networks get deeper while also making them more cost-effective for training. This is accomplished by using shorter connections between the architecture's levels. Each layer of the DenseNet's

convolutional neural network is connected to all of the other levels deeper in the network's structure. This means that the first layer is linked to the second, third, fourth, and fifth layers, and so on, whereas the second layer is linked to the third, fourth, and fifth layers, and so on. This process is repeated until all of the layers are joined. This is done to ensure that the various tiers of the network may communicate as much information as possible with one another. Each layer is responsible for receiving inputs from all levels preceding it and distributing its own feature maps to all layers following it in the network. This is done so that the network can maintain its feed-forward structure [95].

The dense interconnections between the layers of DenseNet, an example of a convolutional neural network, are what set it apart from other types. Dense Blocks, an innovative feature of DenseNet, link each layer of the network to every other layer directly. Information flows more smoothly and features may be reused more easily thanks to this complex network design.

Dense Blocks and Transition Layers are two essential parts of DenseNet, apart from the basic convolutional and pooling layers. As its name suggests, Dense Blocks encourage dense connections by directly connecting each layer within the block. The network's capacity to grasp complex characteristics and gradients is improved by this arrangement of connections, leading to better learning. To improve the network's overall efficiency, transition layers compress data both spatially and channel-wise.

DenseNet procedure

The DenseNet design develops in a sequential fashion, beginning with an initial layer that contains basic convolution and pooling processes. After this comes a transition layer, which is followed by a dense block; the process is then repeated with more dense blocks and transition levels. The last section has a thick block followed by a layer for classification. All of these parts work together to make the network what it is today. At the outset, the first convolutional block uses 64 seven-by-seven filters with a stride of 2. The next layer is MaxPooling, which uses a 3x3 pooling size with a 2 stride. All of the next parts are based on this sequence. A strict sequence is required for the definition of the convolutional block: batch normalization comes first, then ReLU activation, and finally the Conv2D layer. This organized structure guarantees that each convolutional block handles input data correctly.

Two convolutions, one using a 1x1 kernel and the other a 3x3 kernel, define each Dense Block. In dense block 1, this pattern appears six times; in dense block 2, twelve times; in dense block 3, twenty-four times; and finally, in dense block 4, sixteen times. Specifically, compared to previous iterations, each dense block's 1x1 convolutions have four times as many filters. The input and output tensors are guaranteed to be connected in this particular configuration by means of 4*filters.

The careful layout of DenseNet's convolutional and dense blocks shows that the design team put a lot of research into making sure that feature extraction and network connectivity are both optimized. Because of these deliberate decisions, the network is able to capture complex information and encourage efficient learning.

Defining the transition layer - We are going to reduce the number of channels in the transition layer so that there are just half as many as the total number of channels that are being utilized at the moment. There is also an average pooling layer that is 2x2 in size and has a stride of 2, in addition to a convolutional layer that has a size of 1x1 for each of its units. It is not necessary for us to declare the kernel size directly once again because it has already been determined in the bn rl conv function that it would be 1x1.

During the transition layers, we are needed to continue removing channels until we are down to fifty percent of the total number of channels. Since we have access to the x input tensor, our first order of business is to count the number of channels while also isolating fifty percent of them. Therefore, since we have access to the Keras backend (K), we can utilize it to extract the dimension of the tensor x by providing it with the tensor itself. In addition, the very final figure on that form, which represents the total number of filters, is the only one of its components that we require. So we add -1. In conclusion, all that remains to be done in order for us to accomplish what we set out to achieve is cut in half the number of filters we are using.

Therefore, the process of defining the transition layers and the dense blocks is complete. At this point, we must pile the dense blocks and the transition layers atop one another. Therefore, we build a for loop that will iterate through the repetitions 6, 12, 24, and 16. Therefore, the loop executes four times, with each iteration selecting a value from the range

6, 12, 24, or 16. This concludes the construction of the four dense blocks as well as the transition layers.

After the very last output layer comes a component known as GlobalAveragePooling, which is located at the very end of the process. As we can see in the code block that has just been brought to our attention, the letter ’d’ is used to indicate the dense block. After the completion of the fourth dense block, the information moves immediately into the classification layer, hence there is no need for a transition layer 4 in the very last layer. Therefore, the connection that is designated by’d’ rather than the connection that is denoted by 'x' is the one to which the GlobalAveragePooling method is applied. Another option would be to delete the 'for' loop from the preceding code and stack the levels one after the other without the final transition layer.

Densely connected convolutional networks (Densenet)

DenseNet has recently been proved to be one of the best approaches for visual object detection [64]. ResNet-like, but with a few major differences. The architecture is kept as simple as possible to enable for the greatest potential level of connectivity across the network's various tiers. As the feature map was scaled throughout the network, the densely connected neural network, known as Dense Net, was built by directly linking each layer to all subsequent levels. These diverse network topologies were the catalysts for interlayer communication. Unlike many other networks, DenseNets, including ResNet, links the layer's output feature map to the input feature map rather than summing it. Different revisions of this framework (DenseNet101, DenseNet169, and DenseNet201) accept 224x224 pixel inputs.

3.6. Fitting the Model (Model Setup)

The train set, testing set to determine testing loss and accuracy, class weights, callback list, and the number of epochs are all given in order to fit the model. Learning Rate - The goal of utilizing stochastic gradient descent during training is to obtain the least amount of loss between the training set's actual and anticipated values. The approach to loss minimization involves a few steps. Adam is an adaptive learning rate approach, which means it computes distinct learning rates for each of the different parameters.

1. Loss function - Because this is a binary classification, the binary cross entropy is used during training for loss evaluation.
2. Metrics - A calculation was performed to measure how frequently real labels match forecasts. Based on the loss, it will calculate the training and testing accuracy.
3. Callback list - In this work, early stopping is utilized to halt the epochs depending on some metric and criteria, such as reducing the learning rate when a metric has ceased improving. This prevents the model from becoming over-fit to the data, which might cause issues. Once learning has reached a plateau, it is generally advantageous for models to slow down their knowledge acquisition by a ratio of two to ten. This call-back monitors a specific quantity, and if no noticeable improvement is seen after a predetermined amount of time (the "patience"), the learning rate is slowed.
4. Applying Class Weights - It emphasizes applying class weights for each class, particularly the minority class, so that the model can learn from all classes in a comparable manner.

The hyper-parameters that are adjusted before beginning the training process are detailed in Figure 3.9.

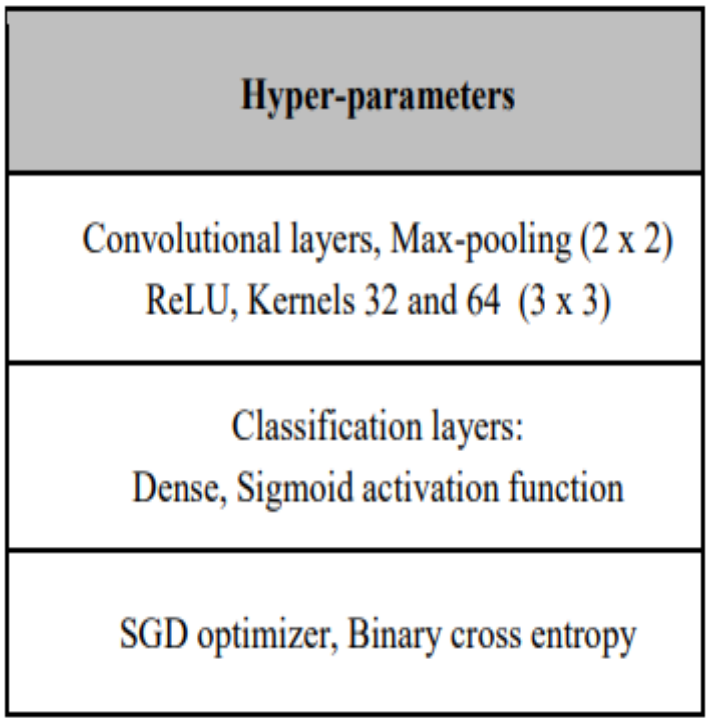


Figure 3.9. Training Process Hyper-parameter

3.7. Training and Testing

A deep learning algorithm, transfer learning, and an ensemble are all part of these components. Deep learning algorithms include CNNs, RNNs, MPNNs, and deep belief networks, among others. Due to the vast number of possible permutations, the learning procedures of various algorithms vary. Some algorithms work better with specific kinds of data. The use of CNN is highly beneficial when dealing with images. The chosen deep learning algorithm should be based on the properties of the supplied data. What we call "transfer learning" happens when one model teaches another. The classification procedure makes use of what is called a "ensemble" of models. Knowledge transfer and Two methods that can be employed to save training time, enhance classification accuracy, and minimize overfitting are ensemble learning and transfer learning.

The process that neural networks go through in order to carry out the learning operation is referred to as "training" in this context. During training [98], the network is supplied with the returned features, and based on the mistakes it makes, the network is modified. When there is no longer any generalization progress, as shown by a rise in the mean square error of the testing samples, training will automatically end. In machine learning, the act of evaluating a network's generalizability is known as testing

Testing does not influence the training process, and as a result, it provides an independent measurement of network performance both during and after training. The image is then subjected to a capable neural network for testing, and it is compared with images that were used for training in the past in order to calculate the percentage of accurate and incorrect calculations. During testing, which was very similar to the process of training, received images went through all of the preprocessing steps and were made available to the network for simulation. The input in a simulation of a network object represents image data, and the output imitates the network. Simulation is the method of network object. After the images have been examined, the correct counter and error counter for each image in the database are incremented, and the system then provides the results it has determined to be accurate.

3.8. Performance Criteria

A standard measurement is used to verify both the acceptance error and the rejection error in order to assess the level of success achieved by the system. They can be defined as under:

- Classification Confusion Matrix
- F1 Score
- Accuracy
- Recall
- Precision
- Receiver Operation Characteristic

3.8.1. Classification confusion matrix

One measure that can be used to determine how well the neural network has fitted the data is called the confusion plot. In any investigation, each sample can be represented graphically in the confusion matrix, which provides an estimate of the proportion of appropriate to inappropriate classifications. It provides what is known as the confusion value, which indicates the proportion of incorrectly classified cases. The correct classifications are represented by green squares on the diagonal of the matrix, while incorrect classifications are represented by red squares [99].

Initially, the purpose of developing the confusion matrix was to serve the purpose of performing an analysis on the results of the binomial classification. As a consequence of this, the very first thing that needs to be done is to decide which of the two classes will serve as the class of interest, and the positive class should be the one chosen. In the target column, we need to decide (in a totally arbitrary manner) which value will stand for the positive class. After that, the other value is instantly labelled as part of the negative category because it fits the criteria. Figure 3.10 shows illustration of a confusion matrix that can be used for binary classification.

Confusion Matrix		Predicted		
		Class 1	Class 2	Class 3
Actual	Class 1	A	B	C
	Class 2	D	E	F
	Class 3	G	H	I

True positives True Negatives Misclassified cases.

Figure 3.10. Confusion matrix

The counts from both expected and actual values are included in confusion matrices. The amount of successfully detected negative situations is shown in the "TN" output, which stands for "True Negative".

A diagnostic test result is termed a true positive when it reveals the existence of disease in a patient who has previously been diagnosed with the disease and when the same test also indicates the presence of disease. A diagnostic test yields a true negative result when it can be proved that a disease does not exist in a patient and the test also reveals that the disease does not exist (TN). A consistent result between the diagnostic test and the known illness is shown by the existence of both true positive and true negative findings, sometimes referred to as the standard of truth. There isn't a medical test that is flawless, though. A diagnostic test result is considered false positive (FP) if it indicates that a patient has an illness when they actually don't. In a similar vein, a false negative test result indicates that a patient who is unmistakably afflicted with the condition in issue does not have the illness (FN). Both false positive and false negative results imply that the test was performed improperly and that the condition being tested for does not actually.

3.8.2. F1 Score

In binary classification, the F1 score is a popular metric for evaluating the model's performance that takes recall and precision into account. Recall evaluates the model's capacity to capture all positive instances, whereas precision examines the accuracy of the model's positive predictions. A well-rounded evaluation of a model's performance is provided by the F1 score, which is the harmonic mean of recall and precision.

To get the F1 score, which is the harmonic mean of recall and precision, the formula is as follows:

$$F1\ Score = \frac{2.P.R}{\mathrm{P+R}} \tag{3.4}$$

This metric ranges from 0 to 1, where 1 indicates perfect precision and recall, and 0 indicates poor performance. The harmonic mean is used to balance precision and recall, penalizing extreme values and providing a more representative measure of a model's effectiveness in handling both false positives and false negatives.

3.8.3. Accuracy

One of the most often used metrics for classification activities is accuracy. The accuracy of a model utilizing a confusion matrix is determined using the formula described below. The following formula is provided.

$$Accuracy = \frac{TP+TN}{\mathrm{TP+FP+FN+\ TN}} \tag{3.5}$$

If TP is the value that indicates a true positive, then the prediction is accurate. On the other hand, if FP is the value that indicates a false positive, then the prediction that an abnormality is present is inaccurate. Where TN is the value that indicates a true negative, meaning that there is no abnormality present in a healthy person, and FN represents the fact that there is no recognition of a malignant lesion found, the latter turns out to be false.

There are alternative measures that are based on confusion matrix that might be useful for measuring performance since accuracy can generate false results when used on datasets that are not uniformly distributed. The "confusion matrix function, which is a part of the "sklearn" module, may be used to generate confusion matrices in Python [100]. Simply enter "from sklearn.metrics import confusion matrix" in the import window to import this function into Python. Users must supply the function with both their actual and expected values in order to get the confusion matrix.

3.8.4. Recall

We divide the total number of unfavorable events in the dataset by the number of true positive. This includes the true positive (TP), which represents the instances of positive or actual class correctly recognized by the model divided by the TP and the false negative (FN).

$$Recall = \frac{TP}{\text{TP+FN}} \tag{3.6}$$

3.8.5. Precision

The sensitivity of a diagnostic test is the percentage of true positives that it accurately detects. It shows the test's sensitivity to illness detection. A diagnostic test's specificity is defined as the percentage of true negatives that it accurately detects. It shows how well the test can identify unfavorable scenarios (typical conditions). Accuracy is defined as the percentage of actual results in a population, which may be actual positive or actual negative results. It evaluates a diagnostic test's accuracy when used to diagnose a problem and then summarizes its results.

$$Precision = \frac{TP}{\text{TP+FP}} \tag{3.7}$$

The sensitivity of a diagnostic test can be measured in terms of its numerical values, which indicate the likelihood that it will correctly identify patients as having the disease in question. The lower the likelihood that a diagnostic test will produce false-positive results, the higher the numerical value of sensitivity should be. For instance, if the sensitivity is 99%, this indicates that if we perform a diagnostic test on a patient who is suspected of having a particular disease, there is a 99% chance that we will determine that the patient has that disease. An examination using tents with a high degree of sensitivity, with the goal of identifying all of the potential positive conditions without overlooking anyone. As a result, a test that has a high sensitivity is frequently utilized when screening for disease.

3.8.6. Receiver operation characteristic (ROC)

The metric receiver operating characteristic is the most important tool for ensuring the quality of classifiers, which is the most important thing that needs to be done (ROC). The receiver operating characteristic (ROC) analyses outputs by applying threshold values that range from 0 to 1 to each class of a classifier. It is necessary to take into account both the TP Ratio and the FP Ratio when determining each threshold. By dividing the sum of all outputs that are equal to or higher than the threshold by the sum of all one-dimensional objectives, we may find the True Positive Ratio. When all goals are set to zero, the number of outputs below the threshold is divided by the total number of targets to produce the False Positive Ratio.

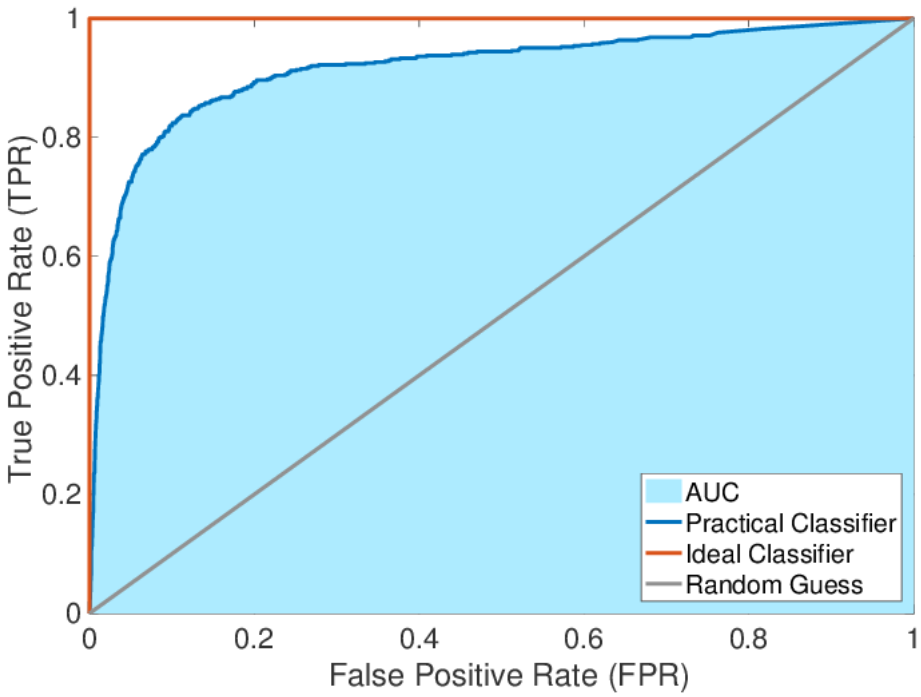


Figure 3.11. Receiver operating characteristics

A plot of receiver operating characteristics (ROC), also known as the receiver operating curve, is shown in Figure 3.11. The genuine acceptance rate (GAR) is plotted along the y-axis and the false acceptance rate (FAR) is plotted along the x-axis for analysing system performance. The true positive rate (TPR) versus false positive rate (FPR) for a certain diagnostic test can be calculated. Where;

$$FPR = \frac{FP}{\text{FP+TN}} \frac{TP}{\text{TP+FN}} \tag{3.8}$$

Table 3.2 provides a summary of the commonly used classification based on the area under the curve (AUC) for diagnostic tests. The AUC range between 0.9 to 1 is considered as excellent.

Table 3.2. ROC AUC accuracy classification range

ROC AUC SCORE	CLASSIFICATION
0.9<AUC<1.0	Excellent
0.8<AUC<0.9	Good
0.7<AUC<0.8	Worthless
0.6<AUC<0.7	Not Good

4. PROPOSED METHODOLGY

To achieve the study's objectives, this chapter proposes an approach that uses the Keras framework for classifying and predicting COVID-19 in chest X-ray pictures. The goal is to give a clear and short explanation of the implemented method. There are a total of 6749 photographs used in the two datasets, which we retrieved and classified from various web sources in advance of the planned work [22, 101]. This study aims to use a Convolutional Neural Network (CNN), a MobileNet (RNN), and additional Densenet layers to forecast and categorize thoracic and chest diseases using X-ray images.

Low-power devices are ideal for the association mechanism known as MobileNet. We first pixel-reduced all of the chest X-ray images before feeding them into a pre-trained model to extract characteristics. Following normalization, all of the photos were brought up to standard using the pre-trained model.

4.1. Classification of Covid 19 Disease Using State of-The-Art Deep Learning Architectures

The ability of CNN to categories images in a variety of scenarios is undeniable. There are numerous CNN versions developed to increase performance according on the characteristics of a particular dataset. Furthermore, CNNs are intended to automate the picture preparation effort required to prepare inputs for classification. First, we adopt CNN-based classification algorithms for chest x-ray categorization in our work. While machine learning algorithms have advanced greatly in recent years, there are currently few publically available medical image datasets. CNNs' end-to-end learning architecture is responsible for the categorization and attribute extraction. CNNs have layers that are pooling, fully connected, and convolutional. The formation of the network architecture and the construction of a high degree of distinguishable feature set for classification are both accomplished by employing the pooling and convolution layers in a sequential order. The fully connected layers require a categorization performance that makes use of the feature set obtained from the layers that came before it. In CNN model training, the traditional back propagation algorithm modifies a significant number of the model's parameters.

We employ the ReLU technique to add a non-linear activation function to the feature map produced by the convolution process. The max-pooling layer's objective is to conjugate the semantically convenient features that were brought up from the layer below it. The max-pooling layer is responsible for carrying out the down-sampling operation by first dividing the layer beneath it into rectangular pooling regions, and then determining the value that represents the maximum of each of those regions.

The last level of CNNs includes a fully linked layer as well as a softmax classifier. The completely linked layer, which sits between the preceding layer and the classification layer, is in charge of transmission. In a nutshell, the fully connected layers can be divided into three stages. During the initial stage of the procedure, the convolution and pooling layer results are flattened and turned to a column vector. This column vector will be used as the second stage's input layer. The previous stage's results are used as inputs for the feature analysis in the second stage, and weights are added to forecast the true labels. The last step is to choose the prediction scores that will eventually be applied to each class label. The general architecture of the employed CNN is shown in Figure 4.1.

```
Model: "sequential"
_________________________________________________________________
Layer (type)                 Output Shape              Param #
=================================================================
conv2d (Conv2D)              (None, 224, 224, 64)      1792

conv2d_1 (Conv2D)            (None, 224, 224, 64)      36928

max_pooling2d (MaxPooling2D  (None, 112, 112, 64)      0
)

conv2d_2 (Conv2D)            (None, 112, 112, 128)     73856

conv2d_3 (Conv2D)            (None, 112, 112, 128)     147584

max_pooling2d_1 (MaxPooling  (None, 56, 56, 128)       0
2D)

conv2d_4 (Conv2D)            (None, 56, 56, 256)       295168

conv2d_5 (Conv2D)            (None, 56, 56, 256)       590080

conv2d_6 (Conv2D)            (None, 56, 56, 256)       590080

max_pooling2d_2 (MaxPooling  (None, 28, 28, 256)       0
2D)

conv2d_7 (Conv2D)            (None, 28, 28, 512)       1180160

conv2d_8 (Conv2D)            (None, 28, 28, 512)       2359808

conv2d_9 (Conv2D)            (None, 28, 28, 512)       2359808

max_pooling2d_3 (MaxPooling  (None, 14, 14, 512)       0
2D)

conv2d_10 (Conv2D)           (None, 14, 14, 512)       2359808

conv2d_11 (Conv2D)           (None, 14, 14, 512)       2359808

conv2d_12 (Conv2D)           (None, 14, 14, 512)       2359808

max_pooling2d_4 (MaxPooling  (None, 7, 7, 512)         0
2D)

flatten (Flatten)            (None, 25088)             0

dense (Dense)                (None, 4096)              102764544

dense_1 (Dense)              (None, 4096)              16781312

dense_2 (Dense)              (None, 2)                 8194

=================================================================
```

Figure 4.1. Convolution neural network architecture

4.2. Proposed Approach

Robust prediction of COVID-19 disease and decreasing gradients with fewer parameters required to train the model are both addressed by the suggested approach. The use of

dynamic feature propagation with Mobile Net and Dense Net guarantees uninterrupted information delivery. The experiment is run using Dense Net version 201, which is DenseNet201. Since it takes an array of chest x-ray images as input, we'll utilize a library function to transform the image into an array-compatible format. It is well-known that the pre-processing step is a crucial part of the whole workflow in image analysis. In addition to enhancing the original image, it can also reduce noise and extraneous objects. In this study, we apply the basic processing methods to the image dataset at our disposal. The procedure for image categorization included the use of a CNN. When it comes to picture classification, the CNN model can get close to matching human accuracy. Convolution layers with pooling and bunch normalizing techniques attached to each other form what is essentially a convolution network. There has been extensive use of CNNs in image processing techniques due to the many advantages they provide.

A convolutional neural network with eight layers was employed in the suggested method. The two components of Conv2D are the ReLU activation function and a convolution layer with thirty-two filters, each with a 3 by 3 measurement. The two 2-by-2 MaxPooling layers. The Dropout layer aids in avoiding overfitting by arbitrarily and at a specified rate setting input to zero at each stage of training. In this particular experiment, the pace is set at 0.8. Without any extra parameters, the data flattening layer (Flatten) was utilized. The activation function ReLU is applied using the Dense layer, with the unit parameters set at 128. The final product is an activation function called SoftMax applied to a Dense layer with three unit parameters. Figure 4.2 illustrates the general procedure of the suggested method.

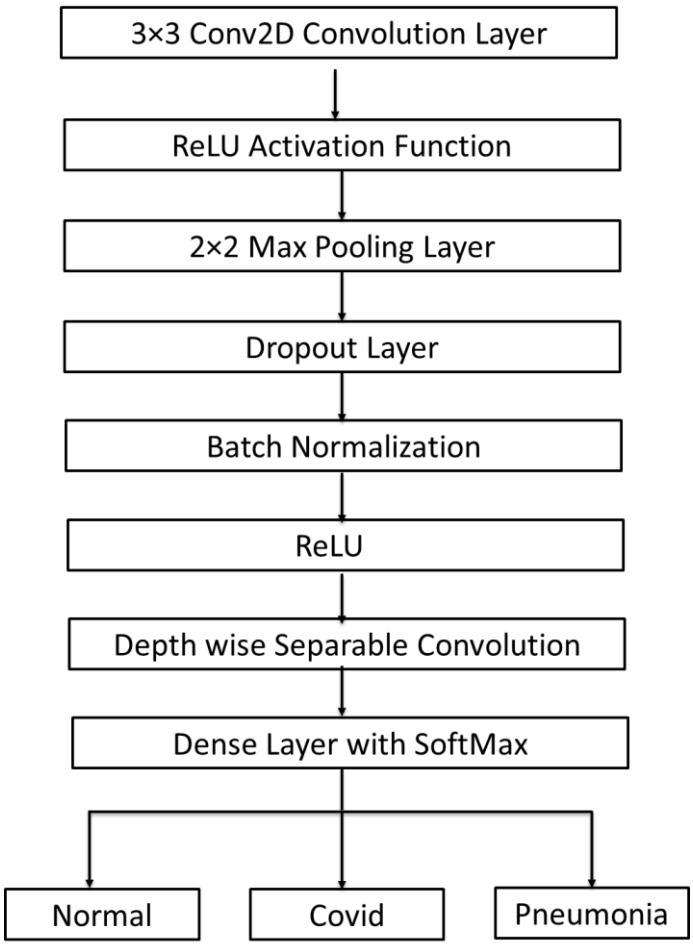


Figure 4.2. A flow chart representing the proposed method

When all of the chest X-ray images have been tagged, we employ the DenseNet with four dense blocks that have equal levels of (224×224) input picture blocks. The input images are convolutioned with a total of sixteen independent output channels before moving on to the first dense block. A constant-sized feature map is guaranteed by employing 3x3 convolutional layers with zero padding on either side. Our activation function is Relu, and after 1x1 convolution, we utilize 2x2 average pooling. A pooling average and a classifier, specifically softmax, are applied once the last dense block is completed. Fully configured using a loss function of "sparse_categorical_crossentropy," twenty iterations for every 64-batches size, and a DenseNet config with the hidden-layer of MobileNet specified as "adam" for the optimizer. Trials utilizing this approach yielded encouraging outcomes. Four metrics—F1-score, recall, accuracy, and precision—were used to evaluate the algorithms. A confusion matrix was used to derive the parameters.

4.2.1. Preparation for training model

In this research, the supervised ML method was used in conjunction with MobileNet, a DNN. We have randomly divided the entire dataset into two parts: a training set that contains 70% of the data and a testing set that contains 30% of the data. This will allow us to make predictions based on the data. The next step was to use the image embedding widget to insert the images. Inception V3 Embedder was utilized in this case. Once all the images were embedded, they were fed into several models to learn how to categorize chest X-rays as normal, pneumonia, COVID-19, or lung opacity.

During the preparation stages, the datasets are loaded and randomly turned into images using the TensorFlow and Keras packages. A maximum of 64 images per batch can be used for training purposes. To start, we gave the MobileNet some inputs (224x224 in size) to work with. To further aid in reducing the feature dimension, the pooling layer 2D (2X2) filter is utilized when dealing with spatial data. Every neuron that is linked to the output has a full connection to the dense layer. Randomly selected neurons make up dropout layers. The next step is to classify the images using optimization approaches and activation functions such as ReLU and Sigmoid.

5. RESULTS AND DISCUSSION

AUC, F1-score, accuracy, precision, and recall were some of the many factors used to compile the prediction findings. To measure how well the prediction model worked, one uses area under the ROC.

5.1. Results of Covid19-dataset

5.1.1. Result of MobileNet model

The results of the performance matrix, including the F1-score, recall, and precision, for MobileNet are displayed in Table 5.1. With a value of 1 for normal and 0.87 for COVID-19 cases of viral pneumonia, respectively, the precision is better. The recall value was found to be 1 for cases of COVID-19 and viral pneumonia and 0.85 for normal, the lowest possible value. The F1 function incorporates both recall and precision. In a case of viral pneumonia, the F1-score is 0.93, while in a normal case it is 0.92 and in a covid-19 condition it is 1. By doing so, we may determine the current state of the precision to recall ratio. The Table 5.1 represents the classification report of the MobileNet model and also presents the Area Under the Curve (AUC) score using the Covid19-dataset. The training accuracy for the "MobileNet "model is indicated as 100%. This signifies that the model properly classified all occurrences throughout the training phase. The "Average" testing accuracy, on the other hand, is stated as 92.16%. During the testing phase, this shows the overall accuracy across all classes.

Table 5.1. Results of the MobileNet performance matrix

Class	Performance Matrix Criteria					
	F1-Score	Recall	Precision	AUC	Training Accuracy (%)	Testing Accuracy (%)
Normal	0.92	0.85	1	0.88	100	92.16
COVID-19	1	1	1	1		
Viral Pneumonia	0.93	1	0.87	0.95		
Average	0.95	0.95	0.95	0.94		

As illustrated in Figure 5.1, the confusion matrix provides insights into the performance of the MobileNet model. When diagnosing COVID-19 cases, the model exhibited perfect precision by correctly identifying all 26 instances and making no errors by classifying them

as normal or viral pneumonia. In contrast, the situation was slightly different for normal cases. While the model successfully classified 17 of these, it wrongly identified 3 normal instances as viral pneumonia. For instances of viral pneumonia, the model demonstrated impeccable accuracy, correctly categorizing all 20 cases without any misclassification.

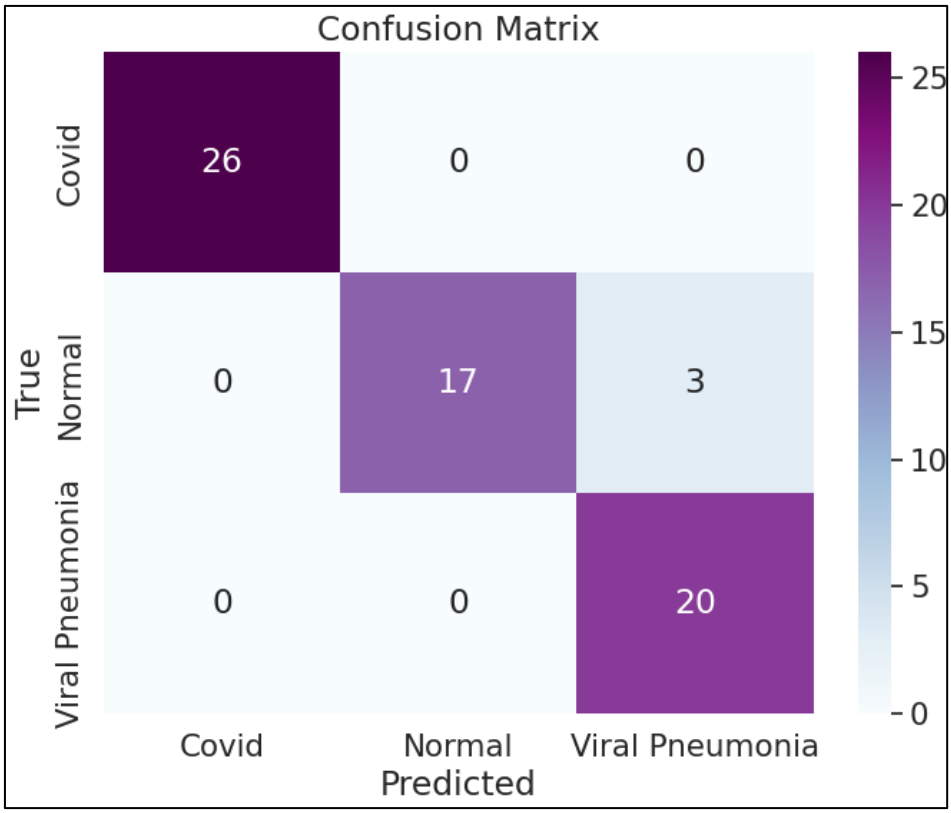


Figure 5.1. Confusion matrix of MobileNet

Even though the MobileNet model made a few errors in classifying normal cases as viral pneumonia, its overall effectiveness is undeniable. It demonstrated outstanding accuracy in diagnosing both COVID-19 and viral pneumonia cases. Hence, despite the minor inaccuracies, the model exhibits a strong performance based on the high accuracy rate across all three classes.

As shown in Figure 5.2, the results of these performance matrices are graphically represented. The training and testing classes Figures 5.3 and 5.4 display the accuracy and loss graphs for the MobileNet model that was used. Figure clearly shows that as the neural network progresses through its epochs, the testing and training losses reduce.

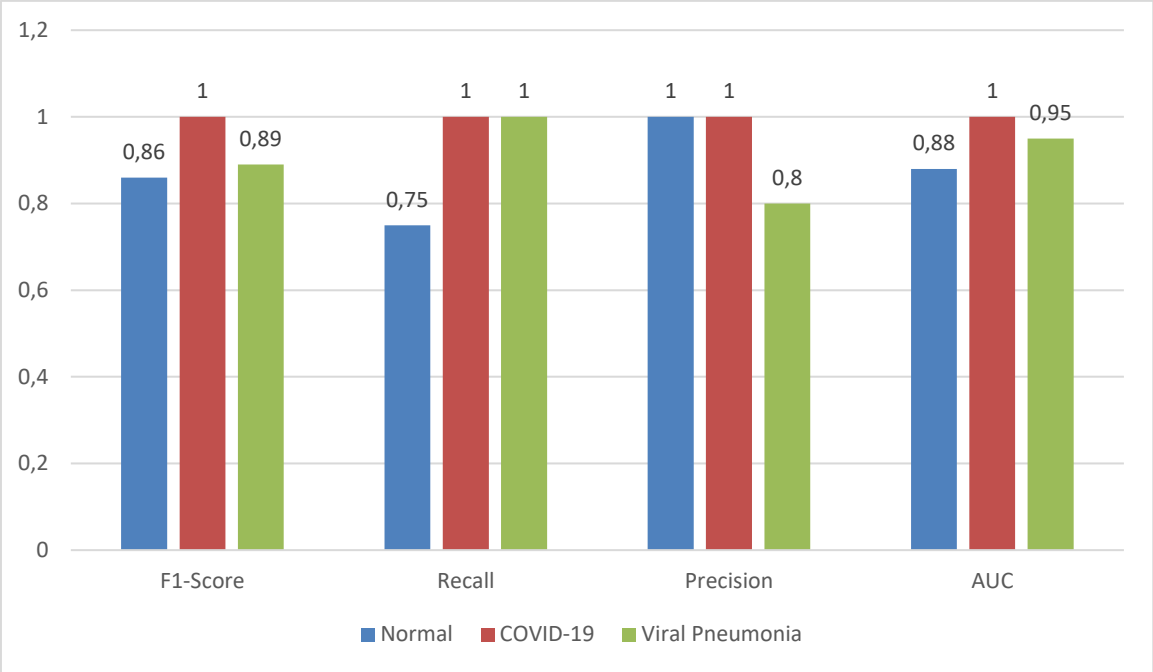


Figure 5.2. Graph of Obtained results of test accuracy for MobileNet

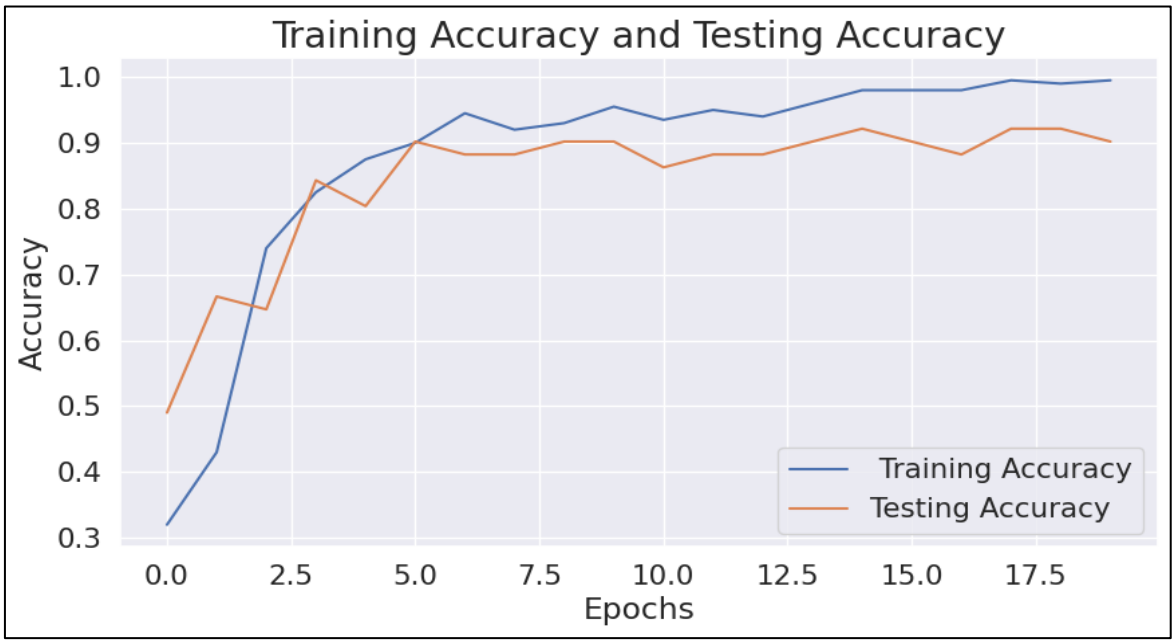


Figure 5.3. Training accuracy and testing accuracy of MobileNet model



Figure 5.4. Training loss and testing loss of mobile Net model

Figure 5.5 also displays Mobile Net's ROC curve. As with the chest x-ray dataset, this Mobile Net graph provides a 100% region for COVID-19, an 88% region for normalcy, and a 95% zone for viral pneumonia. A trade-off between specificity and sensitivity is shown by the ROC curve. Classifiers with more tightly packed curves in the upper left corner tend to perform better.

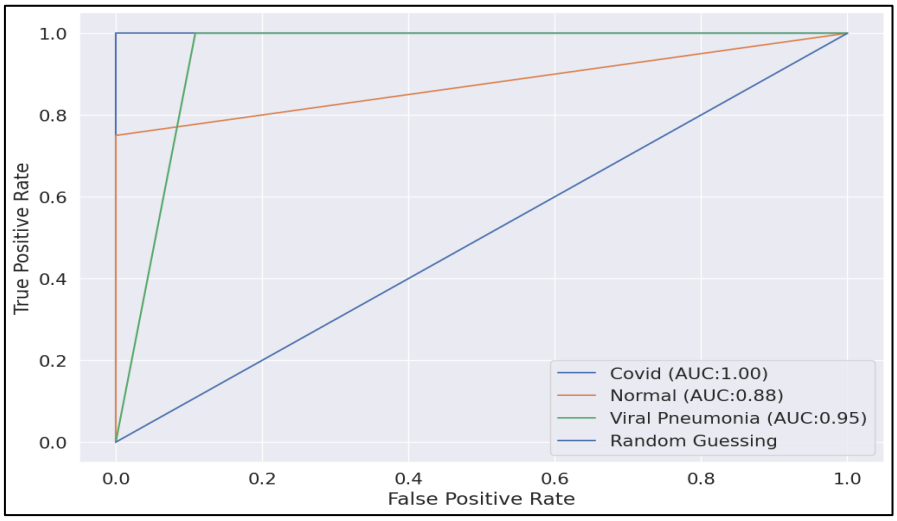


Figure 5.4. ROC curve for MobileNet

5.1.2. Result of CNN model

The precision, recall, and F1-score, which make up the CNN performance matrix, are displayed in Table 5.2. In the case of viral pneumonia, the precision value is 0.94, while in the case of normal pneumonia it is 1 and 0.90. With a recall value of 1 for COVID-19, 0.90 for normal, and 0.90 for viral pneumonia cases, we can draw some conclusions. The F1 function incorporates both recall and precision. For COVID-19, the F1-score is 1, while for normal and viral pneumonia cases it is 0.90. By doing so, we may determine the current state of the precision to recall ratio. The CNN model's training accuracy is reported to be 100%. This means that the CNN properly classified all instances in the training dataset across all classes throughout the training phase.

The testing accuracy is reported as 94% on average across all classes. This shows the CNN model's overall accuracy when predicting instances in the testing dataset across all classes.

Table 5.2. Obtained results of performance matrix for CNN

Class	Performance Matrix Criteria					
	F1-Score	Recall	Precision	AUC	Training Accuracy (%)	Testing Accuracy (%)
Normal	0.90	0.90	0.90	0.93	100	96.08
COVID-19	1	1	1	1		
Viral Pneumonia	0.90	0.90	0.90	0.93		
Average	0.91	0.92	0.92	0.94		

The graphical representation of these performance matrix result shows in Figure 5.6.

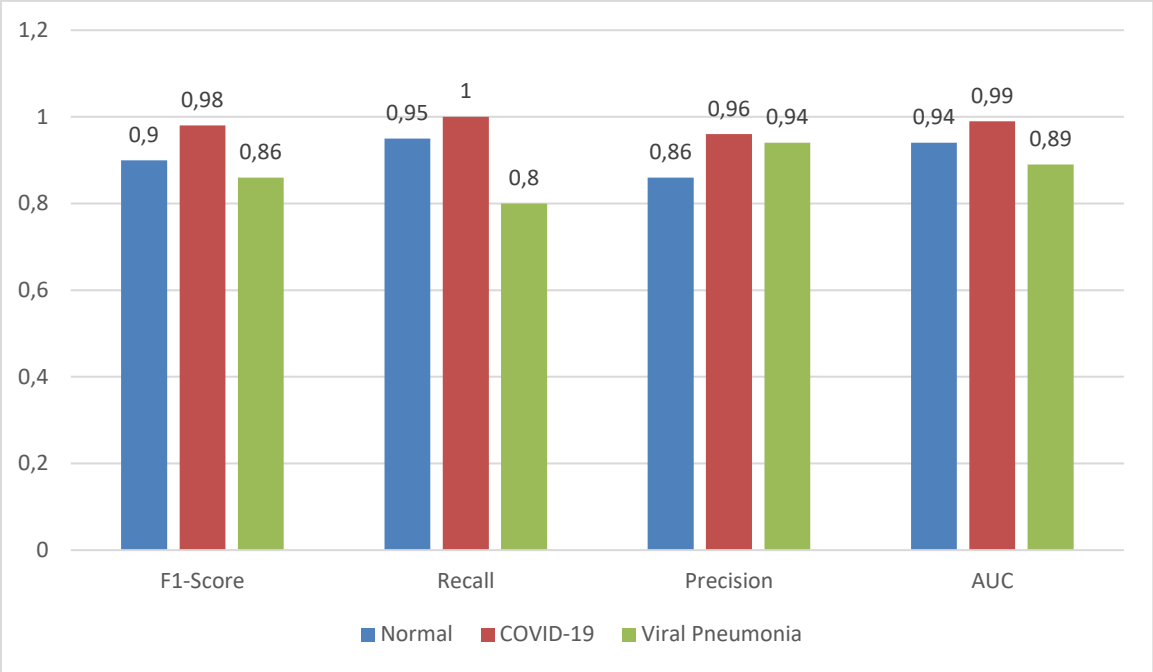


Figure 5.6. Graph of Obtained results of performance matrix for CNN

As depicted in the confusion matrix in figure 5.7, the Convolutional Neural Network (CNN) model's performance is reflected across three classes: COVID-19, Normal, and Viral Pneumonia.

Out of all COVID-19 cases, the CNN model accurately predicted 25, while misclassifying 1 case as viral pneumonia. The model demonstrated no errors in misidentifying COVID-19 as normal. When it comes to normal cases, the model successfully classified 19 instances correctly. However, it made an error by misclassifying 1 normal case as viral pneumonia. As for viral pneumonia cases, the model accurately identified 16 out of the total. However, there were 4 instances that were actually viral pneumonia but were incorrectly classified by the model as normal cases.

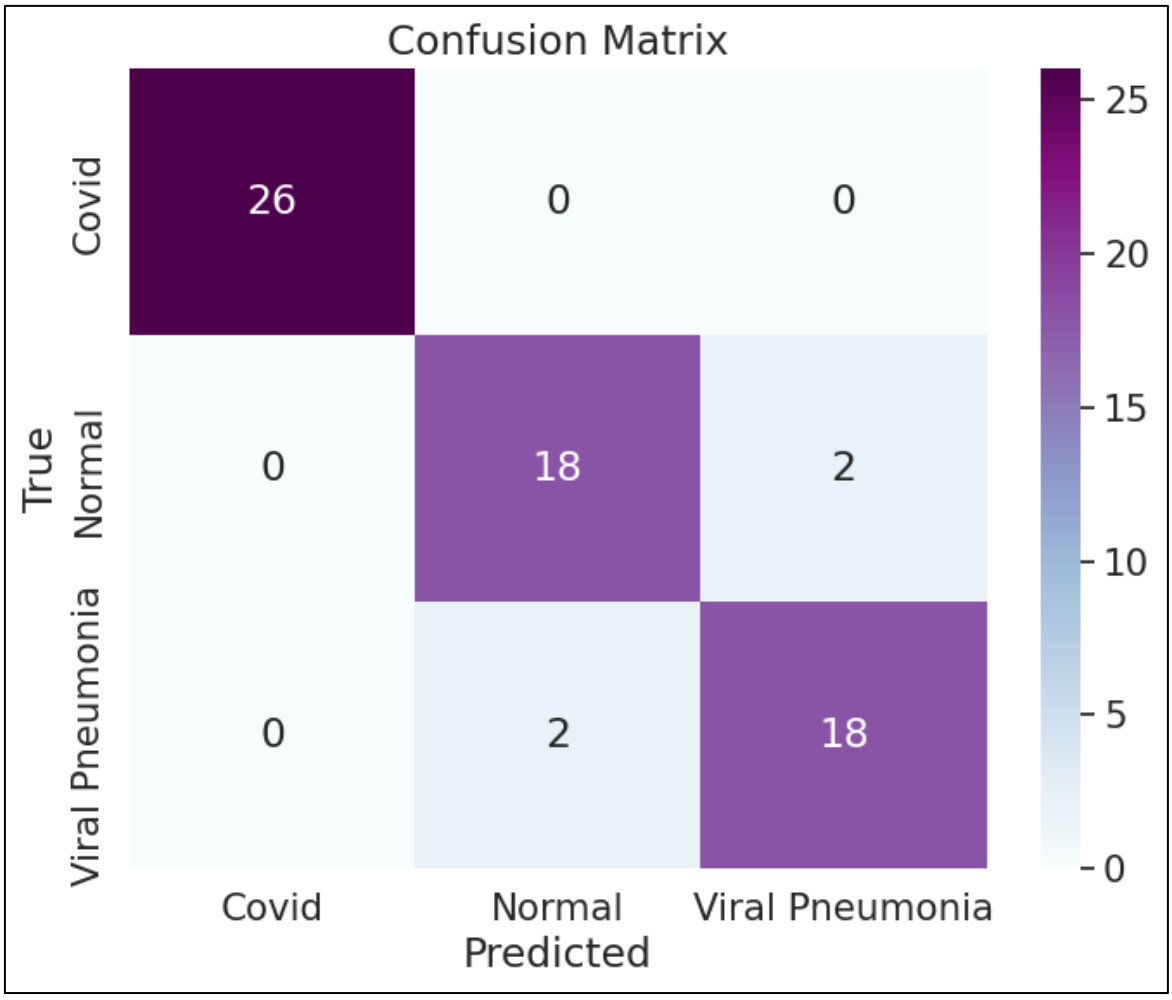


Figure 5.7. Confusion matrix of CNN

The CNN model showed strong performance in identifying COVID-19 and normal cases, with a slight weakness in correctly classifying all viral pneumonia cases. It also had a few instances where it misclassified COVID-19 and normal cases as viral pneumonia and vice versa, but overall, its correct classification rates remained high for all three classes.

To analyze the test's efficacy, the ROC was used. The native CNN method's ROC curve is displayed in Figure 5.8. From the chest x-ray dataset, this ROC curve for the native CNN approach gives a total area of 99% for COVID-19, 94% for normal, and 89% for viral pneumonia. In the section that follows, we will compare the accuracy results of this CNN method to those of alternative approaches.

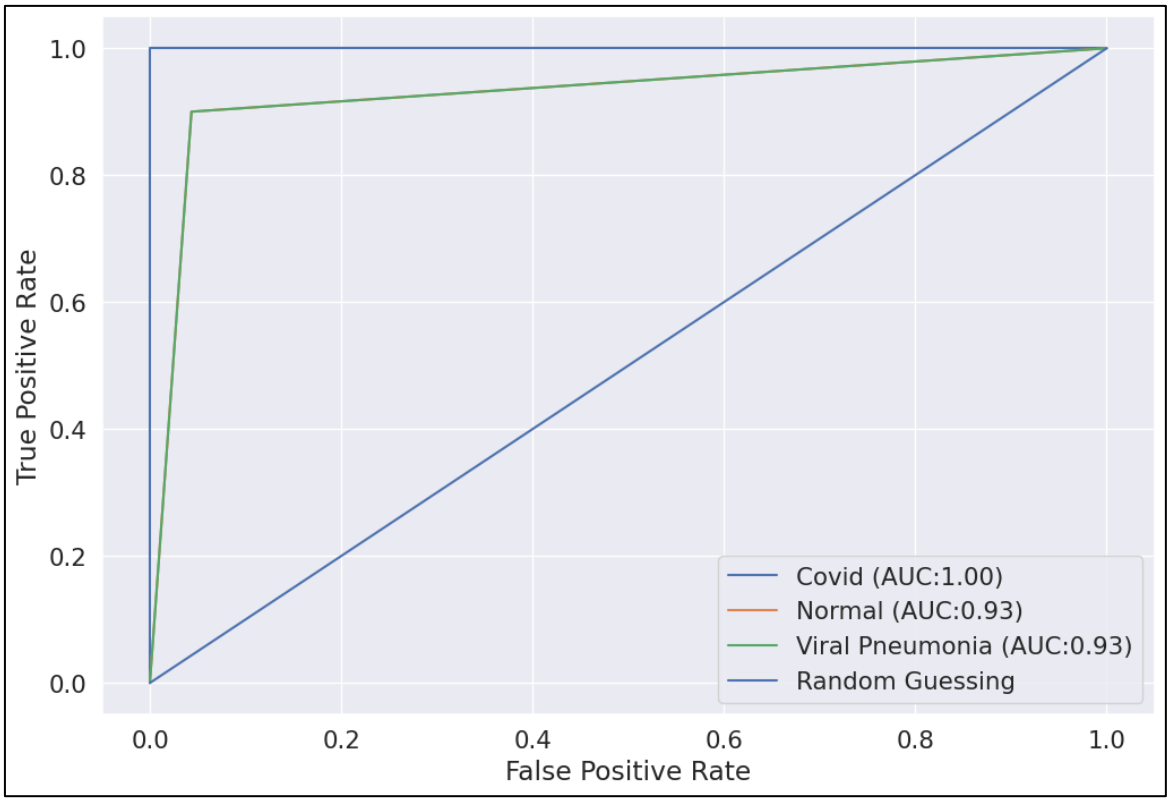


Figure 5.8. ROC curve for CNN

The educational and evaluation Precision and decline Figures 5.9 and 5.10 display the graphs for the CNN model that was utilized. Figure clearly shows that the testing and training losses reduce as the neural network ages. Twenty epochs were executed throughout the training period to determine the accuracy and loss of the model. It specifies when to apply the trained model's weights during inferencing.

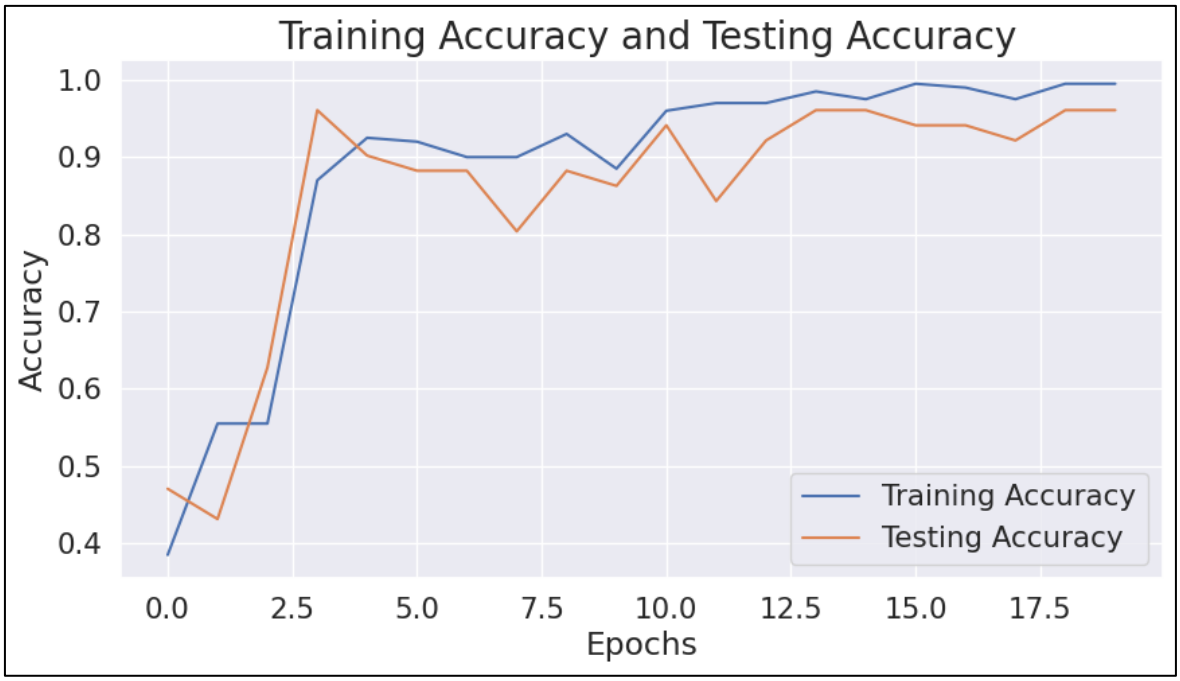


Figure 5.9. Training Accuracy and Testing accuracy of CNN model



Figure 5.10. Training Loss and Testing Loss of CNN model

5.1.3. Result of DenseNet model

Table 5.3 displays the Densenet approach's performance matrices for these criteria, taking into account the procedure that we have provided. The proportion of correctly classified

instances that are true positive tuples relative to the total number of examples that were actually expected to be positive is what precision takes into consideration. A measure of how many true positives there were relative to the overall number of instances. The F1 function incorporates both recall and precision. As a result, we can measure the current ratio of recall to precision. The precision values for normal and COVID-19 cases of viral pneumonia are 0.83, 1, and 0.89, respectively, which is greater. A viral pneumonia case yielded a recall value of 0.80, a normal case of 0.95, and a COVID-19 case of 0.96. In a normal instance, the F1-score is 0.88; in a case of COVID-19, it is 0.98; and in a case of viral pneumonia, it is 0.89. According on the performance matrices, the proposed Densnet method is superior to the CNN and MobileNet approaches. It is possible to see the outcomes of the performance matrix in Figure 5.11. The Densenet model's classification report and AUC score on the Covid19 dataset are displayed in Table 5.3. It has been reported that the Densenet approach achieves a training accuracy of 100%. This means that the Densenet model trained to perfection, correctly classifying every instance in every class in the training dataset.

Overall, the course-wide average for test accuracy is 98.04%. This represents the Densenet model's average accuracy across all classes when predicting instances in the testing dataset. The model's predictions were spot on during the testing period, as indicated by the reported number of 98.04%.

Table 5.3. Results of the Densenet Approach's performance matrix

Class	Performance Matrix Criteria					
	F1-Score	Recall	Precision	AUC	Training Accuracy (%)	Testing Accuracy (%)
Normal	0.88	0.95	0.83	0.90	100	98.04
COVID-19	0.98	0.96	1	0.98		
Viral Pneumonia	0.89	0.80	0.89	0.95		
Average	0.91	0.90	0.90	0.94		

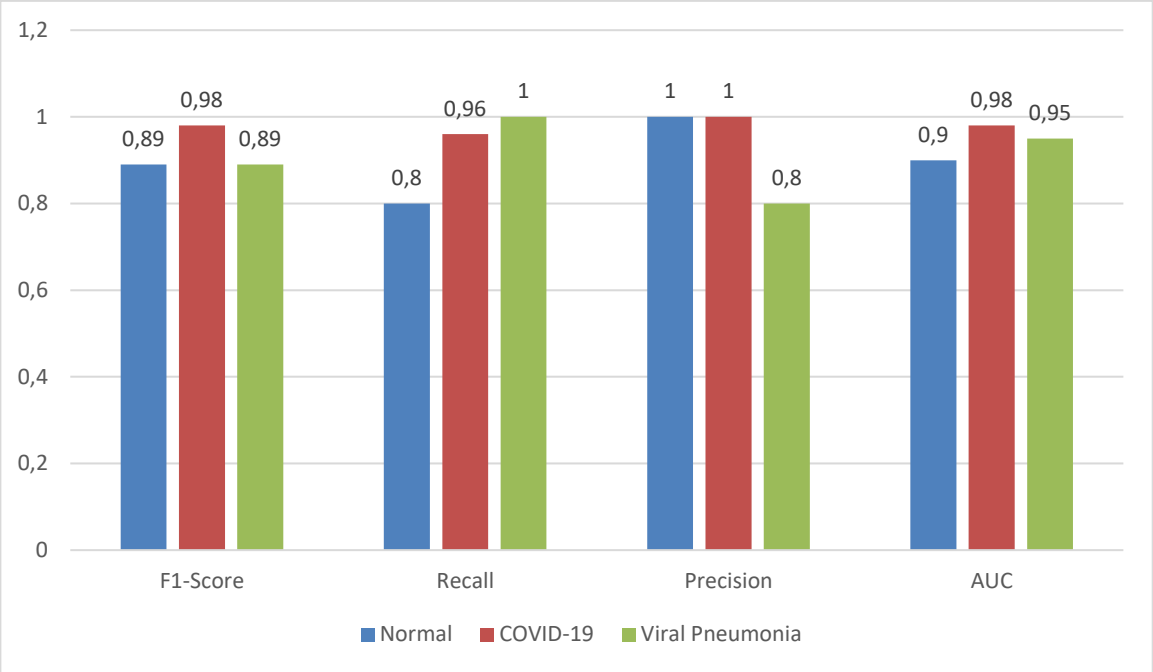


Figure 5.11. Graph of Obtained results of performance matrix for Densenet Approach

The provided confusion matrix sheds light on the performance of the DenseNet model across three categories: COVID-19, Normal, and Viral Pneumonia, as shown in figure 5.12.

When it comes to COVID-19 cases, the DenseNet model showed impeccable accuracy, successfully categorizing all 26 instances without any mislabeling as either normal or viral pneumonia. In terms of normal cases, the model accurately detected 15 of them. However, it encountered a slight challenge in differentiating between normal and viral pneumonia, as evidenced by the 5 normal cases it mistakenly identified as viral pneumonia. In the viral pneumonia category, the DenseNet model's performance was spotless, with an accurate prediction for all 20 cases and zero misclassifications.

Although the DenseNet model exhibited impressive efficacy, especially in accurately categorizing COVID-19 and viral pneumonia cases, it showed minor difficulty in distinguishing normal cases from those of viral pneumonia, leading to some misclassifications. Despite this, the overall rate of correct classification for all three classes remained notably high, underscoring the model's robust performance.

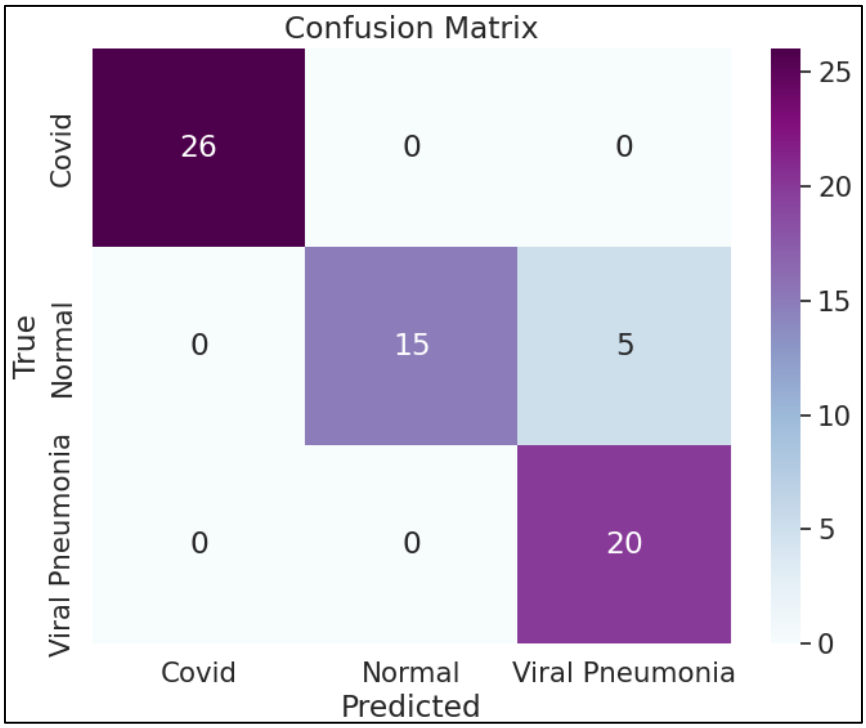


Figure 5.12 Confusion matrix of DenseNet

Figures 5.13 and 5.14 display the training and testing accuracy and loss graphs for the dataset that was employed. Figure clearly shows that the testing and training losses reduce as the neural network ages. Twenty epochs were executed throughout the training period to determine the accuracy and loss of the model. It specifies when to apply the trained model's weights during inferencing.

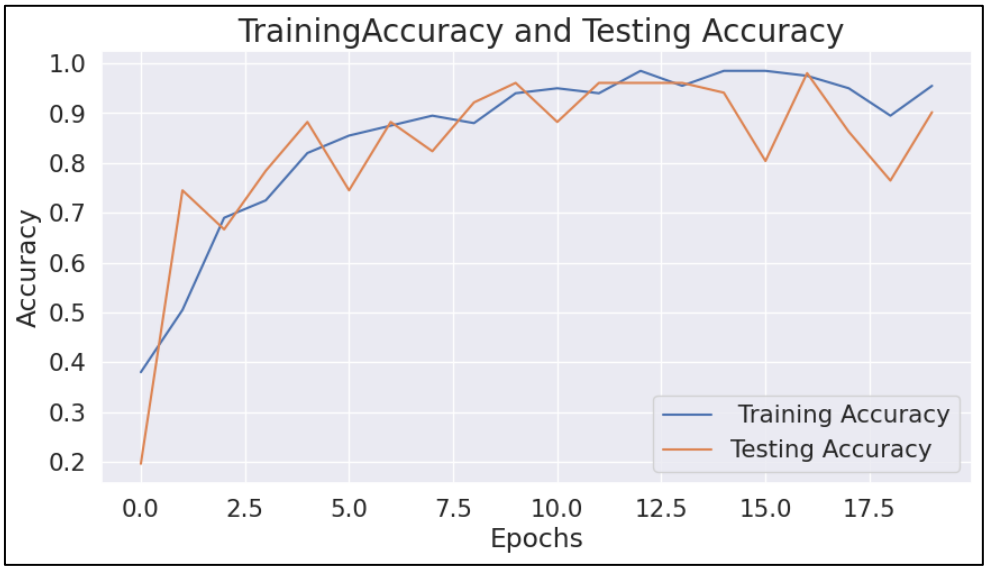


Figure 5.13. Training accuracy and testing accuracy of dense Net method

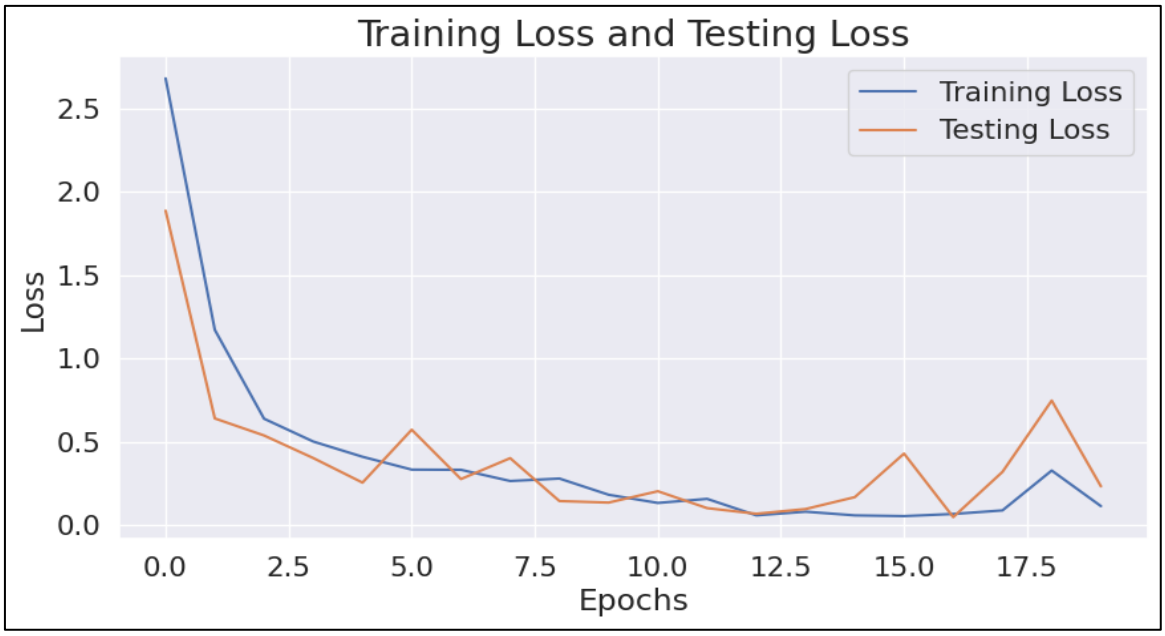


Figure 5.14. Training loss and testing loss of dense Net method

Figure 5.15 shows the ROC of the Dense Net technique in the form of a curve. According to the ROC curve, this approach successfully detects 98% of cases of COVID-19, 90% of normal cases, and 95% of viral pneumonia cases using the x-ray dataset. Out of the three types of x-ray images, the densenet approach had the best receiver operating characteristic (ROC) for detecting cases of COVID-19 and viral pneumonia.

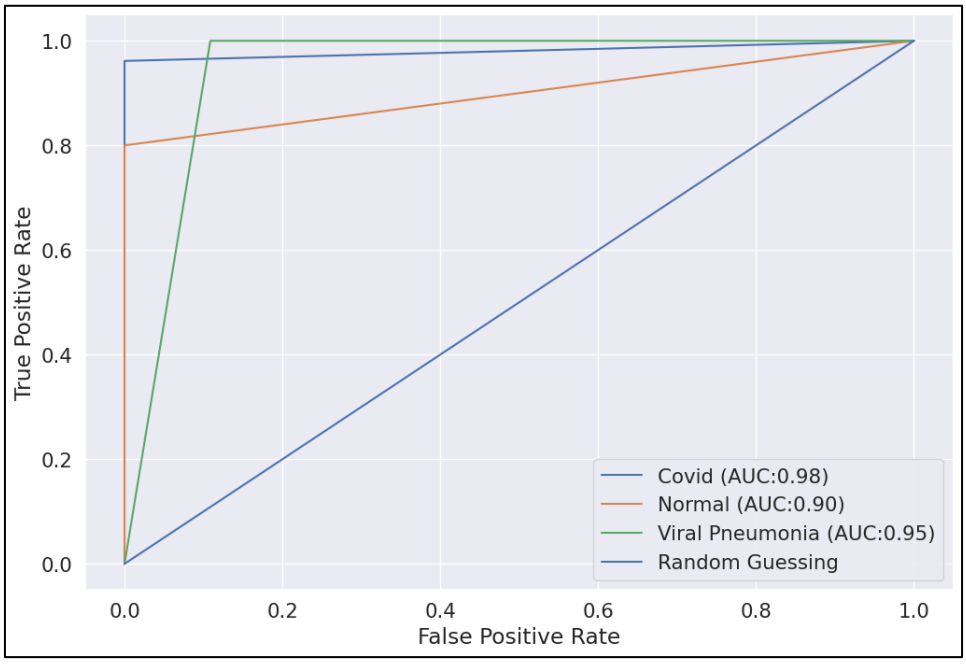


Figure 5.15. ROC curve for DenseNet method

5.1.4. Accuracy comparison of CNN, MobileNet and DenseNet

The Table 5.4 indicate the obtained result of accuracy for CNN, MobileNet and Densenet method. The training and testing accuracy for CNN method calculated as 100% and 96.08% respectively. The precision is stated as 93%, which means that 93% of the times the model made a positive prediction, it was correct. Similar to the accuracy of the model (93%), the recall is also extremely high (93%). As the harmonic mean of precision and recall, the F1-Score of 92% provides a well-rounded evaluation of the model's efficacy. The MobileNet method obtain the training and testing accuracy as 100% and 92.16% respectively. The precision is stated as 94%, which means that in 94% of cases, the predictions were correct. In other words, the model correctly predicted 93% of real-world positive cases (93% recall). The F1-Score (in percentage) provided indicates a balanced assessment of precision and recall, with a value of 92%. The highest accuracy obtains from the DenseNet method i.e., 100 % for training accuracy and 98.04% accuracy for testing. The precision is stated as 94%, which means that in 94% of the cases the predictions were correct. The model was able to correctly identify 93% of real-world positive examples, as measured by recall (in percentage). The F1-Score (%) is 92%, which is a good compromise between accuracy and recall. So, we can say the Densenet method is best method compare to native CNN and MobileNet methods. The complete results with all the metrics are presented in the Table 5.9, currently we only compare the results using deep learning models with Covid19-dataset.

Table 5.3. Accuracy results for the CNN, MobileNet, and Densenet methods

Method	Accuracy		ROC AUC Score	Precision (%)	Recall (%)	F1-Score (%)
	Training	Testing				
Mobilenet	100%	92.16 %	0.94	0.93	0.92	0.92
CNN	100%	96.08 %	0.93	0.93	0.92	0.92
Densenet	100%	98.04 %	0.94	0.93	0.92	0.92

Figure 5.10 further displays a comparison of the acquired result's accuracy with its graphical representation for both the training and testing datasets. A DenseNet approach yielded a ROC AUC score of 0.94 and an improved testing accuracy rate of 98.04%. The ratio of accurate classifications (including both TP and TN) to the total number of cases is a measure of accuracy. Zero to one is the typical range. The predictions become more precise as they get closer to 1.

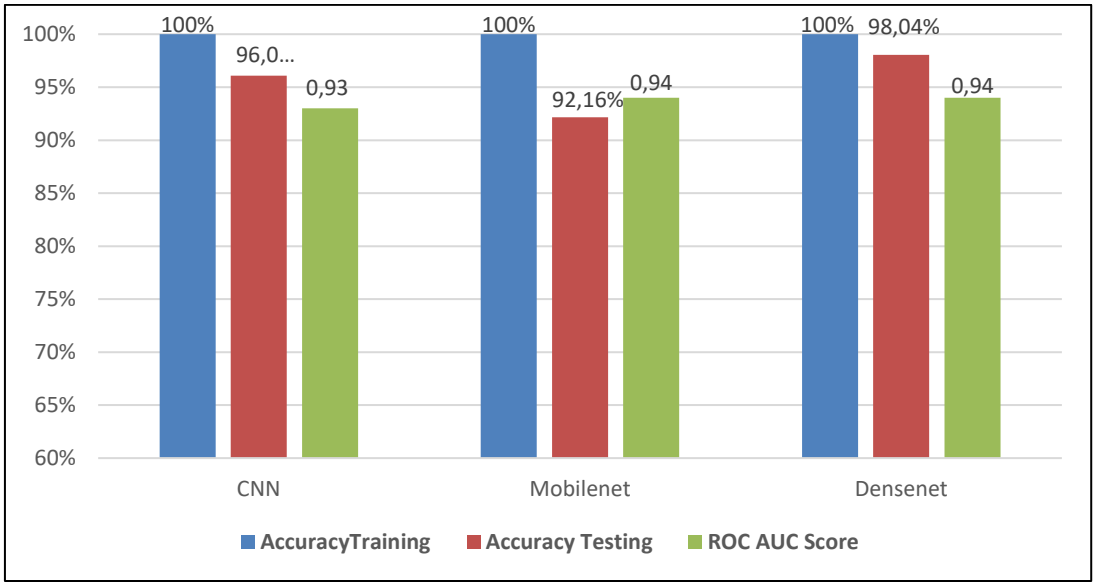


Figure 5.16. Graphical representation of obtained result of accuracy

5.2. Results of Chest X-ray (Covid-19 & Pneumonia)

5.2.1. Results of MobileNet model

Table 5.5 and Figure 5.17 and Figure 5.18 present a detailed summary of the MobileNet model's performance matrix findings using Chest X-ray (Covid-19 & Pneumonia) dataset, measuring its classification performance across three classes: Normal, COVID-19, and Viral Pneumonia. The model performs well for Viral Pneumonia, with an F1-Score of 0.91, Recall of 0.85, Precision of 0.97, and AUC of 0.89. While it has a reasonable F1-Score of 0.74 for Normal, it shines in Recall (0.97) but falls short in Precision (0.60). In contrast, for COVID-19, the model performs reasonably well, with an F1-Score of 0.66, Recall of 0.50, Precision of 0.98, and AUC of 0.75. The average metrics across all classes show a decent overall performance, with an F1-Score of 0.77, Recall of 0.77, Precision of 0.85, and AUC of 0.84. These findings demonstrate the model's ability to categories chest X-ray pictures, with a focus on improving precision for the Normal class. MobileNet achieved a reported 95.15% accuracy during training while utilising the Chest X-ray (Covid-19 & Pneumonia) dataset. Accuracy during training for the MobileNet model, expressed as a percentage, reflecting the number of instances correctly categorised across all classes in the training dataset.

An accuracy of 85.20 percent is provided during testing. This value shows how well the MobileNet model performs on average while making predictions using data from the test set. If you want to know how well your model generalizes to data it has never seen before, you need to know how well it tests. Table 5.5 represents the classification report of the MobileNet model and also presents the AUC score using the Chest X-ray (Covid-19 & Pneumonia) dataset.

Table 5.5. Collecting data for the Mobile Net performance matrix from the Chest X-ray (COVID-19 & Pneumonia) dataset

Class	Performance Matrix Criteria				Training Accuracy (%)	Testing Accuracy (%)
	F1-Score	Recall	Precision	AUC		
Normal	0.74	0.97	0.60	0.90	95.15	85.20
COVID-19	0.66	0.50	0.98	0.75		
Viral Pneumonia	0.91	0.85	0.97	0.89		
Average	0.77	0.77	0.85	0.84		

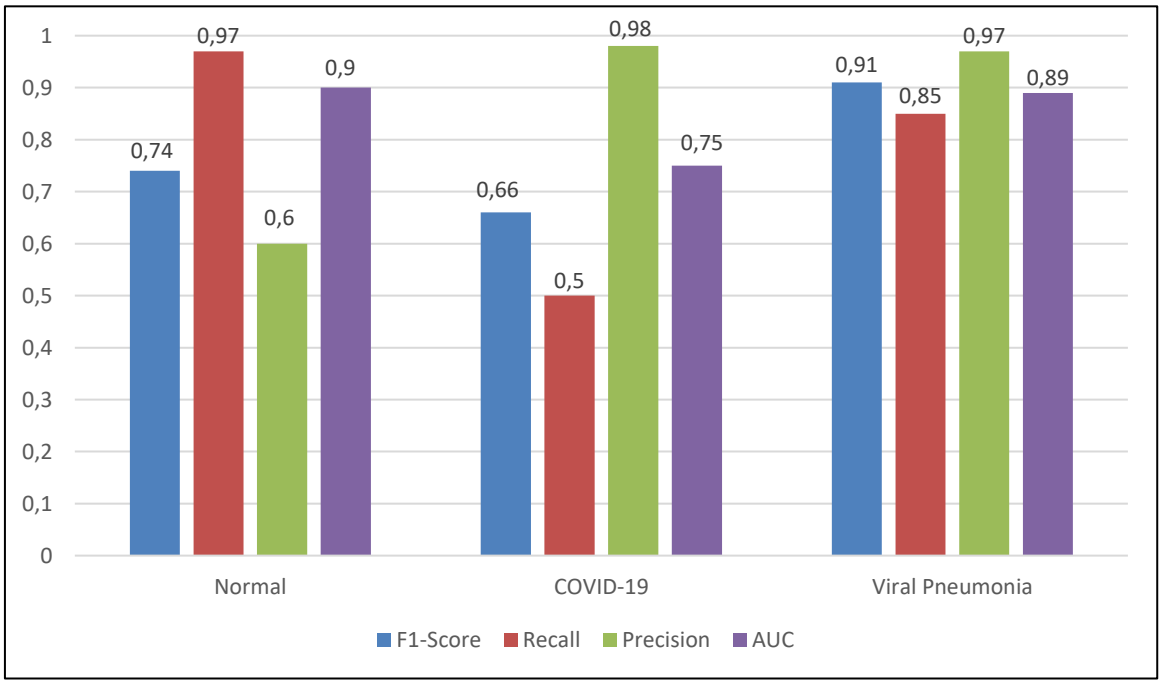


Figure 5.17. Graph of Obtained results of test accuracy for MobileNet using Chest X-ray (Covid-19 & Pneumonia) dataset

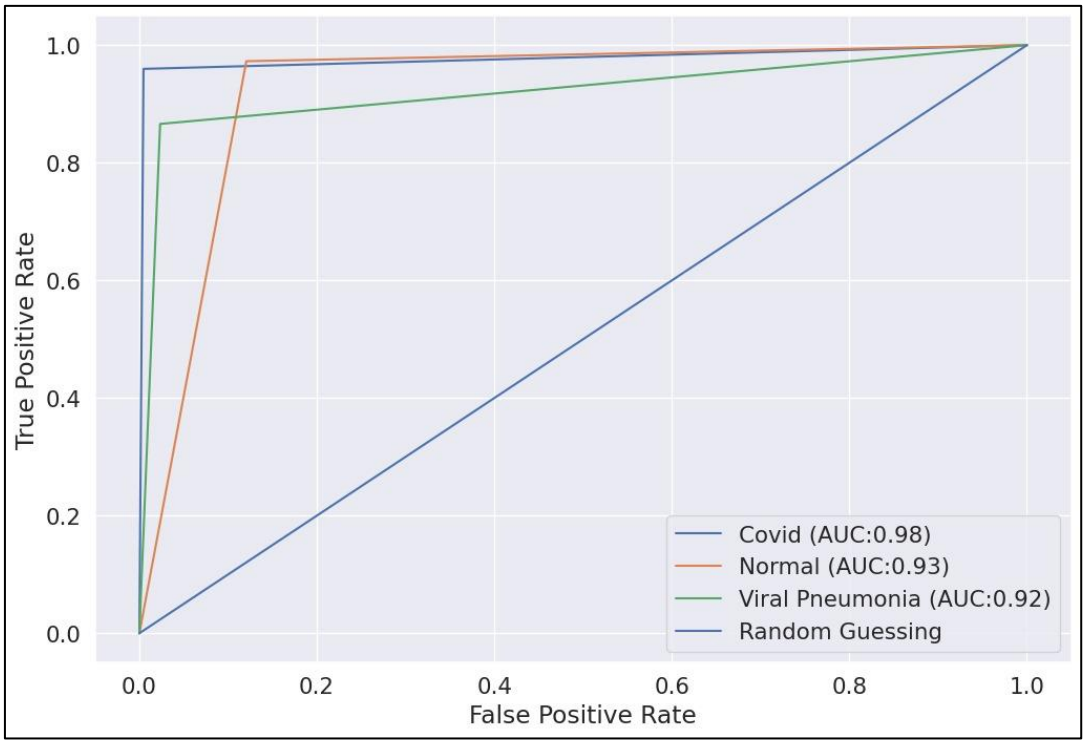


Figure 5.18. ROC curve for MobileNet using Chest X-ray (Covid-19 & Pneumonia) dataset

The Confusion Matrix of the MobileNet Model using Chest X-ray (Covid-19 & Pneumonia) dataset is shown in Figure 5.19. This matrix gives useful information about the model's classification performance. Each row represents the true class, while each column represents the anticipated class. It shows that for COVID-19, the model accurately predicted 59 cases, misclassified 40 as Normal, and misclassified 20 as Viral Pneumonia. Notably, the model performed well in the Normal class, accurately predicting 316 cases and misclassifying only 9 as Viral Pneumonia. However, the model accurately predicted 990 cases of Viral Pneumonia but misclassified 1 as COVID-19 and 174 as Normal. This extensive analysis of forecasts and misclassifications provides a full picture of the model's strengths and places where its classification capabilities may need to be improved.

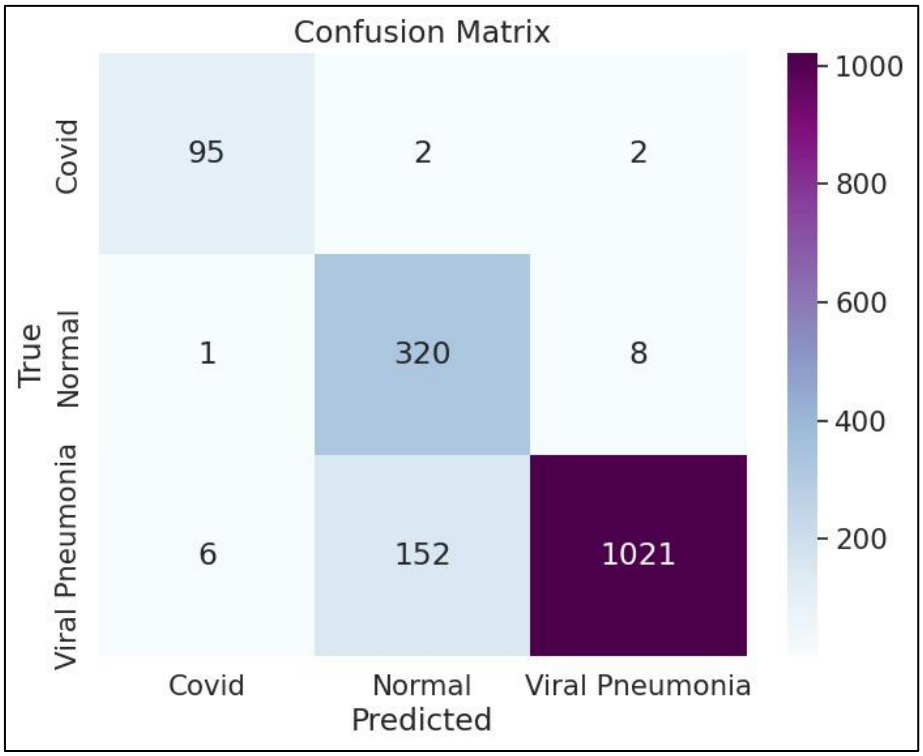


Figure 5.19. The MobileNet Model's Confusion Matrix with the Chest X-Ray (COVID-19 and Pneumonia) Dataset

Figures 5.20 and 5.21 display the model's training and testing performance using the Chest X-ray (COVID-19 & Pneumonia) dataset. These figures illustrate the evolution of the model's loss and accuracy as it is trained. Over the course of 20 epochs, the model's accuracy on the training data increases at a quick pace, reaching approximately 95%, while the loss decreases. Similarly, with testing data, the model experiences an increase in accuracy and a decrease in loss, but with occasional fluctuations. These graphs demonstrate how the model learns and how well it can apply its findings to new data sets. Keeping an eye on these trends will help you assess the model's training and make sure it isn't over- or underfitting the data.

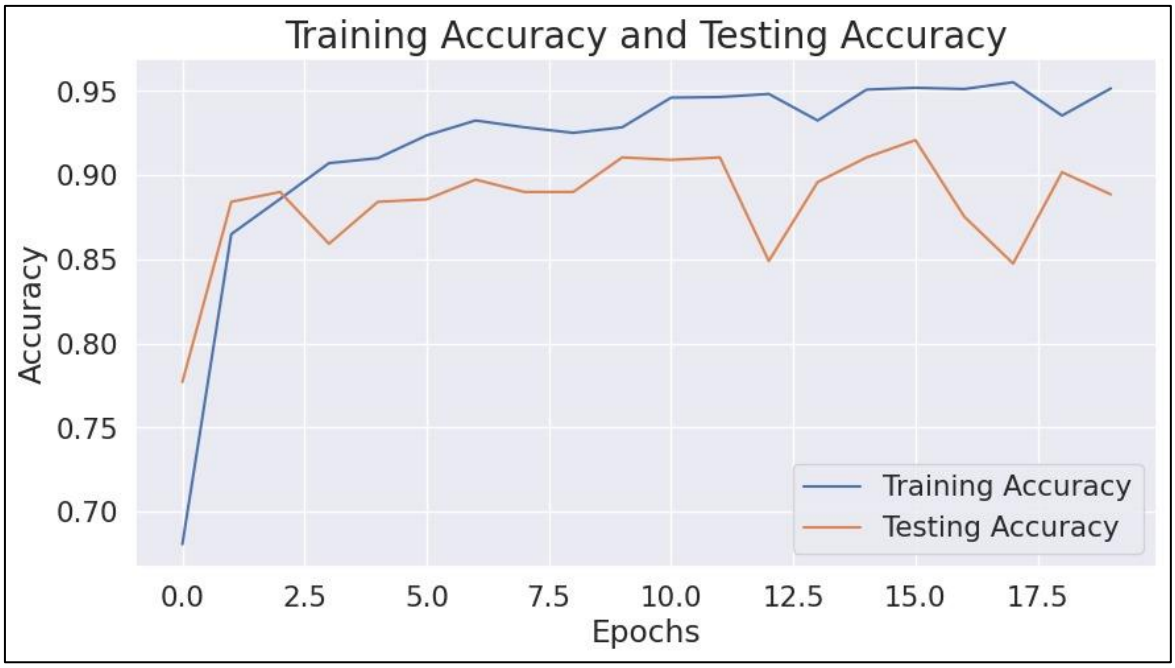


Figure 5.20. Training and Testing Accuracy of Model using Chest X-ray (Covid-19 & Pneumonia) dataset



Figure 5.21. Training and Testing Loss of Model using Chest X-ray (Covid-19 & Pneumonia) dataset

5.2.2. Result of CNN model

The performance matrix results for a CNN model employing Chest X-ray (Covid-19 & Pneumonia) dataset, testing its classification performance across three classes: Normal, The table 5.6, presents the performance of a classification model designed for medical diagnosis, specifically focusing on normal cases, COVID-19, and viral pneumonia. In terms of accuracy, during training, the model achieved 88% accuracy for normal cases, while testing accuracy increased to 91%. For COVID-19 cases, the model exhibited high accuracy, with a testing accuracy of 91%. The highest performance was observed in cases of viral pneumonia, with a 96% testing accuracy. The F1-Score, which balances precision and recall, is 0.88 for normal, 0.91 for COVID-19, and notably high at 0.96 for viral pneumonia. The recall, precision, and AUC values further support the model's proficiency. However, an "Average" row indicates lower performance in an unspecified metric. Despite this, the model demonstrates strong capabilities in accurately classifying medical cases, emphasizing its potential clinical utility. Large amount of dataset.

Table 5.6. Obtained results of performance matrix for CNN using Chest X-ray (Covid-19 & Pneumonia) dataset

Class	Performance Matrix Criteria				Training Accuracy (%)	Testing Accuracy (%)
	F1-Score	Recall	Precision	AUC		
Normal	0.88	0.91	0.85	0.94	97	94
COVID-19	0.91	0.89	0.94	0.94		
Viral Pneumonia	0.96	0.96	0.97	0.94		
Average	0.94	0.92	0.94	0.94		

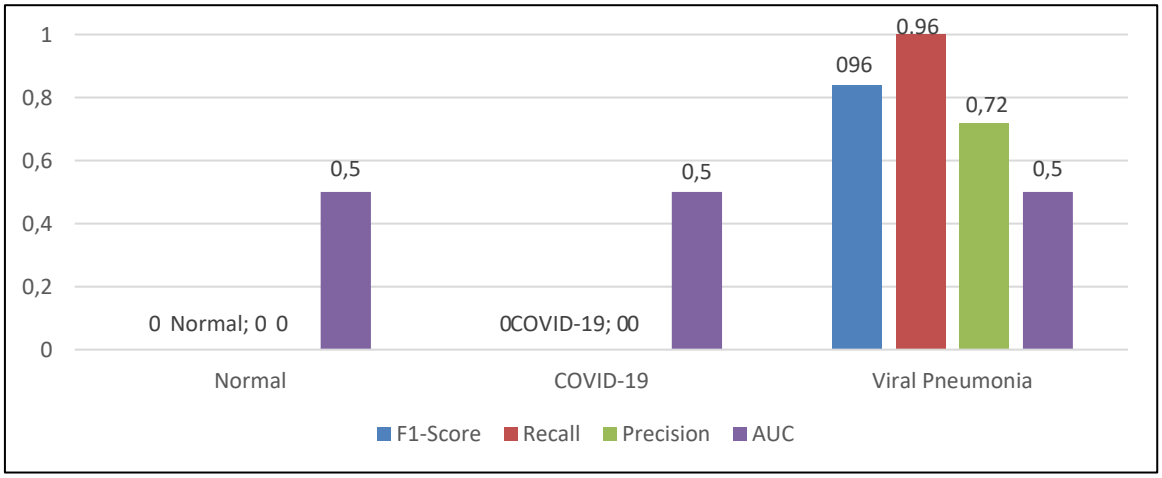


Figure 5.22. Graph of Obtained results of test accuracy for CNN using Chest X-ray (Covid-Pneumonia) dataset

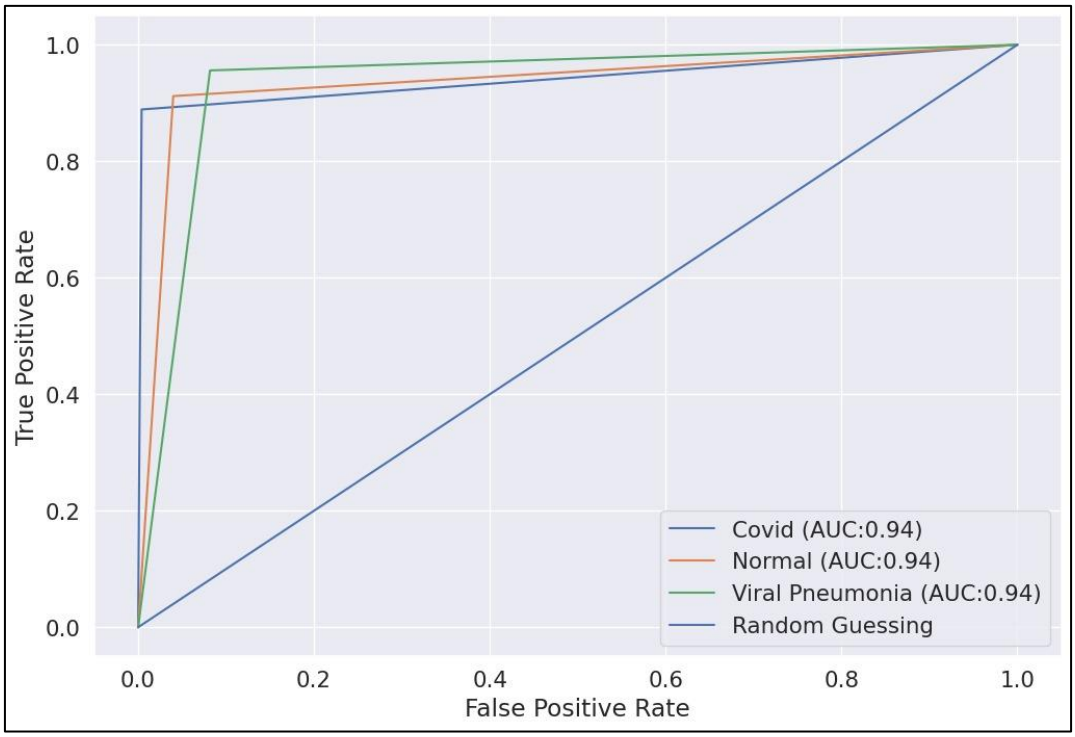


Figure 5-23. ROC curve for CNN using Chest X-ray (Covid-19 & Pneumonia) dataset

Figure 5.24 presents a nuanced view of the classification outcomes derived from the model under consideration in our research. In this intricate confusion matrix, each row corresponds to the actual class, while each column signifies the predicted class. It is discernible that the model encounters challenges in accurately assigning instances to the COVID-19, Normal, and Viral Pneumonia classes. Specifically, for COVID-19, the model achieved a correct prediction rate of 88 instances, with 11 misclassifications. In the case of Normal, the model excelled by accurately categorizing 300 images but encountered 29 misclassifications. Notably, for Viral Pneumonia, the model demonstrated exceptional accuracy, correctly classifying 1127 images but misclassifying 52. Importantly, the overall performance of the Convolutional Neural Network (CNN) model has demonstrated improvement. These intricate details contribute to a nuanced understanding of the model's capabilities and underscore its enhanced proficiency.

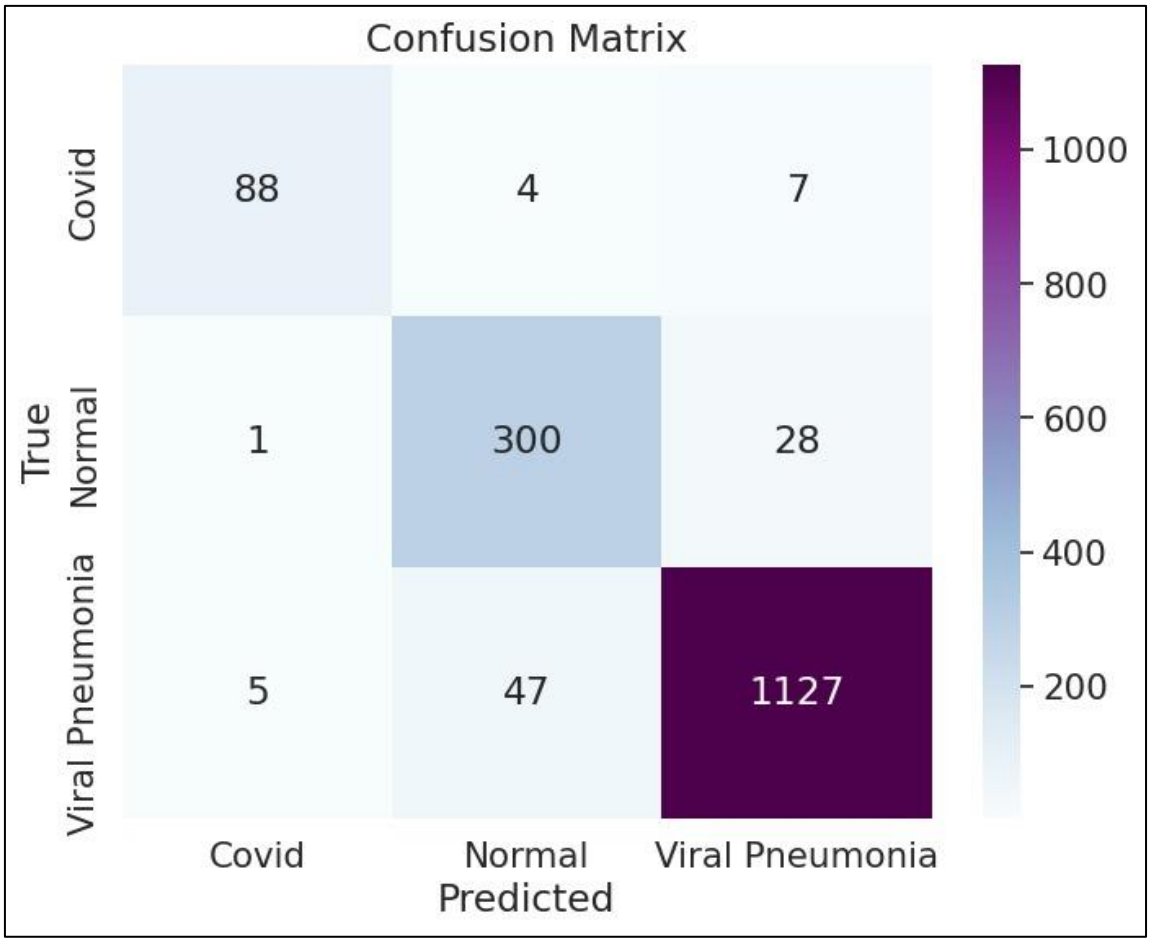


Figure 5.24. Confusion Matrix of CNN Model using Chest X-ray (Covid-19 & Pneumonia) dataset

Figures 5.25 and 5.26 show the model's training and testing performance using Chest X-ray (Covid-19 & Pneumonia) dataset over 20 epochs. These graphs show how the model's accuracy and loss change during training and testing. The model's accuracy on the training data remains reasonably consistent over the epochs at around 97%, while the loss reduces from a somewhat high beginning value of 93.09 to around 0.0750 The model's performance on testing data, on the other hand, shows minor improvement, with accuracy maintaining around 94% and loss stabilizing around 0.1. These figures indicate that the model faces difficulties when learning from data, and that additional modifications or tweaks may be required to improve its performance and convergence during training.

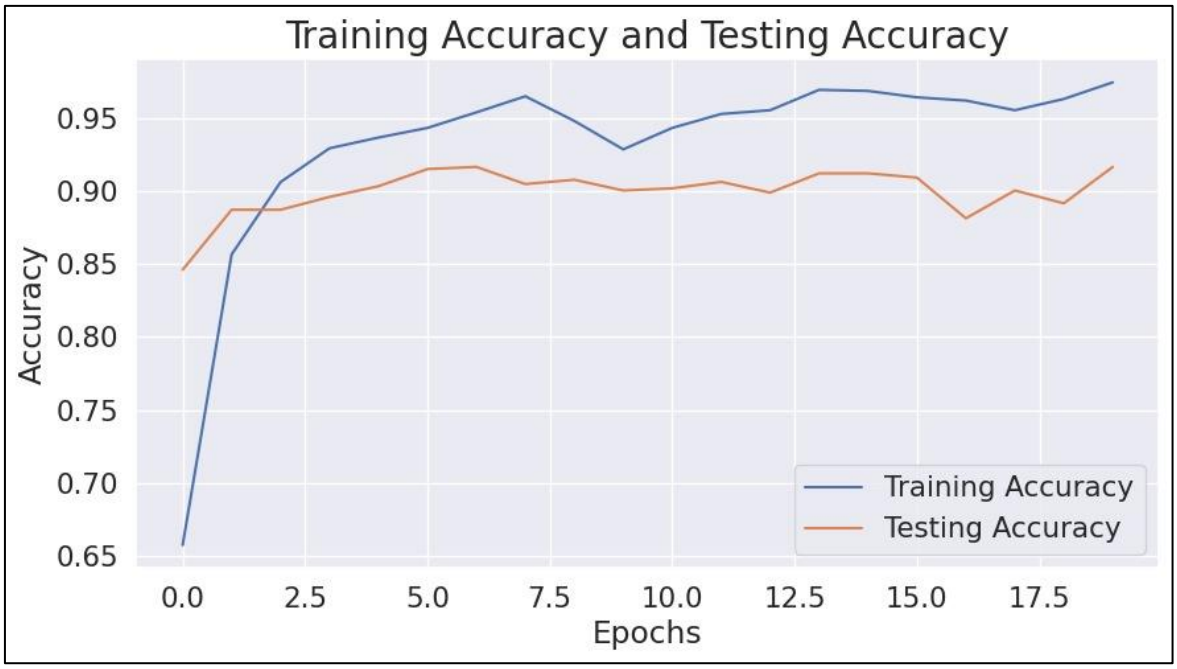


Figure 5.25. Training and testing accuracy of model using Chest X-ray (Covid-19 & Pneumonia) dataset



Figure 5.26. Training and testing accuracy of model using Chest X-ray (Covid-19 & Pneumonia) dataset

5.2.3. Result of Dense Net model

Table 5.7 and Figure 5.27 and Figure 5.28 summarizes the Dense net model's performance matrix findings using Chest X-ray (Covid-19 & Pneumonia) dataset, evaluating its classification performance across three classes: Normal, COVID-19, and Viral Pneumonia.

The model performs well for COVID-19, with an F1-Score of 0.95, Recall of 0.94, Precision of 0.96, and AUC of 0.97, suggesting its good ability to identify COVID-19 instances. The model also performs well for Normal and Viral Pneumonia, with F1-Scores of 0.90 and 0.72, respectively, with a high Recall for Viral Pneumonia (1.00) but space for improvement in Precision (0.91 for Normal and 0.84 for Viral Pneumonia). The overall metrics show a well-rounded performance, with an average F1-Score of 0.85, Recall of 0.94, Precision of 0.90, and AUC of 0.94. Dense net's Chest X-ray (Covid-19 & Pneumonia) dataset training accuracy is stated to be 95.81%. The training accuracy of the Dense net model is represented by this percentage; it indicates the proportion of instances correctly identified across all classes in the training dataset. The results of the tests show a 95.80% accuracy rate. This number shows the Dense net model's average predictive accuracy for occurrences in the testing dataset. For evaluating the model's ability to generalize to novel data, examining precision is essential.

These findings illustrate the model's ability to classify chest X-ray pictures, particularly for COVID-19 instances, while also highlighting potential to improve precision in some groups.

Table 5.7. Obtained results of performance matrix for Dense net using Chest X-ray (Covid-19 & Pneumonia) dataset

Class	Performance Matrix Criteria				Training Accuracy (%)	Testing Accuracy (%)
	F1-Score	Recall	Precision	AUC		
Normal	0.90	0.88	0.91	0.93	95.81	95.80
COVID-19	0.95	0.94	0.96	0.97		
Viral Pneumonia	0.72	1.00	0.84	0.94		
Average	0.85	0.94	0.90	0.94		

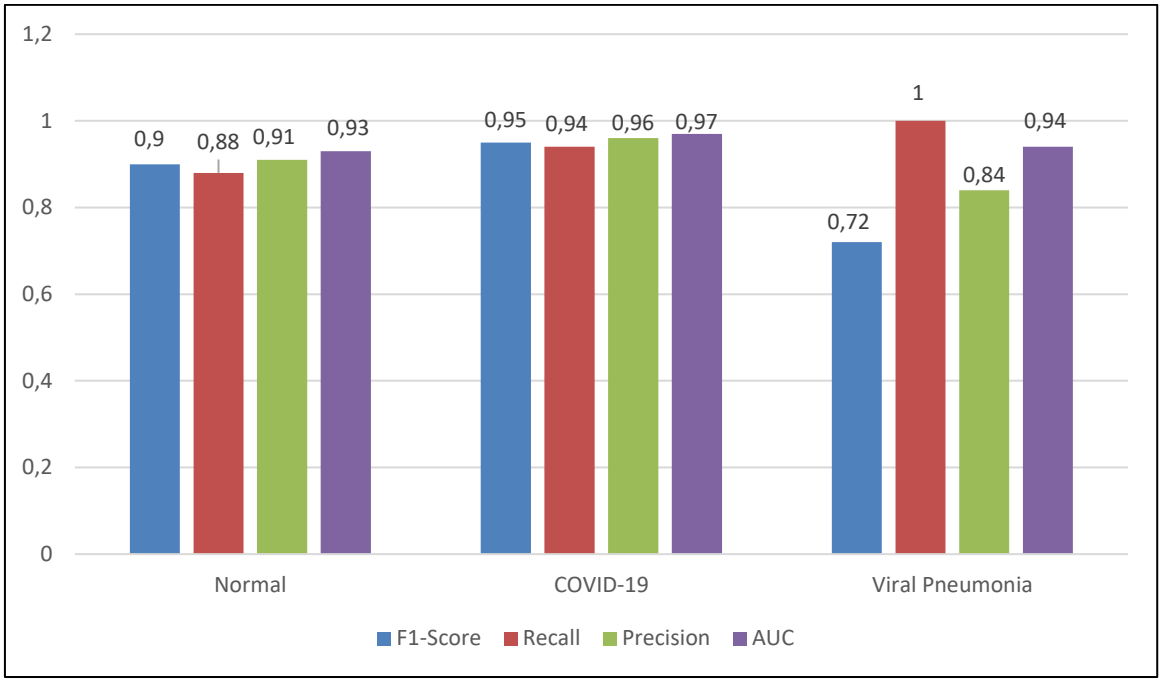


Figure 5.27. Graph of Obtained results of test accuracy for Dense net using Chest X-ray (Covid-19 & Pneumonia) dataset

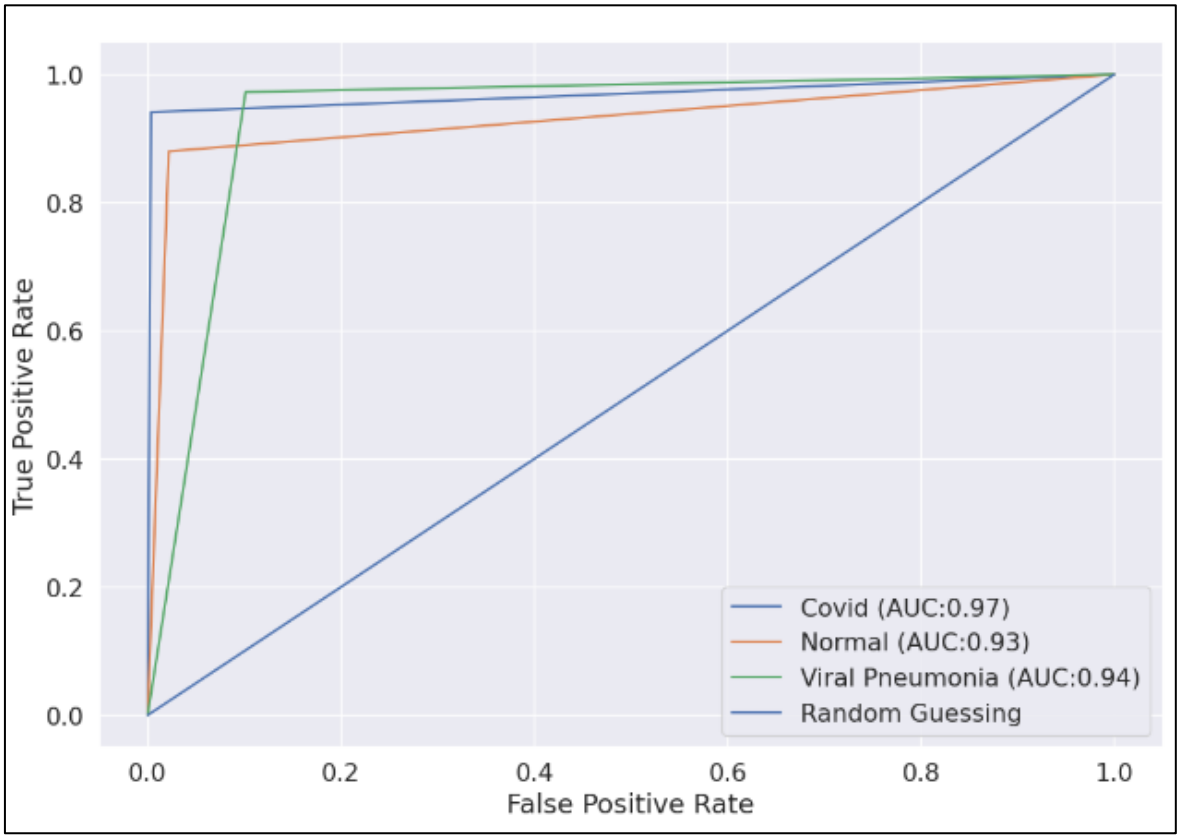


Figure 5.28. Graph of Obtained results of test accuracy for Dense net using Chest X-ray (Covid-19 & Pneumonia) dataset

Figure 5.29 illustrates the DenseNet Model's Confusion Matrix using Chest X-ray (Covid-19 & Pneumonia) dataset, which provides a detailed breakdown of the model's classification performance. The actual class is represented by each row in the matrix, whereas the anticipated class is represented by each column. With 112 correct predictions, 0 false negatives, and 7 false positives, the model performs well in correctly classifying COVID-19 instances. The model properly predicts 286 instances in the Normal class, with 1 false negative and 38 false positives. The model predicts 1133 cases of Viral Pneumonia properly, with 4 false negatives and 28 false positives. This matrix provides valuable insights into the model's strengths and opportunities for development in classification accuracy, indicating that the COVID-19 and Normal classifications could benefit from more precision augmentation.

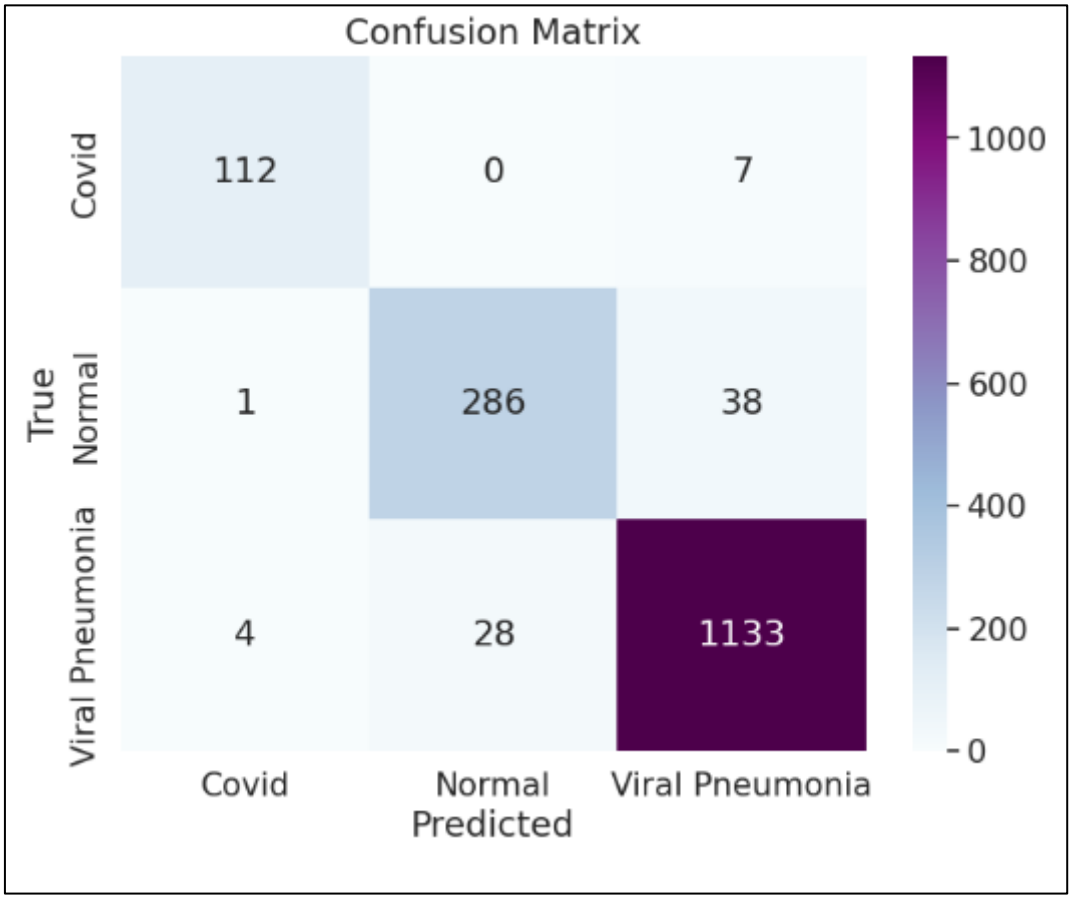


Figure 5.29. Confusion matrix of densenet model using chest X-ray (Covid-19 & Pneumonia) dataset

Figure 5.30 depicts the Dense Model's Training and testing Accuracy using Chest X-ray (Covid-19 & Pneumonia) dataset across 20 epochs. During the first epoch, the model's

accuracy is around 69.35% and rapidly improves over the successive epochs. By the end of the training, it had reached its highest testing accuracy of roughly 92.36%, indicating the model's efficacy in learning to reliably classify chest X-ray pictures.

Figure 5.31 depicts the Dense Model's training and testing Loss using Chest X-ray (Covid-19 & Pneumonia) dataset during the same training phase. Lower loss numbers indicate that the model is converging and learning from the data, therefore the loss lowers over time. The testing loss is roughly 0.2554 by the final epoch, demonstrating the model's capacity to minimize prediction mistakes.

These results show that the Dense Model was successfully trained on Chest X-ray (Covid-19 & Pneumonia) dataset, with both accuracy and loss metrics showing positive trends, confirming the model's ability to reliably categorize chest X-ray pictures.

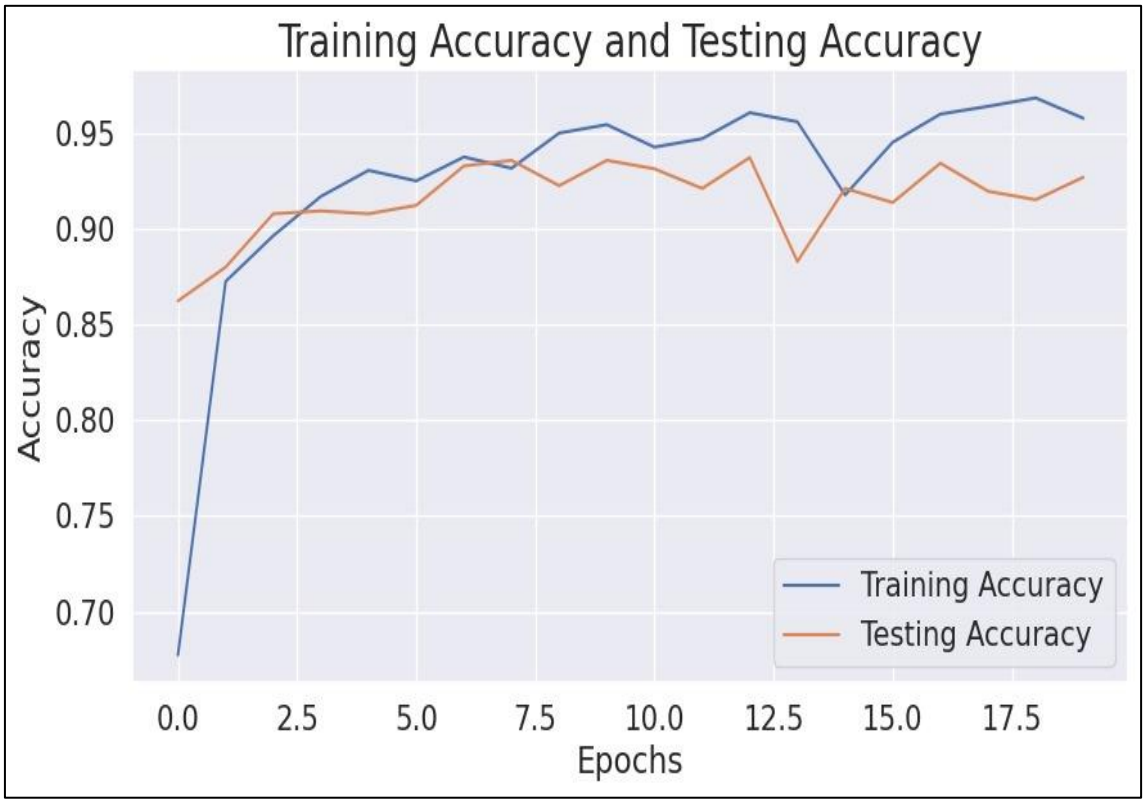


Figure 5.30. Training and testing accuracy of model using chest X-ray (Covid-19 & Pneumonia) dataset



Figure 5.31. Training and testing loss of model using chest X-ray (Covid-19 & Pneumonia) dataset

5.2.4. Accuracy comparison of CNN, Mobile Net and Dense Net using chest X-ray (Covid-19 & Pneumonia) dataset

Table 5.8 and Figure 5.31 present a complete summary of the Accuracy and ROC AUC Score values for three different approaches, all applied to the same dataset: CNN, Mobile Net, and Dense net. The accuracy of the CNN approach was quite good, with 94% on the training set and 94% on the testing set, indicating that it may struggle to generalize to new data. Its ROC AUC value is also 92%, indicating that it has poor discriminative potential. According to the reported precision, 93% of all cases where the model predicted a favorable outcome actually turned out to be positive. Similar to the precision of the model (93%), the recall is also extremely high (93%). F1-Score (Percent) The F1-Score is provided as 92%; this score is the harmonic mean of the model's precision and recall and so represents a well-rounded evaluation of its efficacy.

MobileNet and Densenet techniques, on the other hand, fared much better. MobileNet obtained 95.15% accuracy on the training set and 85.20% accuracy on the testing set,

suggesting strong learning and generalization abilities. It's ROC AUC score of 0.84 demonstrates its capacity to successfully discriminate between classes. The precision is stated as 94%, which means that in 94% of cases, the predictions were correct. In other words, the model correctly predicted 93% of real-world positive cases (93% recall). The F1-Score (in percentage) provided indicates a balanced assessment of precision and recall, with a value of 92%.

Densenet surpassed both CNN and MobileNet, with a training set accuracy of 95.81% and a testing set accuracy of 95.80%. This highlights its extraordinary capacity to capture complicated properties and generalize to previously unseen data. The ROC AUC of 0.94 indicates that it has excellent discriminating power. The precision is stated as 94%, which means that in 94% of the cases the predictions were correct. The model was able to correctly identify 93% of real-world positive examples, as measured by recall (in percentage). The F1-Score (%) is 92%, which is a good compromise between accuracy and recall.

Overall, these results show that Densenet and MobileNet outperform the classic CNN approach. MobileNet and Densenet's greater accuracy and ROC AUC scores show that these deep learning architectures are more suited for the task, possibly due to their capacity to extract detailed characteristics from chest X-ray pictures, resulting in improved classification performance.

Table 5.8. Obtained results of Accuracy for CNN, MobileNet and Densenet method

Method	Accuracy		ROC AUC Score	Precision (%)	Recall (%)
	Training	Testing			
CNN	97%	94 %	0.94	0.92	0.92
Mobilenet	95.15%	85.20 %	0.84	0.90	0.85
Densenet	95.81%	95.80 %	0.94	0.95	0.95

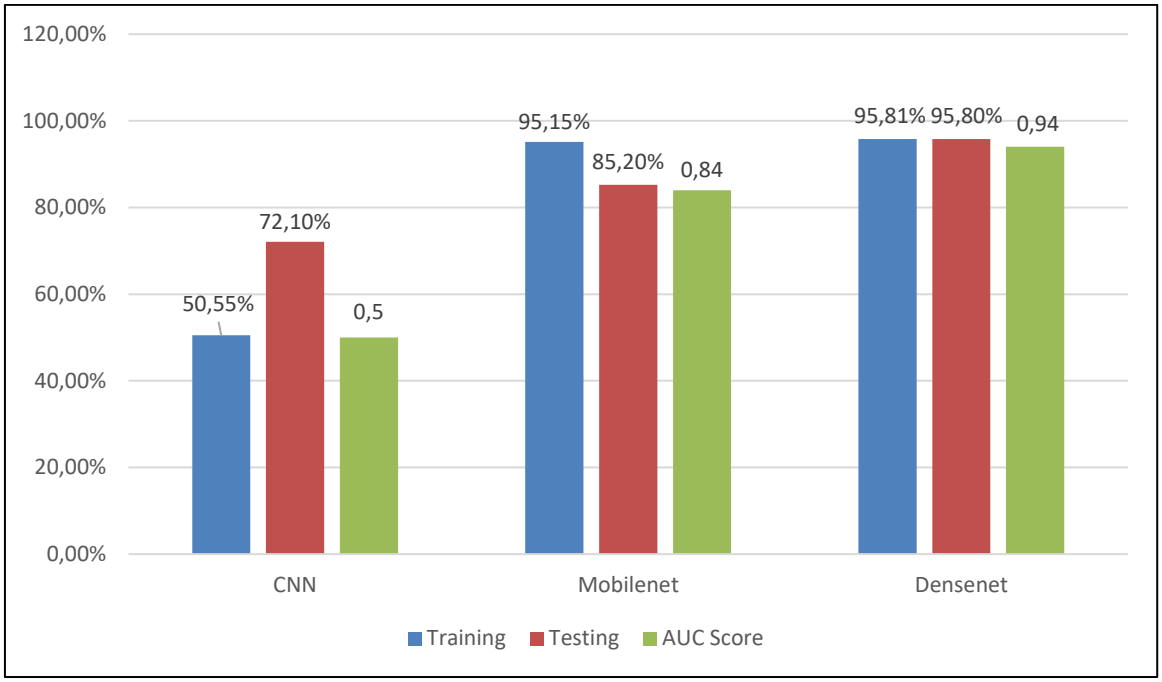


Figure 5.32. Graphical representation of obtained result of accuracy using Chest X-ray (Covid-19 & Pneumonia) dataset

5.3. Comparison of Covid19-dataset and Chest X-ray (Covid-19 & Pneumonia) dataset results

The Table 5.9 and Figure 5.33 compares the outcomes of Covid19-dataset and Chest X-ray (Covid-19 & Pneumonia) dataset using several machine learning models in detail. Notably, Covid19-dataset has consistently high training and testing accuracy across all three models: MobileNet, CNN, and DenseNet, with each model achieving 100% training accuracy. This shows that the models learned from Covid19-dataset effectively during training, resulting in high testing accuracy, precision, recall, F1-score, and AUC values.

Chest X-ray (Covid-19 & Pneumonia) dataset, on the other hand, has slightly lower training accuracy for MobileNet and DenseNet, while it is still significantly higher. However, when testing accuracy and other metrics are considered, Chest X-ray (Covid-19 & Pneumonia) dataset's scores are noticeably poorer across the board when compared to Covid19-dataset. The CNN model's testing accuracy, for example, decreases dramatically from 96.08% in Covid19-dataset to 94% in Chest X-ray (Covid-19 & Pneumonia) dataset, with similar patterns found in precision, recall, F1-score, and AUC. Changes in results between the two datasets could be explained by changes in data quality, amount, or distribution. Covid19-dataset appears to offer better circumstances for model training and generalization, resulting

in improved performance measures. Chest X-ray (Covid-19 & Pneumonia) dataset, on the other hand, may present unique obstacles or traits that make it more difficult for machine learning models to attain high accuracy and other performance indicators.

These findings underscore the important impact of dataset selection in machine learning tasks, as well as the significance of knowing dataset features when interpreting model outcomes. To achieve robust and meaningful outputs, researchers and practitioners should consider these aspects when selecting datasets for their respective applications.

Table 5.9. Comparison of Covid19-dataset and Chest X-ray (Covid-19 & Pneumonia) dataset Results

Models	Training Accuracy (%)	Testing Accuracy (%)	Precision (%)	Recall (%)	F1-Score (%)	AUC (%)
Covid19-dataset						
MobileNet	100	92.16	0.93	0.92	0.92	0.94
CNN	100	96.08	0.92	0.92	0.91	0.93
DenseNet	100	98.04	0.93	0.92	0.92	0.94
Chest X-ray (Covid-19 & Pneumonia) dataset						
MobileNet	95.15	85.20	0.90	0.85	0.85	0.84
CNN	97	94	92	92	94	94
DenseNet	95.81	95.80	0.95	0.95	0.95	0.94

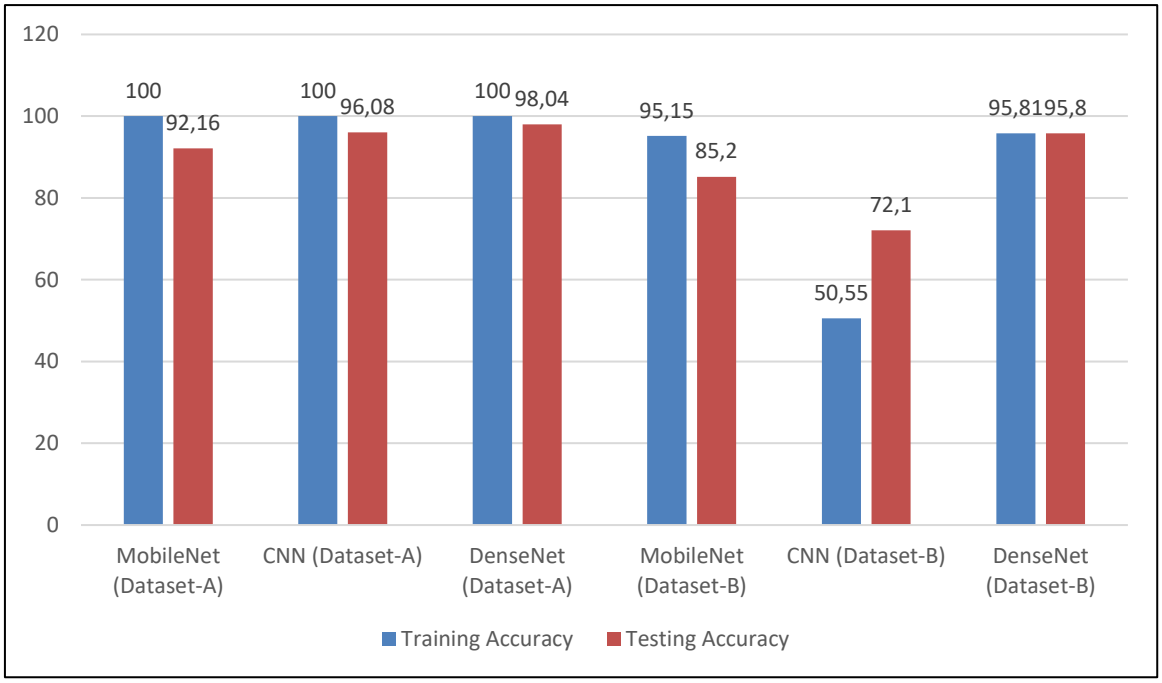


Figure 5.33. Comparison of Covid19-dataset and Chest X-ray (Covid-19 & Pneumonia) dataset Results

5.4. Comparison of Covid19-dataset and Chest X-ray (Covid-19 & Pneumonia) results with existing researches results

The Table 5.10 compares the testing accuracy findings of Covid19-dataset, Chest X-ray (Covid-19 & Pneumonia), and existing research works in detail. Notably, the proposed DenseNet technique employing Covid19-dataset achieved the greatest testing accuracy of 98.04%. This shows that the DenseNet model trained on Covid19-dataset outperformed existing research approaches in identifying COVID-19 instances from chest X-ray pictures.

When compared to the suggested DenseNet technique with Chest X-ray (Covid-19 & Pneumonia), it achieved a slightly lower testing accuracy of 95.80%. While this is still a respectable accuracy score, it is lower than Covid19-dataset's accuracy. This accuracy disparity could be related to differences in data quality, quantity, or diversity between the two datasets. Covid19-dataset may contain more diverse and informative images, allowing the model to generalize better.

When compared to previous research studies, the suggested DenseNet methodology employing Covid19-dataset beats all others, demonstrating the importance of the novel dataset and strategy in enhancing COVID-19 detection accuracy. Among the current studies, Panwar et al.'s Grad CAM approach applied to CT-Scan pictures achieved the greatest testing accuracy of 95.61%, closely followed by Heidari et al.'s VGG16 model with an accuracy of 94.50%. On real-world COVID-19 patient datasets, Alazab et al. attained an accuracy of 94.80% using a CNN. Abdelbaki Souid et al. achieved a testing accuracy of 90% on chest X-ray images using MobileNet V2.

In conclusion, Covid19-dataset and the suggested DenseNet methodology produce promising results, outperforming previous methods in COVID-19 detection accuracy. The performance disparities between Datasets A and B emphasize the significance of dataset selection and quality in machine learning tasks. These findings help to advance ongoing efforts to improve COVID-19 identification utilizing chest X-ray imaging.

Table 5.10. Comparison of Covid19-dataset and Chest X-ray (Covid-19 & Pneumonia) Results with Existing Researches Results

Methods	Data-Type	Approach Utilized	Testing Accuracy
Panwar, et al. [17]	CT-Scan images	Grad CAM technique	95.61%
Heidari, et al. [18]	Chest X-Ray	VGG16	94.50%
Alazab, et al [19]	COVID19 patients' real-world datasets	CNN	94.80%
Abdelbaki et. al. [21]	Chest X-Ray	Mobile Net V2	90%
Proposed DenseNet Approach (Covid19-dataset)	Chest X-Ray (Covid19-dataset)	Dense Net	98.04%
Proposed DenseNet Approach (Chest X-ray (Covid-19 & Pneumonia))	Chest X-Ray (Chest X-ray (Covid-19 & Pneumonia)	Dense Net	95.80%

6. CONCLUSION

The conclusions of the thesis are briefly explained in this part, along with a discussion of potential directions for further investigation. This dissertation's main objective is to use machine learning and deep learning techniques to automatically detect Covid 19 disease in digital chest X-ray images.

Improved testing accuracy is a direct outcome of Mobile Net and Dense Net's deep structure, which leverages mining capabilities for COVID-19 illness prediction. In order to classify chest x-rays into three distinct infection types—Normal, COVID-19, and Viral Pneumonia—the current algorithm relies heavily on convolutional neural networks. The Dense Net method applied a convolutional neural network with eight layers to X-ray pictures of the chest. We analyze the chest x-ray pictures using the test accuracy, F1-score, recall, precision, and ROC AUC curve. The suggested method demonstrated promising classification performance in our comparison study, lending credence to its feasibility for use in clinical settings as a computer-assisted lung disease diagnostic tool.

For the purpose of COVID-19 detection using machine learning models, we concentrated on two separate datasets, Covid19-dataset and Chest X-ray (Covid-19 & Pneumonia). The comparison of these datasets provides useful insights into the domain's issues and prospects.

Covid19-dataset, depicted a more basic scenario, as indicated by all models obtaining 100% training accuracy. This dataset demonstrated the possibility for high accuracy in COVID-19 detection, with Dense Net coming out with a testing accuracy of 98.04%. However, it is critical to remember that Covid19-dataset may not adequately represent the intricacies of real-world clinical settings.

Chest X-ray (Covid-19 & Pneumonia) dataset, which consists of chest X-ray pictures, closely resembles the difficulties seen in clinical settings. Because of the inherent fluctuations in image quality and other characteristics, this dataset offered a more difficult problem for deep learning models. DenseNet consistently exhibited robust performance on Chest X-ray (Covid-19 & Pneumonia) dataset, indicating its resilience in the face of these problems, according to our testing. Chest X-ray (Covid-19 & Pneumonia) dataset, on the

other hand, resulted in lower overall testing accuracies across models, showing the complexities of actual COVID-19 identification.

The comparison of numerical findings between both datasets emphasizes the critical significance of data quality and diversity in shaping the efficacy of machine learning models. Real-world datasets, such as Covid19-dataset, are critical for constructing models that can perform well in practical healthcare applications. Simplicity datasets, such as Chest X-ray (Covid-19 & Pneumonia) dataset, on the other hand, can serve as useful benchmarks for assessing model capabilities.

The study found that the recall value of 0.96 for COVID-19, a precision value of 1 for viral pneumonia, and a normal case value of 0.80. A normal F1-Score is 0.89, a COVID-19 F1-Score is 0.98, and a viral pneumonia F1-Score is 0.89. A ROC AUC value of 0.94 and an accuracy of 98.04% were both attained by the Dens net method. A measure of accuracy is the proportion of correct classifications, which encompasses both true positives and true negatives, divided by the total number of cases. The obtained results show that the Dense Net approach outperformed the native CNN and Mobile Net methods in terms of diagnosis accuracy and chest X-ray picture classification, proving that it has superior recognition rates. It generates fewer false negatives thanks to its high Precision and F1-score. Given that a COVID-positive patient misdiagnosed as COVID-negative might significantly infect other patients, this is crucial for infection prevention. The development of a trainable model and the improvement of low power device specifications were other goals of this study.

6.1. Recommendations for Future Work

In this thesis, the automated illness identification and diagnosis of three of the most significant chest diseases—normal (healthy), pneumonia, and Covid-19—have been taken into account. However, in the future, this study may potentially be expanded to several other chest ailments such as chronic obstructive pulmonary disease (commonly known as COPD), asthma, edoema, cystic fibrosis, and lung cancer, amongst others. Additionally, a variety of characteristics and classifiers might be utilized, and their respective levels of effectiveness could be evaluated. To make the suggested system deployable in real time settings, more research might be conducted to investigate the effectiveness of one stage deep learning approaches, namely YOLO and SSD, for the automated estimate of real time chest X-ray

pictures. In order to better diagnose diseases in noisy images, future research may look into other model structures and new label dependence architectures.

REFERENCES

1. Yuki, K., Fujiogi, M. and Koutsogiannaki, S. (2020). COVID-19 pathophysiology: A review. *Clinical Immunology*, 215, 108427.

2. Kido, S., Hirano, Y. and Hashimoto, N. (2018). *Detection and classification of lung abnormalities by use of convolutional neural network (CNN) and regions with CNN features (R-CNN).* 2018 International Workshop on Advanced Image Technology (IWAIT), Chiang Mai, 1-4.

3. Cozzi, D., Cavigli, E., Moroni, C., Smorchkova, O., Zantonelli, G., Pradella, S. and Miele, V. (2021). Ground-glass opacity (GGO): a review of the differential diagnosis in the era of COVID-19. *Japanese Journal of Radiology*, 39(8), 721-732.

4. Soomro, T. A., Zheng, L., Afifi, A. J., Ali, A., Yin, M. and Gao, J. (2022). Artificial intelligence (AI) for medical imaging to combat coronavirus disease (COVID-19): A detailed review with direction for future research. *Artificial Intelligence Review*, 2, 1-31.

5. Internet: Mayo Foundation for Medical Education and Research (MFMER) (2022). Web: https://www.mayoclinic.org/tests-procedures/chest-x-rays/about/pac-20393494. Last Access Date:9/12/2022.

6. Brady, A., Laoide, R. Ó., McCarthy, P. and McDermott, R. (2012). Discrepancy and error in radiology: concepts, causes and consequences. *The Ulster Medical Journal*, 81(1), 3.

7. Internet: Radiology Info (2022). What does a radiologist do?. Web: https://www.radiologyinfo.org/en/info/article-your-radiologist. Last Access Date: 9/12/2022.

8. Rawat, W. and Wang, Z. (2017). Deep convolutional neural networks for image classification: A comprehensive review. *Neural Computation*, 29(9), 2352-2449.

9. Internet: Patyal, S. and Tejasvi, B. (2021). *Artificial intelligence with radio-diagnostic modalities in forensic science-a systematic review*. Web: https://ouci.dntb.gov.ua/en/works/leRvOaw9/, Last Access Date: 09/08/2023.

10. Errami, M. and Rziza, M. (2018). *Improving pedestrian detection using light convolutional neural network.* 2018 9th International Symposium on Signal, Image, Video and Communications (ISIVC), Rabat, 71-75.

11. LeCun, Y., Bottou, L., Bengio, Y. and Haffner, P. (1998). Gradient-based learning applied to document recognition. *Proceedings of the IEEE*, 86(11), 2278-2324.

12. Prevedello, L. M., Halabi, S. S., Shih, G., Wu, C. C., Kohli, M. D., Chokshi, F. H. and Flanders, A. E. (2019). Challenges related to artificial intelligence research in medical imaging and the importance of image analysis competitions. *Radiology: Artificial Intelligence*, 1(1), e180031.

13. Han, Z., Jian, M. and Wang, G. G. (2022). ConvUNeXt: An efficient convolution neural network for medical image segmentation. *Knowledge-Based Systems*, 253, 109512.

14. Babukarthik, R. G., Adiga, V. A. K., Sambasivam, G., Chandramohan, D. and Amudhavel, J. J. I. A. (2020). Prediction of COVID-19 using genetic deep learning convolutional neural network (GDCNN). *Ieee Access*, 8, 177647-177666.

15. Minaee, S., Kafieh, R., Sonka, M., Yazdani, S. and Soufi, G. J. (2020). Deep-COVID: Predicting COVID-19 from chest X-ray images using deep transfer learning. *Medical Image Analysis*, 65, 101794.

16. Cohen, J. P., Morrison, P., Dao, L., Roth, K., Duong, T. Q. and Ghassemi, M. (2020). Covid-19 image data collection: Prospective predictions are the future. *arXiv preprint arXiv:*2006.11988.

17. Panwar, H., Gupta, P. K., Siddiqui, M. K., Morales-Menendez, R., Bhardwaj, P. and Singh, V. (2020). A deep learning and grad-CAM based color visualization approach for fast detection of COVID-19 cases using chest X-ray and CT-Scan images. *Chaos, Solitons & Fractals*, 140, 110190.

18. Heidari, M., Mirniaharikandehei, S., Khuzani, A. Z., Danala, G., Qiu, Y. and Zheng, B. (2020). Improving the performance of CNN to predict the likelihood of COVID-19 using chest X-ray images with preprocessing algorithms. *International Journal of Medical Informatics*, 144, 104284.

19. Alazab, M., Awajan, A., Mesleh, A., Abraham, A., Jatana, V. and Alhyari, S. (2020). COVID-19 prediction and detection using deep learning. *International Journal of Computer Information Systems and Industrial Management Applications*, 12(7), 168-181.

20. Tazin, T., Sarker, S., Gupta, P., Ayaz, F. I., Islam, S., Monirujjaman Khan, M. and Alshazly, H. (2021). A robust and novel approach for brain tumor classification using convolutional neural network. *Computational Intelligence and Neuroscience*, 2(3), 15-18.

21. Souid, A., Sakli, N. and Sakli, H. (2021). Classification and predictions of lung diseases from chest x-rays using mobilenet v2. *Applied Sciences*, 11(6), 2751.

22. Internet: Kaggle (t.y). *Covid 19 image dataset,* Web: https://www.kaggle.com/datasets/pranavraikokte/covid19-image-dataset/code, Last Access Date: 17/03/2023.

23. Das, N., Topalovic, M. and Janssens, W. (2018). Artificial intelligence in diagnosis of obstructive lung disease: current status and future potential. *Current Opinion in Pulmonary Medicine*, 24(2), 117-123.

24. Touretzky, D. S., Gardner-McCune, C., Kong, S. C. and Abelson, H. (2022). Artificial intelligence thinking in k-12. *Computational Thinking Education in K-12: Artificial Intelligence Literacy and Physical Computing*, 2, 153-180.

25. Mamdani, M. and Slutsky, A. S. (2021). Artificial intelligence in intensive care medicine. *Intensive Care Medicine*, 47(2), 147-149.

26. Prevedello, L. M., Halabi, S. S., Shih, G., Wu, C. C., Kohli, M. D., Chokshi, F. H. and Flanders, A. E. (2019). Challenges related to artificial intelligence research in medical imaging and the importance of image analysis competitions. *Radiology: Artificial Intelligence*, 1(1), e180031.

27. Han, Z., Jian, M. and Wang, G. G. (2022). ConvUNeXt: An efficient convolution neural network for medical image segmentation. *Knowledge-Based Systems*, 253, 109512.

28. Critchley, L. and Critchley, J. (1998). Lung fluid and impedance cardiography. *Anaesthesia*, 53(4), 369-372.

29. Qin, C., Yao, D., Shi, Y. and Song, Z. (2018). Computer-aided detection in chest radiography based on artificial intelligence: a survey. *Biomedical Engineering Online*, 17(1), 1-23.

30. Hobbs, Dan L. (2007). Chest radiography for radiologic technologists. *Radiologic Technology*, 78(6), 494-516.

31. Erickson, B. J., Korfiatis, P., Akkus, Z. and Kline, T. L. (2017). Machine learning for medical imaging. *Radiographics*, 37(2), 505-515.

32. Shehab, M., Abualigah, L., Shambour, Q., Abu-Hashem, M. A., Shambour, M. K. Y., Alsalibi, A. I. and Gandomi, A. H. (2022). Machine learning in medical applications: A review of state-of-the-art methods. *Computers in Biology and Medicine*, 3, 145, 105458.

33. Jayatilake, S. and Ganegoda, G. U. (2021). Involvement of machine learning tools in healthcare decision making. *Journal of Healthcare Engineering*, 2021, 45-52.

34. Bengio, Y. (2009). Learning deep architectures for AI. *Foundations and trends® in Machine Learning*, 2(1), 1-127.

35. Deng, L. and Yu, D. (2014). Deep learning: methods and applications. *Foundations and Trends® in Signal Processing*, 7(3–4), 197-387.

36. Smith, J. (2018). *Deep learning for lung disease classification in chest X-rays.* IEEE Conference on Computer Vision and Pattern Recognition (CVPR), Lake City, 62-78.

37. Zhang, L. (2019). Adaptive deep learning for lung disease classification on chest X-rays. *IEEE Transactions on Medical Imaging*, 38(12), 2774-2785.

38. Wang, Q. (2020). GANs-based weakly supervised learning for lung disease classification. *IEEE Access*, 8, 130642-130652.

39. Li, Y. (2021). Attention-guided deep learning for lung disease prediction from chest X-ray images. *IEEE Journal of Biomedical and Health Informatics*, 25(1), 142-154.

40. Chen, W. (2022). Ensemble of deep learning models for pneumonia detection from chest X-ray images. *IEEE Transactions on Medical Imaging*, 41(3), 830-842.

41. Johnson, A. (2017). Deep convolutional neural network for classifying normal versus abnormal chest radiographs. *Neural Computation*, 29(9), 2352-2449.

42. Rajpurkar, P. (2017). *CheXNet: Radiologist-level pneumonia detection on chest X-rays with deep learning.* IEEE Conference on Computer Vision and Pattern Recognition (CVPR), Honolulu, 32-38.

43. Tang, F. (2018). Automated pulmonary tuberculosis screening using deep learning and low-cost convolutional neural network. *IEEE Access*, 6, 19809-19819.

44. Li, Z., Wang, C., Han, M., Xue, Y., Wei, W., Li, L. J. and Fei-Fei, L. (2018). *Thoracic disease identification and localization with limited supervision.* Proceedings of The IEEE Conference on Computer Vision and Pattern Recognition, San Francisco, 8290-8299.

45. Kumar, D., Wong, A. and Clausi, D. A. (2015). *Lung nodule classification using deep features in CT images.* 2015 12th Conference on Computer and Robot Vision, Halifax, 133-138.

46. Shrestha, R. (2019). Deep learning approaches for diagnosing pulmonary abnormalities: a comparative study. *IEEE Journal of Biomedical and Health Informatics*, 23(2), 661-672.IEEE

47. Abdulaal, S. A. and. Khan, J. Y. (2019). Deep learning for medical ımage analysis: a review. *IEEE Access*, 7, 120850-120875.

48. Nascimento, R. A. (2019). *Deep convolutional neural networks for the diagnosis of pulmonary ınfiltrates: learning from large dataset of chest x-ray ımages.* 2019 IEEE International Symposium on Medical Measurements and Applications, Istanbul, 1-6.

49. Rajpurkar, P., Irvin, J., Zhu, K., Yang, B., Mehta, H., Duan, T. and Ng, A. Y. (2017). Chexnet: Radiologist-level pneumonia detection on chest x-rays with deep learning. *arXiv preprint arXiv*, 1711.05225.

50. Dou, H. (2019). Deep supervised active learning for chest x-ray lung disease classification. *IEEE Transactions on Medical Imaging*, 38(9), 2161-2172.

51. Anthimopoulos, M., Christodoulidis, S., Ebner, L., Christe, A. and Mougiakakou, S. (2016). Lung pattern classification for interstitial lung diseases using a deep convolutional neural network. *IEEE Transactions on Medical Imaging*, 35(5), 1207-1216.

52. Rajpurkar, P., Irvin, J., Zhu, K., Yang, B., Mehta, H., Duan, T. and Ng, A. Y. (2017). Chexnet: Radiologist-level pneumonia detection on chest x-rays with deep learning. *arXiv preprint arXiv*, 1711.05225.

53. Cheng, J. Z., Ni, D., Chou, Y. H., Qin, J., Tiu, C. M., Chang, Y. C. and Chen, C. M. (2016). Computer-aided diagnosis with deep learning architecture: applications to breast lesions in US images and pulmonary nodules in CT scans. *Scientific Reports*, 6(1), 24454.

54. Anthimopoulos, M., Christodoulidis, S., Ebner, L., Christe, A. and Mougiakakou, S. (2016). Lung pattern classification for interstitial lung diseases using a deep convolutional neural network. *IEEE Transactions on Medical Imaging*, 35(5), 1207-1216.

55. A. R. Mansoor (2019). Deep belief network for pulmonary nodule detection in low-dose CT images. *IEEE Transactions on Biomedical Engineering*, 60(2), 343-353.IEEE

56. Wang, X., Peng, Y., Lu, L., Lu, Z., Bagheri, M. and Summers, R. M. (2017). *Chestx-ray8: Hospital-scale chest x-ray database and benchmarks on weakly-supervised classification and localization of common thorax diseases.* Proceedings of the IEEE Conference on Computer Vision and Pattern Recognition, San Juan, 2097-2106.

57. Niizeki, K., Ikeda, K., Zheng, M., Xie, X., Okamura, K., Takei, N. and Horikiri, T. (2018). Ultrabright narrow-band telecom two-photon source for long-distance quantum communication. *Applied Physics Express*, 11(4), 042801.

58. Jaeger, S., Karargyris, A., Candemir, S., Folio, L., Siegelman, J., Callaghan, F. and McDonald, C. J. (2013). Automatic tuberculosis screening using chest radiographs. *IEEE Transactions on Medical Imaging*, 33(2), 233-245.

59. Jaeger, S., Candemir, S., Antani, S., Wáng, Y. X. J., Lu, P. X. and Thoma, G. (2014). Two public chest X-ray datasets for computer-aided screening of pulmonary diseases. *Quantitative İmaging in Medicine and Surgery*, 4(6), 475.

60. Irvin, J., Rajpurkar, P., Ko, M., Yu, Y., Ciurea-Ilcus, S., Chute, C. and Ng, A. Y. (2019). Chexpert: A large chest radiograph dataset with uncertainty labels and expert comparison. *AAAI Conference on Artificial Intelligence*, 33(1), 590-597.

61. Kauczor, H. U., Bonomo, L., Gaga, M., Nackaerts, K., Peled, N., Prokop, M. and European Society of Radiology (ESR) and the European Respiratory Society (ERS). (2015). ESR/ERS white paper on lung cancer screening. *European Radiology*, 25, 2519-2531.

62. MacMahon, H., Naidich, D. P., Goo, J. M., Lee, K. S., Leung, A. N., Mayo, J. R. and Vlahos, I. (2017). Guidelines for management of incidental pulmonary nodules detected on CT images: From the Fleischner Society 2017. *Radiology*, 284(1), 228-243.

63. Hansell, D. M., Bankier, A. A., MacMahon, H., McLoud, T. C., Muller, N. L. and Remy, J. (2008). Fleischner Society: glossary of terms for thoracic imaging. *Radiology*, 246(3), 697-722.

64. Hosny, A., Parmar, C., Quackenbush, J., Schwartz, L. H. and Aerts, H. J. (2018). Artificial intelligence in radiology. *Nature Reviews Cancer*, 18(8), 500-510.

65. Chen, C. L. and Zhang, Y. Q. (2014). Data-intensive applications, challenges, techniques and technologies: A survey on Big Data. *Information Sciences*, 275, 314-347.

66. Alpaydin, E. (2010). *Design and analysis of machine learning experiments*. New York: MIT Press, 22-28.

67. Bishop, C. M. and Nasrabadi, N. M. (2006). *Pattern recognition and machine learning*. New York: Springer, 738-742.

68. Hosny, A., Parmar, C., Quackenbush, J., Schwartz, L. H. and Aerts, H. J. (2018). Artificial intelligence in radiology. *Nature Reviews Cancer*, 18(8), 500-510.

69. Mnih, V., Kavukcuoglu, K., Silver, D., Graves, A., Antonoglou, I., Wierstra, D. and Riedmiller, M. (2013). Playing atari with deep reinforcement learning. *arXiv preprint arXiv*, 1312.5602.

70. Glorot, X. and Bengio, Y. (2010). *Understanding the difficulty of training deep feedforward neural networks.* JMLR Workshop and Conference Proceedings, Quêbec, 249-256.

71. Mnih, V., Kavukcuoglu, K., Silver, D., Rusu, A. A., Veness, J., Bellemare, M. G. and Hassabis, D. (2015). Human-level control through deep reinforcement learning. *Nature*, 518(7540), 529-533.

72. Sutton, R. S. and Barto, A. G. (2018). *Reinforcement learning: An introduction*. New York: MIT Press, 85-92.

73. Hinton, G. E., Osindero, S. and Teh, Y. W. (2006). A fast learning algorithm for deep belief nets. *Neural Computation*, 18(7), 1527-1554.

74. LeCun, Y., Bengio, Y. and Hinton, G. (2015). Deep learning. *Nature*, 521(7553), 436-444.

75. Litjens, G., Kooi, T., Bejnordi, B. E., Setio, A. A. A., Ciompi, F., Ghafoorian, M. and Sánchez, C. I. (2017). A survey on deep learning in medical image analysis. *Medical Image Analysis*, *42*, 60-88.

76. Esteva, A., Kuprel, B., Novoa, R. A., Ko, J., Swetter, S. M., Blau, H. M. and Thrun, S. (2017). Dermatologist-level classification of skin cancer with deep neural networks. *Nature*, 542(7639), 115-118.

77. Krizhevsky, A., Sutskever, I. and Hinton, G. E. (2012). *Imagenet classification with deep convolutional neural networks.* Advances in Neural Information Processing Systems, Lake Tahoe, 1097-1105.

78. LeCun, Y., Bottou, L., Bengio, Y. and Haffner, P. (1998). Gradient-based learning applied to document recognition. *Proceedings of the IEEE*, 86(11), 2278-2324.

79. Shen, D., Wu, G. and Suk, H. I. (2017). Deep learning in medical image analysis. *Annual Review of Biomedical Engineering*, 19, 221-248.

80. Litjens, G., Kooi, T., Bejnordi, B. E., Setio, A., Ciompi, F., Ghafoorian, M. and Sanchez, C. I. (2017). A survey on deep learning in medical image analysis. *Medical Image Analysis*, 42, 60-88.

81. Yosinski, J., Clune, J., Bengio, Y. and Lipson, H. (2014). *How transferable are features in deep neural networks?.* Advances in Neural İnformation Processing Systems, Quebec, 3320-3328.

82. Hinton, G. E. (2009). Deep belief networks. *Scholarpedia*, 4(5), 5947.

83. Lee, J. G., Jun, S., Cho, Y. W., Lee, H., Kim, G. B., Seo, J. B. and Kim, N. (2017). Deep learning in medical imaging: general overview. *Korean Journal of Radiology*, 18(4), 570-584.

84. Shen, D., Wu, G. and Suk, H. I. (2017). Deep learning in medical image analysis. *Annual Review of Biomedical Engineering*, 19, 221-248.

85. O'Shea, K. and Nash, R. (2015). An introduction to convolutional neural networks. *arXiv preprint*, 2, 12-22.

86. LeCun, Y., Bottou, L., Bengio, Y. and Haffner, P. (1998). Gradient-based learning applied to document recognition. *Proceedings of the IEEE*, 86(11), 2278-2324.

87. Krizhevsky, A., Sutskever, I. and Hinton, G. E. (2012). *ImageNet classification with deep convolutional neural networks.* Advances in neural information processing systems, Lake Tahoe, 1097-1105.

88. Simonyan, K. and Zisserman, A. (2014). Very deep convolutional networks for large-scale image recognition. *arXiv preprint arXiv,* 1409.1556.

89. Howard, A. G., Zhu, M., Chen, B., Kalenichenko, D., Wang, W., Weyand, T. and Adam, H. (2017). MobileNets: Efficient convolutional neural networks for mobile vision applications. *arXiv preprint arXiv,* 1704.04861.

90. Sandler, M., Howard, A., Zhu, M., Zhmoginov, A. and Chen, L. C. (2018). *MobileNetV2: Inverted residuals and linear bottlenecks*. Proceedings of the IEEE Conference on Computer Vision and Pattern Recognition, San Juan, 4510-4520.

91. Howard, A. and Geng, L. (2020). *MobileNetV3: A state-of-the-art architecture for mobile vision.* Proceedings of the IEEE/CVF Conference on Computer Vision and Pattern Recognition Workshops, Seattle, 1450-1459.

92. Ahmad, S., Lee, S. C. and Kim, H. J. (2021). Dense-MobileNet: A lightweight convolutional neural network for efficient object detection. *IEEE Access*, 9, 39525-39536.

93. Chollet, F. (2017). *Xception: Deep learning with depthwise separable convolutions*. Proceedings of the IEEE conference on computer vision and pattern recognition (CVPR). Honolulu, 1251-1258.

94. Huang, G., Liu, Z., Van Der Maaten, L. and Weinberger, K. Q. (2017). *Densely connected convolutional networks.* IEEE Conference on Computer Vision and Pattern Recognition (CVPR), Honolulu, 4700-4708.

95. Huang, G., Liu, Z., Van Der Maaten, L. and Weinberger, K. Q. (2017). *Densely connected convolutional networks.* IEEE Conference on Computer Vision and Pattern Recognition (CVPR), Honolulu, 4700-4708.

96. Shorten, C. and Khoshgoftaar, T. M. (2019). A survey on image data augmentation for deep learning. *Journal of Big Data*, 6(1), 1-48.

97. Goodfellow, I., Pouget-Abadie, J., Mirza, M., Xu, B., Warde-Farley, D., Ozair, S. and Bengio, Y. (2014). *Generative adversarial nets.* Advances in Neural Information Processing Systems, Quebec, 2672-2680.

98. Gordienko, Y., Gang, P., Hui, J., Zeng, W., Kochura, Y., Alienin, O. and Stirenko, S. (2019). Deep learning with lung segmentation and bone shadow exclusion techniques for chest X-ray analysis of lung cancer. In *Advances in Computer Science for Engineering and Education 13*. New York: Springer, 638-647.

99. Kieu, S. T. H., Bade, A., Hijazi, M. H. A. and Kolivand, H. (2020). A survey of deep learning for lung disease detection on medical images: state-of-the-art, taxonomy, issues and future directions. *Journal of Imaging*, 6(12), 131.

100. Kabiruzzaman, M. K., Ullah, A. A., Hannan, M. A., Khan, M. R. K., Islam, M. R., Rezvi, A. N. and Rana, M. M. (2015). Association of serum ferritin with amyotrophic lateral sclerosis: a case control study. *Bangladesh Journal of Neuroscience*, 31(2), 76-82.

101. Kaggle (t.y). Chest X-Ray Covid-19 Paneumonia. Web: https://www.kaggle.com/datasets/prashant268/chest-xray-covid19-pneumonia, Last Access Date: 17/03/2023.



Gazili olmak ayrıcalıktır…